Dissertation
submitted to the
Combined Faculties for the Natural Sciences and for Mathematics
of the Ruperto-Carola University of Heidelberg, Germany
for the degree of
Doctor of Natural Sciences

Put forward by
Dipl. Phys. Jan-Bernd Hövener
born in Münster, Westphalia

Oral examination: November 12th, 2008

^{13}C spin hyperpolarization by PASADENA: Instrumentation, preparation of magnetic tracers, and NMR spectroscopy and imaging *in vivo*

Referees: 1. Prof. Dr. Peter Bachert

2. Prof. Dr. Dr. Christoph Cremer

Zusammenfassung

Eine Verstärkung des Kernspinresonanzsignals um einem Faktor von 10^5 wurde von verschiedenen Methoden für die Kernspinhyperpolarisation gezeigt. Dies eröffnet neue Möglichkeiten, wie z.B. die Detektion von Stoffwechselvorgängen in Echtzeit *in vivo*. PASADENA erzielt hohe Kernspinpolarisation (P) im flüssigen Zustand in Sekunden: Die Spinordnung von Parawasserstoff wird mittels einer spin-order-transfer (SOT) Sequenz auf einen dritten Kern übertragen. In dieser Arbeit wurde ein PASADENA Polarisator für Hyperpolarisation von Moleküle in wässriger Lösung entwickelt: $P \sim 0.1$ von ^{13}C Kernen wurde erreicht (10^5-fache Signalverstärkung bei $B_0 = 1.5$ T, T = 293 K). Eine Simulation des PASADENA Experiments für die Berechnung der SOT Sequenz und Voraussage der Polarisationsausbeute wurde angefertigt. Das Biomolekül 1-^{13}C, 2,3-D_2 Succinate (Suc) und das funktionelle Molekül 2,2,3,3-tetraflouropropyl 1-^{13}C, 2,3,3-D_3 propionate (TFPP) wurden hyperpolarisiert ($P \sim 0.1$). Die Stabilität der Polarisationsausbeute wurde in Experimenten und Simulationen untersucht. Die Lebensdauer von Suc, TFPP and 2,2,3,3-hydroxyethyl 1-^{13}C 2,3,3-D_3 propionate (HEP) wurde in Abhängigkeit von Deuterierung der Moleküle und Lösungsmittel, pH und B_0 ermittelt: Die maximale Lebensdauer von Suc $T_1 = (59.7 \pm 3.2)$ s verlängert die Zeitspanne für die *in vivo* Detektion deutlich. Signifikant verstärktes ^{13}C Signal *in vivo* wurde nach der Injektion von hyperpolarisierten Suc und HEP in Magnetresonanzbildgebung und Spektroskopie beobachtet. Dies demonstriert das Potential der PASADENA Hyperpolarisation für die biomedizinische Forschung.

Abstract

Techniques for the enhancement of the nuclear spin polarization (hyperpolarization) have demonstrated ~10^5 fold amplification of ^{13}C NMR signal: new applications like imaging of metabolic processes in real-time and *in vivo* are in reach. PASADENA is a unique technique reaching high nuclear polarization (P) within seconds in liquid state: spin order of parahydrogen is transferred to a third nucleus by an r.f. spin-order-transfer (SOT) sequence. In this work, a semi-automated PASADENA polarizer for hyperpolarization of biomolecules in aqueous solution was constructed: $P \sim 0.1$ on ^{13}C was demonstrated (a ~10^5 fold ^{13}C signal enhancement at $B_0 = 1$ T and T = 293 K). A simulation of the spin dynamics of the PASADENA experiment was developed to calculate the parameters for the SOT sequence and to predict the hyperpolarization yield. New compounds were introduced: the *metabolic tracer* 1-^{13}C, 2,3-D_2 succinate (Suc) and the *functional agent* 2,2,3,3-tetraflouropropyl 1-^{13}C, 2,3,3-D_3 propionate (TFPP) were hyperpolarized ($P \sim 0.1$). The stability of the hyperpolarization was investigated in experiment and simulations. The lifetimes of the ^{13}C hyperpolarization of Suc, TFPP and 2,2,3,3-hydroxyethyl 1-^{13}C 2,3,3-D propionate (HEP) were determined in dependence of molecular deuteration, solvent deuteration, pH and B_0: the maximal $T_1 = (59.7 \pm 3.2)$ s of Suc prolongs the window for *in vivo* detection significantly. Strong enhancement of ^{13}C NMR signal was observed *in vivo* after injection of hyperpolarized Suc and HEP in animals and cell cultures, demonstrating the potential biologically relevant molecules hyperpolarized by PASADENA in biomedical research.

Table of contents

Meiner Familie gewidmet

Publications

Journal articles

Chekmenev E.Y., Hövener J.B., Norton V.A., Harris K.C., Batchelder L.S., Bhattacharya P., Ross B.D., and Weitekamp D.P. (2008) PASADENA Hyperpolarization of Succinic Acid for MRI and NMR Spectroscopy. J. Am. Chem. Soc., 130: 4212-4213.

Hövener J.-B., Rigotti D.J., Amann M., Liu S., Babb J.S., Bachert P., Gass A., Grossman R.I., and Gonen O. (2008) Whole-Brain N-Acetylaspartate MR Spectroscopic Quantification: Performance Comparison of Metabolite versus Lipid Nulling. Am. J. Neuroradiol., 29: 1441-45.

Hövener J.-B., Chekmenev E.Y., Norton V.A., Harris K.C., Perman W.H., Weitekamp D.P., Ross B.D., and Bhattacharya P. (2008) Quality assurance of PASADENA hyperpolarization for ^{13}C Biomolecules. Magn. Reson. Mater. Phys., revised version submitted.

Hövener J.-B., Chekmenev E.Y., Norton V.A., Weitekamp R., Harris K.C., Perman W.H., Robertson L., Weitekamp D.P., Ross B.D., and Bhattacharya P. (2008) PASADENA hyperpolarization of 13C biomolecules: Equipment design and installation. Magn. Reson. Mater. Phys., revised version submitted.

Perman W.H., Bhattacharya P., Leupold J., Lin A.P., Harris K.C., Norton V.A., Hövener J.-B., Weitekamp D.P., and Ross B.D. (2008, submitted) Fast Volumetric Spatial-Spectral MR Imaging of Hyperpolarized ^{13}C-Labeled Compounds using Multiple Echo 3D FIESTA. J. Magn. Reson. Imaging., revision submitted.

Chekmenev E.Y., Chow S.K., Hövener J.-B., Ross B.D., Weitekamp D.P., and Bhattacharya P. (2008) Towards receptor specific ^{13}C hyperpolarized MR contrast agents. J. Am. Chem. Soc., submitted.

Xu V., Chan H., Lin A.P., Sailasuta N., Valencerina S., Tran T., Hövener J.B., and Ross B.D. (2008) Mr Spectroscopy in Diagnosis and Neurological Decision Making. Seminars in Neurology, submitted.

Conference contributions

Achtnichts L., Amann M., Hirsch J., Weier K., Duyar H., Merkle A., Hövener J.B., Sollberger M., Monsch A., Gonen O., and Gass A. (2007) Assessment of whole brain N-acetylaspartate – a new additional MR marker in mild cognitive impairment and Alzheimer's disease Akt Neurol 34 (abstract). DOI: 10.1055/s-2007-987561.

Chekmenev E.Y., Bhattacharya P., Norton V.A., Hövener J.B., Ross B.D., and Weitekamp D.P., Towards hyperpolarized ^{13}C succinate for biomedical MR imaging, Proceedings of the 48th Experimental NMR conference, Asilomar, CA, USA, 2007

Hövener J.-B., Bhattacharya P., Chekmenev E.Y., Norton V.A., Perman W.H., Lin A.P., Harris K.C., Weitekamp D.P., and Ross B.D., Reproducibility and quality assurance in hyperpolarized 13C MRI and MRS Proceedings of the joint annual meeting of the ISMRM and ESMRMB, Berlin, Germany, 2007, pp. 278.

Hövener J.-B., Lin A.P., Tran T., Feng F., Zee C.S., Flannigan B., and Ross B.D., Neurospectroscopy will miss the boat AGAIN: The unmet need for universal standards and a database, Proceedings of the joint annual meeting of the ISMRM and ESMRMB, Berlin, Germany, 2007.

Bhattacharya P., Harris K.C., Chekmenev E.Y., Lin A.P., Norton V.A., Hövener J.B., Perman W.H., Ross B.D., and Weitekamp D.P., How low can we go? Limits of detection in PASADENA ^{13}C hyperpolarization, Proceedings of the joint annual meeting of the ISMRM and ESMRMB, Berlin, Germany, 2007, pp. 227.

Chekmenev E.Y., Bhattacharya P., Hövener J.B., Norton V.A., Perman W.H., Harris K.C., Lin A.P., Weitekamp D.P., and Ross B.D., Toward hyperpolarized ^{13}C succinate imaging of brain cancer, Proceedings of the joint annual meeting of the ISMRM 2007, Berlin, Germany, pp. 121.

Perman W.H., Bhattacharya P., Lin A.P., Hövener J.-B., Harris K.C., Chekmenev E.Y., Norton V.A., Weitekamp D.P., and Ross B.D., Fast spatial-spectral imaging of hyperpolarized 13C compounds using partial fourier multiple echo 3D FIESTA, Proceedings of the joint annual meeting of the ISMRM and ESMRMB, Berlin, Germany, 2007, pp. 267.

Chekmenev E.Y., Hövener J.-B., Perman W.H., Weitekamp D.P., Ross B.D., and Bhattacharya P., PASADENA hyperpolarization of succinic acid for brain tumor imaging, Proceedings of the Annual Meeting of the American Brain Tumor Association, Chicago, IL, USA, 2008.

Hövener J.-B., Chekmenev E.Y., Norton V.A., Weitekamp R.A., Harris K.C., Perman W.H., Robertson L.W., Ross B.D., Weitekamp D.P., and Bhattacharya P., Quality assurance of PASADENA hyperpolarization for 13C Biomolecules, Proceedings of the 49th Experimental NMR Conference, Asilomar, CA, USA, 2008.

Ollerenshaw J., Hövener J.-B., and Weitekamp D.P. (2008) Simulation-based optimization of imaging experiments that detect the metabolism of hyperpolarized biomolecules. Proceedings of the 49th Experimental NMR conference.

Hövener J.-B., Strategies to prolong the T1 time of hyperpolarized molecules, Proceedings of the 16th annual meeting of the International Society for Magentic Resonance in Medicine, Toronto, Canada, 2008, pp. 336.

Chekmenev E.Y., Norton V.A., Hövener J.-B., Perman W.H., Reynolds W.F., Weitekamp D.P., Ross B.D., and Bhattacharya P., Hyperpolarized PASADENA 13C tracers for true MR metabolic imaging, Proceedings of the International Conference on Magnetic Resonance in Biological Systems, San Diego, CA, USA, 2008.

List of abbreviations

ADC	acetylenedicarboxylic acid dimethyl ester
B_0	static magnetic field
B_1	r.f. pulses
(b)SSFP	(**b**alanced) **S**teady **S**tate **F**ree **P**recession
DNP	**D**ynamic **N**uclear **P**olarization
FISP	**F**ast **I**maging with **S**teady State **P**recession, a bSSFP sequence
Fum	1-^{13}C, 2,3-D_2 fumarate
HEA	2-hydroxyethyl 1-^{13}C, 2,3,3-D_3 acrylate
HEP	2-hydroxyethyl 1-^{13}C, 2,3,3-D_3 proprionate
${}^{i}J^{AB}$	J-coupling across *i* bonds between spin A and B
IR	inversion recovery
IUPAC	**I**nternational **U**nion of **P**ure and **A**pplied **C**hemistry
MDE	maleic acid dimethyl ester
MRI	**M**agnetic **R**esonance **I**maging
MRS	**M**agnetic **R**esonance **S**pectroscopy
NMR	**N**uclear **M**agnetic **R**esonance
oH_2	orthohydrogen
$P_{hyp}^{t_a}$	degree of polarization at t_a after production of hyperpolarized sample
PASADENA	**P**arahydrogen **A**nd **S**ynthesis **A**llows for **D**rastically **E**nhanced **N**uclear **A**lignment
PE	polyethyelene
pH_2	parahydrogen
PHIP	**P**ara**h**ydrogen **I**nduced **P**olarization
pO_2	partial oxygen pressure

r.f.	radio frequency
SD	standard deviation of an individual measurement; See Appendix III
SE	standard error, SD of the mean; See Appendix III
SEA	**s**mall-**e**xcitation-angle **a**pproximation
Suc	1-^{13}C, 2,3-D_2 succinate
T_1	longitudinal relaxation time
t_1, t_2, t_3	intervals of Goldman's spin-order-transfer sequence
T_2	transversal relaxation time
t_a	time between production and detection of a hyperpolarized sample
t_α^A	pulse width for a pulse with flip angle α for spin A
TE	echo time
TFPA	2,2,3,3-tetrafluorropropyl 1-^{13}C, 2,3,3-D_3 acrylate
TFPP	2,2,3,3-tetrafluorropropyl 1-^{13}C, 2,3,3-D_3 propionate
TR	repetition time
U^A	peak-to-peak voltage for r.f. pulse for spin A

Introduction

Nuclear magnetic resonance (NMR) is a very successful and versatile tool in many scientific fields. Since the discovery of the magnetic moment of protons by Stern and Gerlach in 1922 [10], the field developed rapidly: NMR was observed first in molecular beams by Rabi in 1938 [11], followed by NMR in condensed matter by Bloch [12] and Purcell [13] in 1946. Since then, NMR spectroscopy has found broad application for example in analytical chemistry, or the elucidation the three-dimensional structure of molecules. In the late 1970s, NMR was introduced to the field of medicine [14]: By now, magnetic resonance imaging (MRI) of protons (^{1}H) has become a standard diagnostic tool, uniquely providing anatomical information *non invasively* and *in vivo*, as other methods e.g. require for harmful radiochemistry (Positron Emission Tomography, PET) or rely on ionizing radiation (X-ray, CT).
The history of NMR is reflected in the Nobel prizes awarded: O. Stern in 1943 “for ... the discovery of the magnetic moment of the proton”, I.I. Rabi in 1944 “for his resonance method for recording the magnetic properties of atomic nuclei”, F. Bloch and E. P. Purcell in 1952 "for their development of new methods for nuclear magnetic precision measurements and discoveries in connection therewith", R. R. Ernst in 1991 “for his contributions to the

development of the methodology of high resolution nuclear magnetic resonance (NMR) spectroscopy", K. Wüthrich in 2002 for "for his development of nuclear magnetic resonance spectroscopy for determining the three-dimensional structure of biological macromolecules in solution", and P. C. Lauterbur and Sir P. Mansfield in 2002 "for their discoveries concerning magnetic resonance imaging ".

NMR in medicine is not limited to the acquisition of images alone: Magnetic resonance spectroscopy (MRS) is a unique tool to observe biochemistry *non invasively* and *in vivo.* MRS has provided unique insights and understanding of fundamental metabolic processes [15]. As a diagnostic modality, MRS holds great potential since metabolic changes can be detected *in vivo* before MRI-visible pathologies occur.
However, NMR is restricted by its inherently low sensitivity. For example, merely a fraction (called polarization) $P \sim 10^{-6}$ of all ^{1}H spins in a sample contribute to the observed NMR signal in an external field of $B_0 = 1.5$ T. The detection of NMR signal is only possible because spins are abundant: 1 cm^3 of water contains $\sim 6.7 \cdot 10^{22}$ protons ($c \approx 111$ M). While this is sufficient to resolve structures of the order of mm with ^{1}H MRI, *in-vivo* MR spectroscopy is limited to a chemical, spatial and temporal resolution of *mM*, *cm*^{3} and *min*. Apart from few exceptions, MRS has not yet found routine clinical application.
The detection of NMR signal is further exacerbated for nuclei other than ^{1}H. The polarization of carbon-13 $P(^{13}\text{C})$, for example, is only about a fourth of the proton polarization $P(^{1}\text{H})$ (caused by a smaller gyromagnetic ratio $\gamma(^{13}\text{C}) \approx ¼ \cdot \gamma(^{1}\text{H})$). Additionally, the natural abundance of ^{13}C is only 1.1 %, while ^{1}H is abundant at ≈ 100 %. Several promising methods aiming at an improved sensitivity of NMR, like superconducting coils or higher field strengths, all operate within the constraints of thermal nuclear spin polarization, and therefore provide only moderate enhancement of the signal to noise ratio (SNR) of the order of 2 – 10 fold.

Hyperpolarization techniques have demonstrated several orders of ^{13}C NMR signal enhancement, induced by large non-equilibrium ^{13}C polarization ($P \sim 1$) [16]. These techniques hold great potential to access new diagnostic parameters: hyperpolarized Helium, for example, is applied for lung imaging in humans since 1995 [64], but does not provide biochemical information. In order to study metabolism with the enhanced sensitivity of hyperpolarization, a hyperpolarized nucleus has to be introduced into the metabolic processes. This requires for a biologically relevant molecule, a *metabolic tracer,* which is taken up rapidly, and relatively long lifetime of the hyperpolarization, to allow penetration of the metabolic cycles. While the T_1 of protons in usually on the order of seconds, low-γ of nuclei like ^{13}C provide significantly longer T_1 and permit the detection of enhanced ^{13}C signal for minutes after the hyperpolarization was formed.

Only recently, hyperpolarization $P_{hyp} > 0.1$ of nuclear spins in molecules suitable for bio-medical research was achieved by (a) a **d**ynamic **n**uclear **p**olarization (DNP) technique and (b) **p**arahydrogen **a**nd **s**ynthesis **a**llow for **d**ramatically **e**nhanced **n**uclear **a**lignement (PASADENA) [16, 17]:

(a) Solid-state DNP techniques [18, 19] are used in to achieve nuclear polarization by first polarizing electrons to $P \approx 1$ and then transferring the polarization to the nuclear spins: A sample of the target molecule and an organic free radical is frozen to T ≈ 10 K in a strong magnetic field (in [16]: $B_0 = 3.35$ T). At this temperature, the equilibrium polarization for carbon is only $P_B(^{13}C) \approx 7.8 \cdot 10^{-4}$; electrons, though, are polarized to $P(e^-) \approx 0.97$ (because of their gyromagnetic ratio $\gamma(e\text{-}) \approx 2600 \cdot \gamma(^{13}C)$) (Eq. 7). Microwave irradiation ($\nu = 94$ GHz at $B_0 = 3.35$ T) is used to transfer the electron polarization to the nuclei. After the polarization process is completed, the sample is rapidly dissolved and transferred to a MR system for signal detection.
This technique benefits from great versatility: nuclei in most molecules can be hyperpolarized. On the downside are the toxicity electron donor, the duration (hrs per ml sample) and the costs, which is of the order of $500.000 for purchase, plus the running expenses for each experiment (superconducting magnet, microwave source, low temperature cryotechnique). Nevertheless, DNP-polarizers are commercially available (HyperSense, Oxford Instruments, UK), and already applied to studies of biochemistry *in vivo*: In recent work, the flux of the ^{13}C label between the carboxylic groups of pyruvate and lactate in a heart was measured [20, 21].

(b) PASADENA is the *only* liquid-state technique and unique in its ability to achieve nuclear polarisation of the order of unity within seconds [22, 23, 24]. It employs the pure spin-order of the singlet spin-isomer of dihydrogen (parahydrogen, pH_2) to produce nuclear polarization (here on ^{13}C): pH_2 is catalytically added to an unsaturated molecule, followed by subsequent transfer of the pH_2-spin order to a third nucleus by means of a field-cycling (2001) and a r.f. spin-order-transfer (SOT) sequence (2006) [1, 17, 25]. Since no superconducting magnet or microwave source is needed, the cost for PASADENA is only a fraction of the cost for DNP. PASADENA, though, is restricted to molecules which have a stable unsaturated precursor.
However, the application of PASADENA is yet limited since (1) the instrumentation for hyperpolarization by SOT sequence is not published in scientific literature nor commercially available, (2) no biomolecules were hyperpolarized yet[1], and (3) no biologically relevant application *in vivo* was demonstrated. As a consequence, PASADENA is available in only a few laboratories (>5).

[1] The only previously reported PASADENA agents which demonstrated P>0.1 are 2-hydroxyethyl 1-^{13}C, 2,3,3-D_3 propionate and maleic dimethyl ester solved in acetone.

These impediments were addressed in the present work:

(1) A new PASADENA polarizer had to be developed and constructed for reliable and stable production of hyperpolarized samples to $P \sim 0.1$ [3].

(2) The pool of PASADENA agents had to be extended to biologically relevant molecules [2, 26].

(3) In case (1) and (2) were achieved, *in vivo* ^{13}C MRI and MRS in animals is envisaged. [27].

The experimental part of this work was conducted in Pasadena, CA, in a joint research project of the Huntington Medical Research Institutes (HMRI) and the California Institute of Technology (CIT).

Chapter 1: Theory

This chapter begins with an introduction to nuclear magnetism and polarization (1.1), followed by a description of liquid-state NMR using the product operator formalism (1.2). A historical overview of parahydrogen-based NMR signal enhancement techniques is given in the beginning of section 1.3, followed by a description of NMR of parahydrogen, the initial PASADENA experiment, and the spin-order transfer to X nuclei. In section 1.4, the product operator formalism (1.2) is employed to simulate the PASADENA experiment, to calculate the spin-order-transfer sequence and to predict the hyperpolarization yield.

1.1 Nuclear Magnetism and Polarization

The magnetic moment $\hat{\mu}$ of a nucleus is proportional to its spin:

$$\hat{\mu} = \gamma \hat{I} \,, \tag{1}$$

where the proportionality constant γ is called gyromagentic ratio (Tab. 1): for $\gamma > 0$, $\hat{I}$ and $\hat{\mu}$ are parallel (e.g. the proton), $\gamma < 0$, $\hat{I}$ and $\hat{\mu}$ anti-parallel (e.g. ^{15}N). The spin is characterized by the angular-momentum quantum number $s = ½ \cdot (0, 1, 2 ..)$ and magnetic spin-quantum number $m \in [-s \;\; -s + 1, .. s - 1, s]$. In this work, we consider only $s = ½$ particles, with the exception of ^{2}H, which is $s = 1$.
The Hamilton operator of a magnetic moment in an external magnetic field B_0 can be described as

$$\hat{H} = -\hbar \vec{B}_0 \cdot \hat{\mu} = -\hbar \gamma \vec{B}_0 \cdot \hat{I} \,, \tag{2}$$

where $\hbar$[1] = Planck's constant over $2 \cdot \pi$. As we will see later, this operator is associated with the Zeeman-effect.
There are two eigenstates for a spin-½ ($s = ½$) in a magnetic field, denoted $|\alpha>$ and $|\beta>$:

$$\begin{aligned} \hat{\mu}\vec{B}_0 |\alpha\rangle &= \gamma \vec{B}_0 \hat{S} |\alpha\rangle = \tfrac{1}{2}\gamma \vec{B}_0 |\alpha\rangle = \tfrac{1}{2}\hbar\omega_0 |\alpha\rangle = E_\alpha |\alpha\rangle \\ \hat{\mu}\vec{B}_0 |\beta\rangle &= \gamma \vec{B}_0 \hat{S} |\beta\rangle = -\tfrac{1}{2}\gamma \vec{B}_0 |\beta\rangle = -\tfrac{1}{2}\hbar\omega_0 |\beta\rangle = E_\beta |\beta\rangle \end{aligned} \,. \tag{3}$$

Transitions between the states can be induced by r.f. irradiation with $\omega_0 = \Delta E / \hbar$:

$$\Delta E = \left| E_\alpha - E_\beta \right| = \hbar \gamma \vec{B}_0 = \hbar \omega_0 \,. \tag{4}$$

Only the *difference* of the populations contributes to the macroscopic magnetization and to the NMR signal:

$$P = \frac{N_\alpha - N_\beta}{N_\alpha + N_\beta} \,, \tag{5}$$

where $N_\alpha + N_\beta = 1$ denote the fractional populations the states, and P the relative population difference. The population of the spin states is described by the Boltzmann distribution:

[1] $\hbar = 1.054571628(53) \cdot 10^{-34}$Js

$$\frac{N_\alpha}{N_\beta} = \frac{\exp\left(-\frac{E_\alpha}{k_b T}\right)}{\exp\left(-\frac{E_\beta}{k_b T}\right)}, \tag{6}$$

where k_B [1] = Boltzmann constant and T = temperature. With Eq. 6 and Eq. 5 follows:

$$P_B = \tanh\left(\frac{\gamma\hbar B_0}{2k_B T}\right) \approx \frac{\gamma\hbar B_0}{2k_B T}. \tag{7}$$

At room temperature (T = 293.15 K) and $B_0 \sim 1$ T, the Boltzmann- or thermal polarization is low: for ^{1}H, only $P_B \sim 10^{-6}$ of the spins in the detection volume contribute to the NMR signal (Tab. 1).

For further reading, the following texts are recommended: [28] for quantum mechanics, [29, 30, 31] for NMR, and [32] for its application in biomedicine.

Tab. 1: Boltzmann polarization P_B (at T= 293.15 K), resonance frequency ($\nu_0 = \omega_0 / (2 \cdot \pi)$), gyromagentic ratio (γ), angular momentum quantum number (S) and natural abundance (N.A.) for selected atomic nuclei and the electron.

	B_0 = 1.5 T		B_0 = 3 T		B_0 = 4.7 T		B_0 = 7 T		γ / 2 · π		N.A.
nuclei	$P_B \cdot 10^6$	ν_0 (MHz)	$P_B \cdot 10^6$	ν_0 (MHz)	$P_B \cdot 10^6$	ν_0 (MHz)	$P_B \cdot 10^6$	ν_0 (MHz)	(MHz/T)	S	(%)
e^-	3441	42037	6882	84074	10782	131717	16057	196174	28024	½	–
^{1}H	5.23	63.86	10.50	127.73	16.4	200.11	24.4	298.03	42.567	½	99.99
^{31}P	1.41	25.85	4.23	51.71	6.63	81.00	9.88	120.65	17.235	½	100
^{23}Na	1.38	16.89	2.77	33.79	4.33	52.93	6.45	78.83	11.262	⅜	100
^{13}C	1.31	16.06	2.63	32.13	4.12	50.33	6.14	74.96	10.708	½	1.1
^{2}H	0.802	9.80	1.60	19.60	2.51	30.71	3.74	45.73	6.5336	1	0.01
19F	0.492	6.01	0.984	12.02	1.54	18.84	2.30	28.05	4.0077	½	100
^{15}N	5.30	-1.45	1.06	-2.89	1.66	-4.53	2.47	-6.74	-4.3156	½	0.36
^{129}Xe	1.45	17.65	2.89	35.31	4.53	55.32	6.74	82.39	-11.770	½	26.4

[1] $k_B = 1.3806504(24) \cdot 10^{-23}$ J/K

1.2 Theory of liquid-state NMR in Hilbert space

For the analysis of a liquid-state NMR experiment, the following items must be considered:

(1) The spin system: Magnetic isotope, chemical shift, J-couplings, relaxation and spin exchange rates.

(2) The NMR pulse sequence: Time evolution in the presence of r.f. fields and pulsed magnetic field gradients.

(3) Detection of the NMR signal: Readout of the transverse magnetization.

These topics are described on the following pages. The theoretical concepts will be used later for the calculation of the spin-order-transfer (SOT) sequence and the simulation of the PASADENA experiment.

Definitions and conventions

Since experiments are focused on ^{13}C, only spin-½ particles are considered. Hilbert space operators are denoted by capital letters in italics ($\hat{S}$). The spin operator for protons is denoted by $\hat{I}$, for other nuclei (like ^{13}C) we use $\hat{S}$. The spin number for individual spins is denoted by s and the magnetic spin-quantum number by m, in capitals S, M if the total-angular momentum of a spin system is considered. Furthermore, e_i denotes the unit vector along an axis I, $\hbar$ is Planck's constant over 2 π, γ is the gyromagnetic ratio and $\nu_0 = \omega_0 / (2 \cdot \pi)$ the resonance frequency on B_0.

(1) The spin system

Hamiltonian for isotropic liquid-state NMR
The basic operator in NMR is the spin operator $\hat{I}$. As an angular momentum operator, it obeys the commutation relation:

$$\left[\hat{I}_i, \hat{I}_j\right] = i\hbar \hat{I}_k \varepsilon_{ijk} \,. \tag{8}$$

The operators $\hat{I}^2$ and $\hat{I}_z$ have simultaneous eigenstates | s, m >, classified by the quantum number l and the magnetic quantum number m ϵ [-s, -s +1, .. , s-1, s], respectively:

$$\begin{aligned} &\hat{I}_z \left|s,m\right\rangle = m\left|s,m\right\rangle \text{ and} \\ &\hat{I}^2 \left|s,m\right\rangle = s\left|s,m\right\rangle. \end{aligned} \tag{9}$$

The Hamiltonian for liquid-state NMR for spin-½ particles consists of three terms:

Zeeman term: Alignment of the spins in the external field $B_0 = B_z$:

$$\hat{H}_Z = -\hat{\mu}\vec{B}_0 = -\hbar\gamma\vec{B}_0\hat{I} = -\hbar\omega_0\hat{I}_z \,. \tag{10}$$

Chemical shift: The electrons surrounding the nucleus shield the external field modify the Zeeman term:

$$\hat{H}_Z = -\hat{\mu}\left(1-\delta\right)\hat{B}_0 \,. \tag{11}$$

Scalar-couplings ("indirect", or J-couplings): Intramolecular interaction of nuclear spins i and j in a molecule, mediated by the binding electrons:

$$\hat{H}^{i,j}_{J\text{-}couplings} = 2\pi \hat{I}^i \tilde{J}^{ij} \hat{I}^j \,. \tag{12}$$

Note the abbreviated writing in the following: $J^{HaHb} = J^{ab}$. ${}^{i}J^{HaHb}$ is used to indicate the number of chemical bonds i between the nuclei a and b. Equation 12 is the general form of the scalar interaction Hamiltonian with the coupling tensor $\tilde{J}^{ij}$, a 3 x 3 real matrix. In an isotropic liquid, $\tilde{J}^{ij}$ is averaged by molecular motion and tumbling:

$$\tilde{J}^{ij} \rightarrow \tfrac{1}{3}\left(J^{ij}_{xx} + J^{ij}_{yy} + J^{ij}_{zz}\right). \tag{13}$$

Further simplifications apply in the so-called weak-coupling limit: In this case, the transversal components ($\hat{I}_x$ and $\hat{I}_y$) of the J-coupling Hamiltonian can be neglected:

$$\left|\tfrac{1}{2}J^{i,j}\right| << \left|\tfrac{1}{2\pi}\left(\delta^i - \delta^j\right)\right|\omega_0 \,. \tag{14}$$

Heteronuclear couplings are always weak. The liquid-state isotropic J-coupling term of the Hamiltonian in the weak-coupling limit reads:

$$\hat{H}^{i,j}_{J\text{-}couplings} = 2\pi J^{ij} \hat{I}^i_z \hat{I}^j_z \,. \tag{15}$$

Altogether, the isotropic liquid-state NMR Hamiltonian for two weakly coupled spins *i* and *j* in a magnetic field B_0 has the following form:

$$\hat{H}^{i,j}_{isotropic} = -\hbar\omega_0 \left(1+\delta^i\right)\hat{I}^i_z - \hbar\omega_0 \left(1+\delta^j\right)\hat{I}^j_Z + 2\pi J^{ij} \hat{I}^i_z \cdot \hat{I}^j_z \,. \tag{16}$$

Note that Planck's constant will be omitted in the following.

Spin ensembles

For all NMR applications, evaluation of the *average* of the *spin ensemble* is sufficient, as we are interested in macroscopic measurements. The density operator $\hat{\rho}$ describes a *spin ensemble*:

$$\hat{\rho} = \sum_{i=1}^{N} w_i \left|\alpha_i\right\rangle\left\langle\alpha_i\right| = \overline{\left|\alpha_i\right\rangle\left\langle\alpha_i\right|}, \tag{17}$$

where w_i indicates the statistical weight of the state α_i in the ensemble. The ensemble average of an operator *A* is evaluated as follows:

$$\left\langle \hat{A} \right\rangle = \mathrm{Tr}\left(\hat{A}\hat{\rho}\right). \tag{18}$$

For an n-spin-½ system in thermal equilibrium in a field B_z, the density operator matrix has the following form:

$$\hat{\rho} = \frac{1}{Z} \cdot \exp\left(-\frac{\hat{H}}{k_B T}\right) \approx \frac{1}{Z} \cdot \left(1 - \frac{\hat{H}}{k_B T} + \ldots\right) \quad , \tag{19}$$

where

$$Z = \sum_{i=1}^{N} \exp\left(-\frac{\hat{H}}{k_B T}\right) \tag{20}$$

is the partition function. For a 1-spin-½ system in the high temperature limit (k_BT >> $\hbar\,\gamma\, B_0$), a good approximation is:

$$\hat{\rho}\left(s = \tfrac{1}{2}\right) \approx \frac{1}{2}\hat{1} - \frac{\hbar\omega_0}{k_B T}\hat{I}_z \,. \tag{21}$$

(2) The NMR pulse sequence

A useful approach for the calculation of the evolution of a spin system is the product operator formalism.

Free evolution
The density matrix evolves according to the von-Neumann equation:

$$i\hbar \partial/\partial t\, \hat{\rho}(t) = \left[\hat{H}, \hat{\rho}(t)\right]. \tag{22}$$

For a time-independent Hamiltonian, the time-evolution operator $\hat{U}(t_0, t_1)$ is specified by the starting time t_0 and the end time t_1:

$$\hat{U}(t_0, t_1) = \exp\left(-i\hat{H} \cdot (t_1 - t_0)\right). \tag{23}$$

The density matrix can be evolved as follows:

$$\hat{\rho}(t_1) = \hat{U}(t_1, t_0)\hat{\rho}(t_0)\hat{U}^{+}(t_1, t_0). \tag{24}$$

For methods to evaluate exponential operators see [30].

Radio-frequency pulses
External manipulations of a spin system by radio-frequency pulses can be represented by rotations. The generators are components of angular momentum operators, hence the operator for a rotation with an angle α around an axis e_j reads:

$$\hat{R}(\alpha, \vec{e}_j) = \exp\left(i\alpha \hat{I}_j\right). \tag{25}$$

The effect of an r.f. pulse on the density matrix is:

$$\hat{\rho}_{\hat{R}} = \hat{R}\ \hat{\rho}_0\ \hat{R}^{+}. \tag{26}$$

(3) Detection of NMR signal

In the NMR experiment the transverse magnetization is detected. The NMR signal *S(t)* is proportional to $M_{trans} = M_x + iM_y$. Hence in the product operator formalism, using $\hat{I}^{+} = \hat{I}_x + i\hat{I}_y$:

$$S(t) \sim M_T(t) \sim \left\langle \hat{I}^{+} \right\rangle = Tr\left(\hat{I}^{+}\hat{\rho}(t)\right). \tag{27}$$

1.3 Parahydrogen and spin-polarization

The spin physics explaining the ^{1}H NMR signal enhancement through addition of parahydrogen to a target molecule was published by Bowers and Weitekamp [22] (July 1986), followed by experimental verification and introduction of the acronym PASADENA one year later [23] (April 1987). Eisenschmid *et al*. published "**P**ara**H**ydrogen **I**nduced **P**olarization" (PHIP) in the same issue of the Journal of the American Chemical Society [33] (August 1987), finding that earlier experiments by Hommeltoft, Berry and Eisenberg [34] (March 1986) indeed demonstrated PASADENA, although interpreted as **C**hemically **I**nduced **D**ynamic **N**uclear **P**olarization (CI-DNP) at that time.

A large number of articles followed, mostly describing applications of PASADENA in chemistry and catalysis, but also investigating the transfer of ^{1}H spin order to heteronuclei by Natterer and Bargon [14, 15, 16, 17, 18, 19, 20]. Much later, in 2001, Golman *et al*. [17] in Malmø, Sweden, were the first to demonstrate the use of PASADENA hyperpolarization *in vivo*, transferring the spin order of ^{1}H to ^{13}C by means of a field-cycling scheme (ALTADENA) introduced by Praciva and Weitekamp in 1988 [24].
PASADENA hyperpolarization of $P > 10$ % on ^{13}C by a r.f. spin-order-transfer (SOT) sequence was first demonstrated by Goldman in 2005 [1] and 2006 [35, 36], using hydroxyethyl propionate (HEP). After the pioneering demonstration of DNP and PASADENA hyperpolarization application *in vivo,* the laboratory in Malmø was closed.

In 2005, the research on PASADENA for *in vivo* research was resumed in the "Enhanced MR laboratories", a joint research group of the California Institute of Technology (D.P. Weitekamp) and the Huntington Medical Research Institutes (B.D Ross), headed by P. Bhattacharya.
The first application *in vivo* of PASADENA molecules in aqueous solution hyperpolarized by a SOT sequence and the suggestion to use PASADENA hyperpolarized biomolecules to detect cancer [4, 37] followed in 2005 – 2007. New approaches to allow PASADENA hyperpolarization of molecules insensitive to Goldman's SOT were presented by Norton and Weitekamp in 2007 [38].

1.3.1 Parahydrogen

Protons are spin-½ particles and obey the Fermi statistics: The wave function associated with the total angular momentum ($\Psi_{\text{tot}}^{\text{ang}}$) of dihydrogen has to be anti-symmetric with respect to the permutation of the two hydrogen atoms. $\Psi_{\text{tot}}^{\text{ang}}$ is formed by the molecular rotation angular momentum ($\Psi_{\text{rot}}^{\text{ang}}$) as well as nuclear ($\Psi_{\text{nucl. spin}}^{\text{ang}}$) and electron ($\Psi_{e^-}^{\text{ang}}$) spin angular momenta. If the electrons are paired and do not contribute, the total angular momentum function combines to:

$$\Psi_{\text{tot}}^{\text{ang}} = \Psi_{\text{nucl. spin}}^{\text{ang}} \cdot \Psi_{\text{rot}}^{\text{ang}} \tag{28}$$

The total nuclear-spin function of two-spin-½ (e.g. H_2) forms four states | S, M >: Three triplets, with a total spin $S = 1$ (symmetric, orthohydrogen (oH_2), $M = -1, 0, +1$), and one singlet, with a total spin $S = 0$ (anti-symmetric, parahydrogen (pH_2), $M = 0$):

$$\begin{aligned}
&|1,+1\rangle = |\alpha,\alpha\rangle \\
&|1,\ 0\rangle = \tfrac{1}{\sqrt{2}}\left(|\alpha,\beta\rangle + |\beta,\alpha\rangle\right) && \textit{symmetric: orthohydrogen} \\
&|1,-1\rangle = |\beta,\beta\rangle \\
&|0,\ 0\rangle = \tfrac{1}{\sqrt{2}}\left(|\alpha,\beta\rangle - |\beta,\alpha\rangle\right) && \textit{antisymmetric: parahydrogen.}
\end{aligned} \tag{29}$$

Thus, the (symmetric) ortho spin angular momentum function requires an anti-symmetric rotational angular momentum function, and likewise the (anti-symmetric) para spin angular momentum function for a symmetric rotational function (Fig. 1).

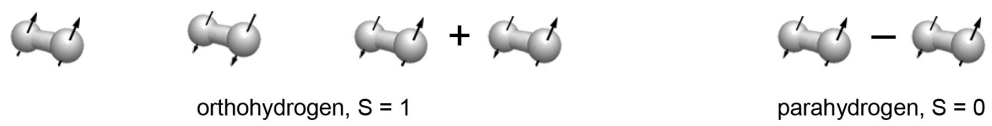

Fig. 1: Ball-and-stick model of the spin isomers of dihydrogen.
Dihydrogen forms three spin triplets ($S = 1$) and one singlet state ($S = 0$). Through catalytic conversion at low temperatures, parahydrogen gas of high purity can be produced in large quantities. As a $S = 0$ spin particle, pH_2 does not give a NMR signal.

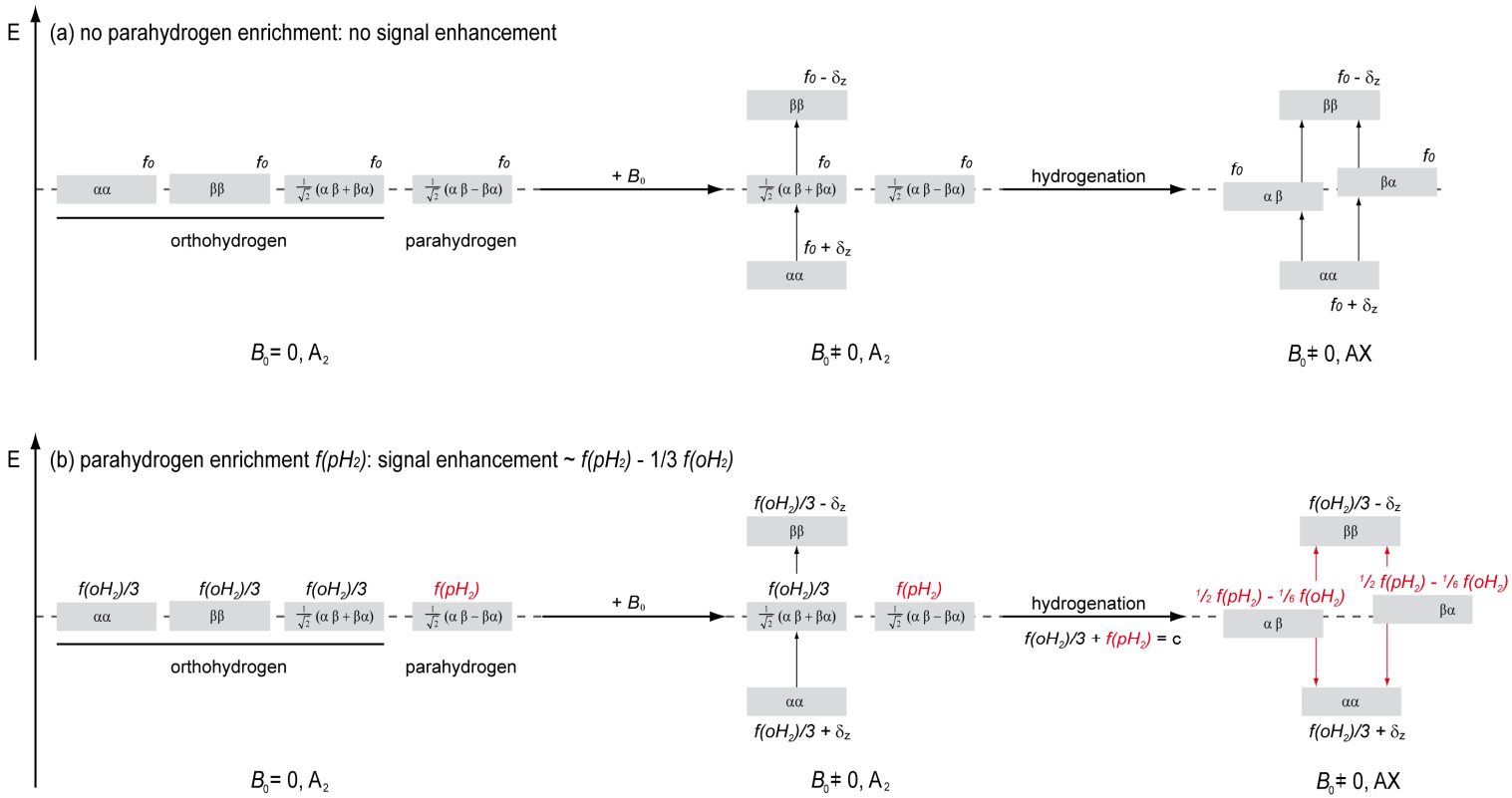

Fig. 2: Energy levels and populations of normal (a) and parahydrogen enriched (b) dihydrogen.

(a) Two magnetically equivalent spin-½ particles (2-spin-½ system, like molecular dihydrogen) form four spin isomers, denoted by $(1,1) = \alpha\alpha$, $(1,-1) = \beta\beta$, $(1,0) = 2^{-½} \cdot (\alpha\beta + \beta\alpha)$, $(0,0) = 2^{-½} \cdot (\alpha\beta - \beta\alpha)^{-½}$ (the numbers in parentheses refer to the total-angular-spin momentum (S,M), Eq. 29). With respect to the permutation of a particle, three of these states are symmetric ($S = 1$: $\alpha\alpha$, $\beta\beta$, $2^{-½} \cdot (\alpha\beta + \beta\alpha)$, orthohydrogen), and one is antisymmetric ($S = 0$: $2^{-½} \cdot (\alpha\beta - \beta\alpha)$, parahydrogen). In absence of an external magnetic field, energies of these states are degenerate ($E_{(1,1)} = E_{(1,-1)} = E_{(1,0)} = E_{(0,0)}$) and equally populated: $f(oH_2)/3 = f(pH_2) = 0.25$ with $1 = f(pH_2) + f(oH_2)$ (left). In a magnetic field, the energy of the $\alpha\alpha$ ($\beta\beta$) state is increased (decreased) by the Zeeman effect by $\Delta E / 2$ (Eq. 10). According to the Boltzmann distribution, this induces a population difference δ_Z (not to be confused with δ of the chemical shift), which can be observed in a NMR experiment: $\Delta E = \hbar\omega$ (middle). Note that parahydrogen is isolated and "NMR silent". If the two spins become non-equivalent (AA' or AX system, right), for example by addition of H_2 to a molecule (hydrogenation), the $M = 0$ composite states $(\alpha\beta + \beta\alpha)^{-½}$ and $(\alpha\beta - \beta\alpha)^{-½}$ are broken into the individual $\alpha\beta$ and $\beta\alpha$ states. The population (p) of the $M = 0$ states is preserved: $p(M = 0) = p(\alpha\beta) + p(\beta\alpha)$. In addition, a new energy shift is introduced by scalar couplings between the nuclear spins mediated by the binding electrons (J-couplings, Eq. 12). Two resonances split by the J-couplings are observed in an NMR experiment (two doublets). The intensities are proportional to the population difference δ, $\sim 10^{-6}$ at 1 T and room temperature.

(b) The population of $(0,0) = 2^{-½} \cdot (\alpha\beta - \beta\alpha)$, parahydrogen, can be enriched to a fraction close to unity $f(pH_2) = 1 - f(oH_2) > 0.99$ by means of catalytic conversion at low temperatures [7]. As long as the spins are magnetically equivalent, the pH_2 spin isomer is isolated and does not contribute to the NMR signal (middle). On the contrary, the overall NMR signal is attenuated since the orthohydrogen fraction is reduced. Only if the two spins become non-equivalent (AA', AX, e.g. by addition of the H_2 to another molecule), the enriched population of pH_2 can be employed for NMR signal enhancement: The large non-equilibrium population (p) of the $M = 0$ states $p(M = 0) = f(oH_2)/3 + f(pH_2)$ is distributed on the population of the now distinct states $\alpha\beta$ and $\beta\alpha$. NMR signal intensities proportional to the population differences (e.g. between $\alpha\beta$ and $\beta\beta$) can be observed: $S^{NMR} \sim p(\alpha\beta) - p(\alpha\alpha) = 0.5 \cdot (f(pH_2) - f(oH_2)/3)\ ) - f(oH_2)/3) - \delta \sim f(pH_2) - f(oH_2)/3$, for example. Relatively to the non-pH_2 enriched signal, a maximal NMR signal enhancement of the order of δ^{-1} can be achieved.

Density operator

Using Eq. 17, the density operator can be constructed for different statistical weights of the states:

$$\hat{\rho}_{H_2} = f\left(pH_2\right) \cdot \left|0,0\right\rangle\left\langle 0,0\right| + \frac{\left(1 - f\left(pH_2\right)\right)}{3} \cdot \left(\left|1,1\right\rangle\left\langle 1,1\right| + \left|1,0\right\rangle\left\langle 1,0\right| + \left|1,\text{-}1\right\rangle\left\langle 1,\text{-}1\right| \right) \tag{30}$$

The density operator for the pH_2 fraction can be constructed using the product-operator formalism [30]:

$$\hat{\rho}_{pH_2} = \frac{1}{4}\hat{1} + \frac{1}{3}\left(1 - 4 \cdot f\left(pH_2\right)\right)\hat{I}_1\hat{I}_2 \overset{f(pH_2)=1}{=} \frac{1}{2}\begin{pmatrix} 0 & 0 & 0 & 0 \\ 0 & 1 & -1 & 0 \\ 0 & -1 & 1 & 0 \\ 0 & 0 & 0 & 0 \end{pmatrix}. \tag{31}$$

NMR of dihydrogen

In thermal equilibrium and in the absence of a magnetic field, the energies of ortho ($S = 1$: $|\alpha,\alpha>$, $|\beta,\beta>$, $2^{-½} \cdot (|\alpha,\beta> + |\beta,\alpha>)$) and parahydrogen ($L = 0$: $2^{-½} \cdot (|\alpha,\beta> - |\beta,\alpha>)$) are degenerated ($E_{(1,1)} = E_{(1,-1)} = E_{(0,1)} = E_{(0,0)}$) and equally populated: $f(oH_2)/3 = f(pH_2) = 0.25$ with $f(pH_2) + f(oH_2) = 1$ (Fig. 2 a, left).

In a magnetic field, the energy of the $|\alpha,\alpha>$ ($|\beta\beta>$) states is increased (decreased) owing to the Zeeman effect (Eq. 10). According to the Boltzmann distribution, this induces a population difference δ_p (not to be confused with δ, the chemical shift) which can be observed in a NMR experiment. Note that the para-state is isolated yields no NMR signal (total spin of the two protons is zero, Fig. 2 a, middle).

If the two spins become magnetically non-equivalent (AA' or AX system, right), for example by addition of H_2 to a molecule (hydrogenation), the $M = 0$ composite states $2^{-½} \cdot (|\alpha,\beta> + |\beta,\alpha>)$ and $2^{-½,} \cdot (|\alpha,\beta> - |\beta,\alpha>)$ turn into the individual $|\alpha\beta>$ and $|\beta\alpha>$ states (Fig. 2 a, right). The total population (p) of the $M = 0$ states is preserved: $p(M = 0) = p(|\alpha,\beta>) + p(|\beta,\alpha>)$. In addition, an additional energy shift is introduced by couplings between the nuclear spins mediated by the binding electrons (J-couplings, Eq. 12). The NMR spectrum shows two J-coupled resonances (two doublets). The intensities are proportional to the population difference δ_p which is of the order of 10^{-6} at $B_0 = 1$ T and room temperature.

NMR with parahydrogen

The population $p(pH_2)$ of parahydrogen $2^{-½} \cdot (|\alpha\beta> - |\beta\alpha>)$ ($S = 0$, $M = 0$) can be increased to unity $f(pH_2) = 1 - f(oH_2) > 0.99$ by means of catalytic conversion at low temperatures (section 2.1, pp. 30) [7]. Since the conversion rate of pure pH_2 and oH_2 in the absence of a catalyst is of the order of months, pH_2 can be stored at room temperature for a very long time of the order of days (Fig. 2 b, left).

As long as the two spins of the dihydrogen molecule are magnetically equivalent (A_2 system) the pH_2 spin isomer does not contribute to the NMR signal (Fig. 2 a and b, middle). In contrast,

the overall NMR signal of pH_2-enriched gas is attenuated since the orthohydrogen fraction is reduced.
Therefore, to access the enriched population of pH_2, it is necessary to break the magnetic equivalence of the spins $A_2 \rightarrow AA'$ or AX, for example by addition of the pH_2 to another molecule. This breaks the $M = 0$ composite states $2^{-½} \cdot (|\alpha,\beta> + |\beta,\alpha>)$ and $2^{-½} \cdot (|\alpha,\beta> - |\beta,\alpha>)$ into the individual $|\alpha,\beta>$ and $|\beta,\alpha>$ states. The large non-equilibrium population (p) of the two $M = 0$ states $p(M = 0) = f(oH_2)/3 + f(pH_2)$ is conserved and distributed among $|\alpha,\beta>$ and $|\beta,\alpha>$. NMR signal intensities S proportional to the population differences (e.g. between $|\alpha,\beta>$ and $|\beta,\beta>$) can be detected, for example (Fig. 2 b, right):

$$S \sim p(|\alpha,\beta>) - p(|\alpha,\alpha>) = 0.5 \cdot (f(pH_2) - f(oH_2)/3)\ ) - f(oH_2)/3) - \delta \sim f(pH_2) - f(oH_2)/3,$$

Relative to the non-pH_2-enriched signal, a maximal NMR signal enhancement of the order of δ^{-1} can be achieved. This effect was called PASADENA: Parahydrogen And Synthesis Allow Dramatically Enhanced Nuclear Alignment [22, 23].

1.3.2 ^{1}H PASADENA

PASADENA is a selective NMR-signal enhancement technique by means of chemical addition of a parahydrogen molecule to another compound [23]. As discussed in the previous section, the maximal polarization achievable with PASADENA $P_{hyp}^{pH_2}$ depends on the fraction of parahydrogen ($f(pH_2)$) and the fraction of orthohydrogen ($f(oH_2)/3$) in the sample:

$$P_{hyp}^{pH_2} \sim f\left(pH_2\right) - \tfrac{1}{3} f\left(oH_2\right). \tag{32}$$

The theory of PASADENA was developed for a spin system consisting of two hydrogens ^1H_a and ^1H_b and an unspecified number of other spins in the surrounding [22]. The latter are introduced for the sole purpose to break the symmetry of the molecule and to generate a chemical-shift difference of ^1H_a and ^1H_b.

The system is described by the density matrix and states of parahydrogen (Eq. 30) and the isotropic liquid-state NMR Hamiltonian with strong homonuclear couplings (Eq. 16):

$$\hat{H}\left({}^1\mathrm{H_a}, {}^1\mathrm{H_b}\right) = -\hbar\omega_a \hat{I}_Z^a - \hbar\omega_b \hat{I}_Z^b + 2\pi\hbar J^{a,b} \hat{I}^a \cdot \hat{I}^b \tag{33}$$

Bowers and Weitekamp [22, 23] suggested to hydrogenate an unsaturated molecule with parahydrogen in a NMR spectrometer, followed by a sequence of free-evolution periods (t_a, t_b, t_c) and r.f. pulses at proton frequency to observe ^{1}H NMR signal enhancement:

(hydrogenation) – t_a – pulse(θ) – t_b – t_a – t_c – pulse(θ) – t_b.

Maximal ^{1}H polarization in the range of $P = 0.14$ and $P = 1$ was predicted.

1.3.3 X-nuclei PASADENA

The first PASADENA experiments demonstrated strong ^{1}H NMR signal enhancement after catalytic addition of parahydrogen to an unsaturated molecule and application of an appropriate r.f. pulse sequence [23, 33]. This effect was broadly used to study hydrogenation reactions [39, 40, 41, 42]. Unfortunately, the use for biomedical applications is limited since the lifetime of proton polarization is relatively short (order of seconds). Therefore, this thesis is focused on hyperpolarization of heteronuclei, here ^{13}C, by means of an r.f. spin-order-transfer (SOT) sequence proposed by Goldman *et al*. [1, 35]. A brief description of the underlying mechanisms is given in the following:

The spin system
The system for Goldman's SOT consists of three spins (3-spin-½): Parahydrogen (^1H_a, ^1H_b, with spin operators $\hat{I}^a$ and $\hat{I}^b$) and a third nucleus (which will be hyperpolarized, e.g. ^{13}C, with spin operator $\hat{S}$). The state after the hydrogenation is constructed as the tensor product of the parahydrogen state | 0,0> and the unpolarized ^{13}C |α/β>:

$$\left|m\left({}^1H_a\right),\, m\left({}^1H_a\right),\, m\left({}^{13}C\right)\right\rangle \;=\; \left|0,0\right\rangle \;\otimes\; \left|{}^{\alpha}\!/_{\beta}\right\rangle \tag{34}$$

The density operator
The density operator is constructed as the tensor product of the operators for pH_2 and unpolarized ^{13}C:

$$\hat{\rho}_0 = \hat{\rho}_{pH_2} \otimes \hat{\rho}_{^{13}C} \tag{35}$$

In the experiment, the parahydrogen is added to the molecule that carries the ^{13}C in a hydrogenation reaction. Since this process is not instantaneous but takes place during a reaction time (t_r) of the order of seconds, the spin systems of molecules which have been hydrogenated first evolve of course for a longer time than molecules which were hydrogenated at the end of t_r. This causes a loss of coherence between the states, but can be avoided by continuous irradiation on ^{1}H frequency during the reaction (^{1}H decoupling). As a consequence, the modelling of the PASADENA experiment can start with the density matrix $\hat{\rho}_0$ (Eqs. 30 and 35).

The Hamiltonian operator
In the case of Goldman's SOT sequence, B_0 is chosen small enough that chemical-shift differences between ^1H_a and ^1H_b can be neglected. The Hamiltonian for the ^1H_a - ^1H_b - ^{13}C system is composed of three Zeeman terms, one strong homonuclear J-coupling term (J^{HaHb}), and two weak heteronuclear J-coupling terms (J^{HaC}, J^{HbC}):

$$\begin{aligned}\hat{H}\left({}^{1}H_a, {}^{1}H_b, {}^{13}C\right) &= \\ &= -h\omega_a \hat{I}_z^a - h\omega_b \hat{I}_z^b + 2\pi J^{H_a,H_b} \hat{I}^a \cdot \hat{I}^b \\ &\quad - h\omega_c \hat{S}_z + 2\pi J^{H_aC} \hat{I}_z^a \cdot \hat{S}_z + 2\pi J^{H_bC} \hat{I}_z^b \cdot \hat{S}_z \ ,\end{aligned} \tag{36}$$

The Hamiltonian can be further simplified: By transformation to the doubly rotating frame (^{13}C and ^{1}H) the Zeeman terms vanish. Only the scalar-coupling terms remain in the *effective* Hamiltonian:

$$\hat{H}_{effective} = 2\pi J^{H_aH_b} \hat{I}^a \cdot \hat{I}^b \ + \ 2\pi J^{H_aC} \hat{I}_z^a \cdot \hat{S}_z \ + \ 2\pi J^{H_bC} \hat{I}_z^b \cdot \hat{S}_z \ . \tag{37}$$

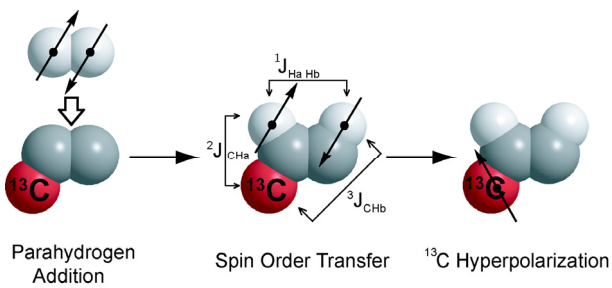

Fig. 3: PASADENA hyperpolarization of X nuclei by transfer of parahydrogen spin-order. Molecular parahydrogen ( ) is added to the precursor ( ) by catalytic hydrogenation (left), followed by perturbation of the coupled spin system by a spin-order-transfer r.f. pulse sequence (involving $^{2}J^{HaC}$, $^{2}J^{HbC}$, $^{3}J^{HaHb}$ couplings, middle) to form non-equilibrium spin polarization on ^{13}C (right). Figure taken from [2].

Goldman's pseudo-spin K

Goldman introduces the pseudo-spin $K = (K_X, K_Y, K_Z)^T$ to combine the two proton spins:

$$\begin{aligned} \hat{K}_X &= \hat{I}_x^a \cdot \hat{I}_x^b + \hat{I}_y^a \cdot \hat{I}_y^b \\ \hat{K}_Y &= \hat{I}_y^a \cdot \hat{I}_x^b - \hat{I}_x^a \cdot \hat{I}_y^b \\ \hat{K}_Z &= \tfrac{1}{2}\left(\hat{I}_z^a - \hat{I}_z^b\right) = -i\left[\hat{K}_X, \hat{K}_Y\right] \end{aligned} \tag{38}$$

The axes in this system are denoted by x_k, y_k, z_k.

Density matrix

In this notation, the density operator takes the following form:

$$\hat{\rho}^{(K)} = \tfrac{1}{8}\left(1 - 4\hat{K}_X - 4\hat{I}_z^a \cdot \hat{I}_z^b\right) \tag{39}$$

The last term of Eq. 39 is constant and can be neglected.

Hamiltonian

The Hamiltonian can reformulated using K_i and $\hat{S}_z$:

$$\hat{H}_{effective} = \hat{H}_A^{(K)}\left(\hat{I}, \hat{S}\right) + \hat{H}_B^{(K)}\left(\hat{I}\right), \tag{40}$$

where

$$\begin{aligned} \hat{H}_A^{(K)}\left(\hat{I}, \hat{S}\right) &= 2a \cdot \hat{S}_z \cdot \hat{K}_Z \\ \hat{H}_B^{(K)}\left(\hat{I}\right) &= b\left(\hat{K}_X + \hat{I}_z^a \cdot \hat{I}_z^b\right) \end{aligned} \tag{41}$$

and $a = ½(J^{HaC} - J^{HbC})$, $b = J^{ab}$.

The geometric picture

By comparison with the Zeeman Hamiltonian of a spin $\hat{I}$ in B_0,

$$\hat{H} = -\left(\gamma \hat{I}\right)\vec{B}_0 = -\omega \hat{I}_z, \tag{42}$$

we see that Eq. 40 has the form of a Zeeman Hamiltonian of spin K' in a fictitious magnetic field $\vec{B}_{zz} = B_{zz}\vec{e}_{zz}$ with a new quantization axis $e_{zz} = \hat{S}_z \cdot a \cdot K_Z + b \cdot K_X$:

$$\begin{aligned} \hat{H}_{effective} &= b \cdot \hat{K}_X + 2a \cdot \hat{S}_z \cdot \hat{K}_Z \\ &= \left(\Gamma \hat{K}'\right) \cdot \vec{B}_{zz}, \end{aligned} \tag{43}$$

where Γ resembles to γ in the Zeeman Hamiltonian $\hat{H} = -\left(\gamma \hat{I}\right)\vec{B}_z$.

The new quantization axis $e_{zz} = \hat{S}_z \cdot a \cdot K_Z + b \cdot K_X$ depends on $\hat{S}_z$ (= ±0.5) and the J-couplings of the molecule.

The e_{zz} vector has the following form:

$$\vec{e}_{zz}^{\pm} = \begin{pmatrix} \sin(\theta) \\ 0 \\ \pm\cos(\theta) \end{pmatrix} \tag{44}$$

We use e_{zz}^{+} for $\hat{S}_z = +0.5$ and e_{zz}^{-} for $\hat{S}_z = -0.5$. e_{zz}^{+} encloses an angle $\theta^{+} = \arctan(b/a)$ with the z_k axis, and e_{zz}^{-} encloses an angle $\theta^{-} = \arctan(-b/a) = \theta^{+} + 90°$. For clarification, a graphical representation is given in Fig. 4.

The Hamiltonians for positive and negative $\hat{S}_z$ are denoted by $H_{\hat{S}+}$ and $H_{\hat{S}-}$:

$$\begin{aligned} \hat{H}_{S+} &= \Omega \hat{K}_{zz}^{+} \\ \hat{H}_{S-} &= \Omega \hat{K}_{zz}^{-} \end{aligned} \tag{45}$$

Thus, the evolution of the PASADENA system can be described as the evolution of two systems evolving under these Hamiltonians. The corresponding density matrix is denoted by $\hat{\rho}^{+}$ and $\hat{\rho}^{-}$.

The quantity θ

The new quantization axis and the z_k-axis enclose and angle |θ|, which is a characteristic parameter for a molecule:

$$\tan(\theta) = \frac{b}{a} = 2\frac{J^{H_a H_b}}{\left(J^{H_a C} - J^{H_b C}\right)}. \tag{46}$$

Goldman's sequence yields $P > 0.5$ only for molecules with $\theta \in [24°, 70°]$. New approaches were developed by Norton and Weitekamp to allow PASADENA hyperpolarization of molecules outside of this range [38].

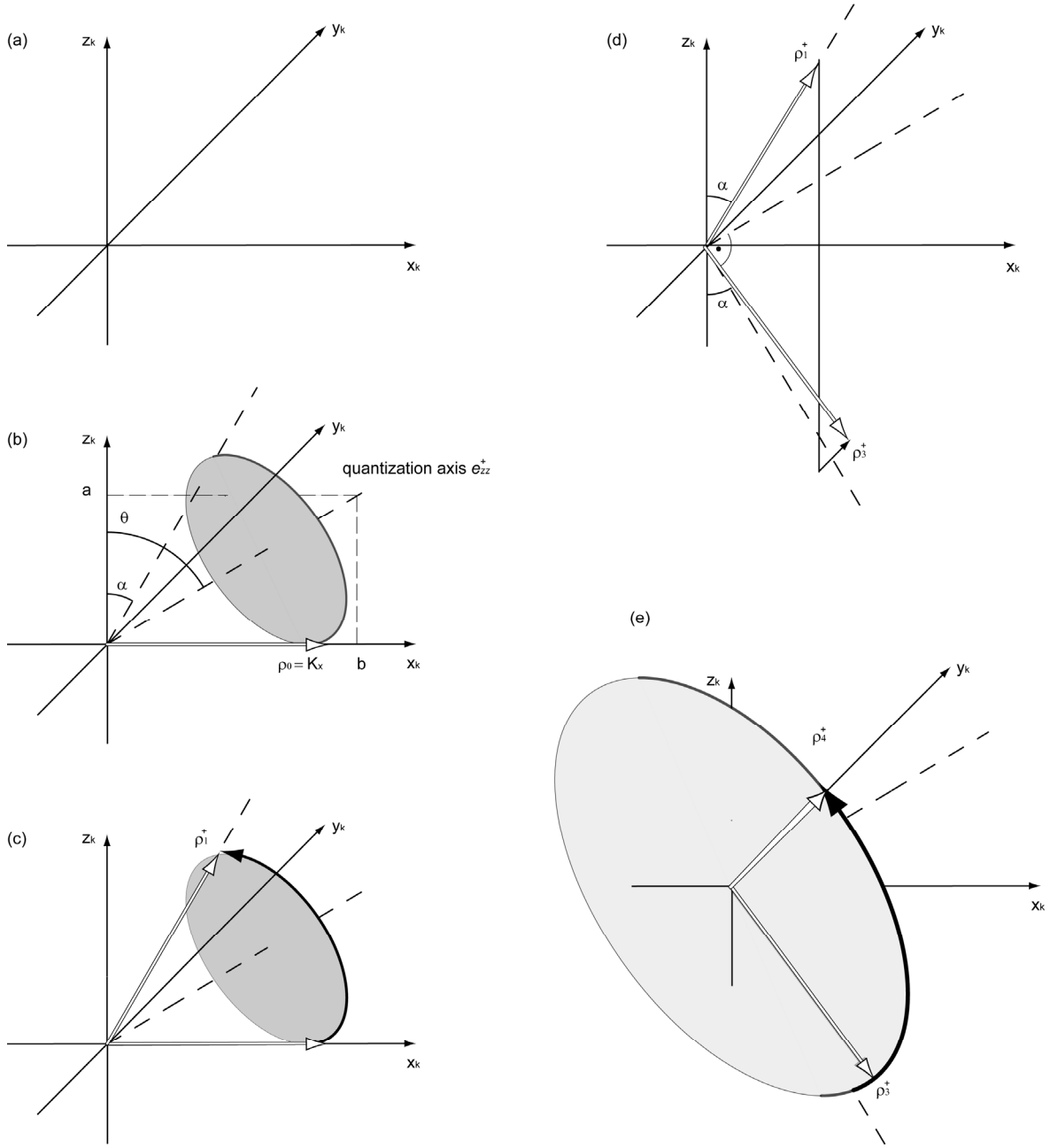

Fig. 4: Trajectory of the density matrix during steps 1 – 4 of Goldman's spin-order-transfer sequence [1].
In the pseudo-spin K notation, the density matrix ρ of the spin system can be expressed in a coordinate system x_k, y_k, z_k (a). After hydrogenation, $\rho_0 = K_x$ (b), and starts precessing around a fictitious magnetic field (along e_{zz}^{+}). After a time t_1, the projection of ρ is at an angle α to the z_k-axis (c), whereupon a $180_x°$ pulse is applied on ^{1}H, flipping the ρ vector into a precession plane perpendicular to the quantisation axis e_{zz} (d). After precession for t_2, ρ is parallel the y_k-axis (e). A $90_y°$ pulse around ^{13}C concludes the first part of the sequence, leaving the density matrix in a K_yS_y state, which is transformed by a $90_x°$ pulse on ^{13}C after an evolution for t_3 in the second part.

Goldman's SOT sequence

The SOT sequence described in [1, 35] consists of two parts:

(1) The initial density matrix ($\hat{\rho}_0 \sim K_x$) is manipulated in four steps ($\hat{\rho}_0$ – $\hat{\rho}_4$) to provide an optimal density matrix ($\hat{\rho}_4 = \hat{S}_x K_y$) for the second part. This requires two free-evolution intervals (t_1, t_2) and two pulses (p_1: $180_x°$ pulse on ^{1}H, p_2: $90_y°$ on ^{13}C) (total: four steps).

(2) From $\hat{\rho}_4 = \hat{S}_x K_y$, a $\sin(2\theta) \cdot \hat{S}_y \approx 1 \cdot \hat{S}_y$ component is formed in the density matrix $\hat{\rho}_5$ after a free-evolution interval (t_3). Subsequently, $\hat{S}_y$ is rotated by a pulse p_3 ($90_x°$ on ^{13}C) into a $\hat{S}_z$ term (density matrix $\hat{\rho}_6$). The size $|\sin(2\theta)|$ of the $\hat{S}_z$ term corresponds to the degree of the ^{13}C hyperpolarization (total: two steps).

The free-evolution intervals t_1, t_2, t_3 are functions of the J-couplings of the molecule. Therefore, a new SOT needs to be calculated for each molecule. A program to calculate the intervals for a given set of J-couplings and to predict the maximal hyperpolarization yield is presented in the next section.

A brief description of Goldman's SOT is given in the following, limited to molecules with $\theta < 60°$. For more details and solutions for molecules with $\theta > 60°$, see [1].

Part One. Goal: $K_y\hat{S}_x$ terms in the density matrix.

(1) Free evolution of $\hat{\rho}_0^+$ for t_1 : $\hat{\rho}_1^+ = U(t_1)\ \hat{\rho}_0^+\ U^\dagger(t_1)$

The starting point after the end of the hydrogenation reaction and ^{1}H decoupling pulses is $\hat{\rho}_0^+ \approx K_x$ (Fig. 4 b, Eq. 39). The time evolution of $\hat{\rho}_0^+$ is a precession around the axis e_{zz}. After a time t_1, the projection into the $x_k - z_k$ plane of $\hat{\rho}_0^+$ will have an angle of $\alpha = 90 - \theta$ to the z_k axis (Fig. 4 c):

$$\hat{\rho}_0^+ \approx \hat{K}_X \xrightarrow{t_1} \hat{\rho}_1^+ \approx \sin(\alpha)\hat{K}_X + \cos(\alpha)\hat{K}_Z + cK_Y\,, \tag{47}$$

where c is a constant describing the K_y component after t_1. The value of t_1 can be calculated from the following equations:

$$\frac{\hat{K}_X(t_1)}{\hat{K}_Z(t_1)} \overset{!}{=} \frac{a}{b} \tag{48}$$

$$t_1 = \frac{1}{\Omega} \cdot \left(\frac{\frac{a}{b}\sin(\theta)\cos(\theta) - \sin^2(\theta)}{\frac{a}{b}\sin(\theta)\cos(\theta) + \cos^2(\theta)} \right). \tag{49}$$

At the end of this step, the K_x and K_z components of $\hat{\rho}^+$ enclose an angle $\alpha = 90 - \theta$ with the z_k axis (Fig. 4 c). In this position, $\hat{\rho}_1^+$ can be flipped into precession plane *perpendicular* to the precession axis (e_{zz}^+) by a 180° pulse, which is done in the following step 2.

(2) Pulse p_1 ($180_x°$ on ^1H or ^{13}C) : $\hat{\rho}_2 = R_{180_x°} \cdot \hat{\rho}_1 \cdot R^{\dagger}_{180_x°}$

By a 180°$_x$ pulse on ^{1}H or ^{13}C, the K_z and K_y components of $\hat{\rho}_1$ change sign: $\hat{\rho}_2$ is now perpendicular to the quantization axis e_{zz}^+ (Fig. 4 d):

$$\hat{\rho}_1^+ \approx \sin(\alpha)\hat{K}_X + \cos(\alpha)\hat{K}_Z + c\hat{K}_Y \xrightarrow{pulse\ 90°_x\ on\ I} \hat{\rho}_2^+ \approx \sin(\alpha)\hat{K}_X - \cos(\alpha)\hat{K}_Z - c\hat{K}_Y . \quad (50)$$

$\hat{\rho}_2^+$ will now precess in a plane perpendicular to e_{zz}^+. From similar considerations follows that $\hat{\rho}_3^-$ is in a plane perpendicular to e_{zz}^-. At some time t_3, $\hat{\rho}$ will be parallel to the y_k - axis, which is the goal of the next step.

(3) Free evolution for t_2 until $\hat{\rho}$ is parallel to y_k: $\hat{\rho}_3^+ = U(t_2)\ \hat{\rho}_2^+\ U^{\dagger}(t_2)$

Since $\hat{\rho}^{\pm}$ is in a plane perpendicular to $e_{zz}^{\pm}$ and continues to precess around $e_{zz}^{\pm}$ in this plane, it will necessarily coincide with the y_k - axis after a certain time t_3:

$$\rho_2^+ \approx \sin(\alpha)\hat{K}_X - \cos(\alpha)\hat{K}_Z + c\hat{K}_Y \xrightarrow{t_2} \rho_3^+ \approx \hat{K}_Y \quad (51)$$

It is easily seen that under the same procedure

$$\rho_3^- \approx -\hat{K}_Y , \quad (52)$$

so that

$$\rho_3 \approx \hat{S}_z\hat{K}_Y . \quad (53)$$

(4) Pulse p_2 ($90_y°$ on ^{13}C) : $\hat{\rho}_4 = R_{90_y^\circ}\ \hat{\rho}_3\ R^{\dagger}_{90_y^\circ}$

The optimal configuration of $\hat{\rho}$ for the second part of the SOT sequence is achieved by a 90$_y$ ° pulse selective on ^{13}C, rotating the $\hat{S}_z$ component of $\hat{\rho}_3$ into $\hat{S}_x$:

$$\hat{\rho}_3 \approx \hat{S}_z\hat{K}_Y \xrightarrow{pulse\ 90_y°\ on\ ^{13}C} \hat{\rho}_4 \approx \hat{S}_x\hat{K}_Y . \quad (54)$$

Part Two. Build-up of $\hat{S}_z$ terms: Hyperpolarization.

(5) Free evolution for t_3: $\hat{\rho}_5 = U(t_3)\ \hat{\rho}_4\ U^{\dagger}(t_3)$

The goal of part one of Goldman's sequence is the preparation of the density matrix to $\hat{\rho}_4 = \hat{S}_x K_y$. This term evolves as follows:

$$\begin{aligned} 2\cdot\hat{S}_x\hat{K}_Y(t) &= \sin(\theta)\cos(\theta)\left(1-\cos(\Omega t)\right)\hat{S}_Y \\ &+\left(\cos^2(\theta)+\sin^2(\theta)\cos(\Omega t)\right)\left(2\hat{S}_X\hat{K}_Y\right)+\sin(\theta)\sin(\Omega t)\left(2\hat{S}_X\hat{K}_Z\right) \end{aligned} \tag{55}$$

After an evolution for t_3 with $\cos(\Omega\ t_3) = -1$, the density matrix consists of a large $\sin(2\theta)\ \cdot \hat{S}_y \approx 1 \cdot \hat{S}_y$ term:

$$\rho_4 \approx 2\hat{K}_Y\hat{S}_x \xrightarrow{t_3} \rho_5 \approx \sin(2\theta)\hat{S}_y + \cos(2\theta)\left(2\hat{K}_Y\hat{S}_x\right) \tag{56}$$

The analytical solution for the third free-evolution interval t_3 is:

$$\begin{aligned} &\cos(\Omega t_3) = -1 \\ &t_3 = \frac{\pi}{\Omega} \end{aligned} \quad , \tag{57}$$

where $\Omega = \sqrt{a^2+b^2}$, a = ½($J^{HaC} + J^{HbC}$), b = J^{HaHb}).

With $\sin(2\theta)\cdot\hat{S}_y \approx 1\cdot\hat{S}_y$, the spin-order transfer from pH_2 to ^{13}C is completed. In the last step, the $\hat{S}_y$ component is rotated x_k to form net polarization ($\hat{S}_z$).

(6) Pulse $90_x°$ on ^{13}C: $\hat{\rho}_6 = R_{90^o_x}\ \cdot\ \hat{\rho}_5\ \cdot\ R^{\dagger}_{90^o_x}$

The $\hat{S}_y \cdot \sin(2\theta)$ component of the density matrix $\hat{\rho}_5$ is turned into the net-polarization ($\hat{S}_z$) by a rotation of $90°_x$ on $\hat{S}$:

$$\hat{\rho}_5 = \sin(2\theta)\hat{S}_y + \cos(2\theta)\left(2\hat{K}_Y\hat{S}_x\right) \xrightarrow{pulse\ 90_x°\ on\ ^{13}C} \hat{\rho}_6 = \sin(2\theta)\hat{S}_z + \cos(2\theta)\left(2\hat{K}_Y\hat{S}_x\right) \tag{58}$$

In case $\sin(2\theta)$ is not close to unity, the last part can be repeated to build-up the polarization.

In order to compensate for dephasing due to B_0 inhomogeneities, two simultaneous $^1H - {}^{13}C$ 180° echo pulses are pasted into each free evolution period. The complete spin-order-transfer sequence is depicted in Fig. 5.

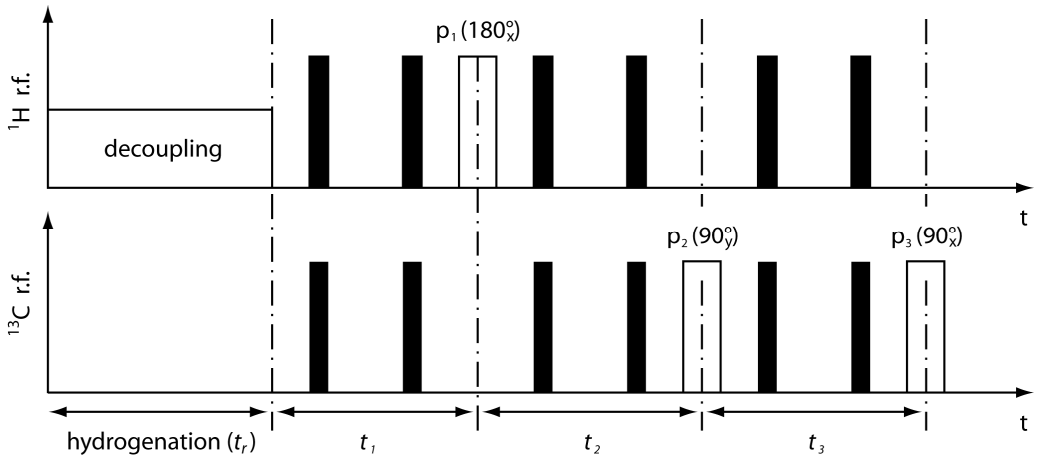

Fig. 5: Spin-order-transfer sequence for PASADENA hyperpolarization of heteronuclei after Goldman and Johannesson [1]. The r.f. sequence depicted above employs the pure spin-order of parahydrogen added to a molecule to form net nuclear polarization on a third, dedicated nucleus (e.g. ^{13}C): A combination of three free-evolution periods (t_1, t_2, t_3) and three pulses (p_1, p_2, p_3) is played out after the decoupling and hydrogenation reaction. The free-evolution intervals t_1, t_2, t_3 depend on the J-couplings of the molecule. To compensate for B_0 inhomogeneities, two 180° pulses are applied simultaneously on ^1H and ^{13}C during each free-evolution period.
White bars: pulses for spin-order transfer. Black bars: 180° pulses.

1.4 Simulation of PASADENA

The theoretical concepts presented in section 1.2 were employed to develop a program to calculate Goldman's SOT sequence and a simulation of the PASADENA experiment.

Calculation of the SOT sequence
A program was developed for the calculation of Goldman's SOT sequence for an arbitrary set of J-couplings. The program was verified by comparison with the data published by Goldman and Johannesson [1] for the molecule HEP. The simulated free-evolution periods correspond to Goldman's values to four significant digits (as published):

$t_1^{\mathrm{HEP}} = 28.28$ ms,
$t_2^{\mathrm{HEP}} = 36.20$ ms,
$t_3^{\mathrm{HEP}} = 50.34$ ms.

Parameters for HEP: $\theta = 49.66°$, ${}^3J^{H_aH_b} = 7.57$ Hz, ${}^3J^{H_aC} = 7.24$ Hz, ${}^2J^{H_bC} = -5.62$ Hz.

Simulation of the X nuclei PASADENA experiment
A simulation was written to predict the theoretical hyperpolarization yield achieved by a SOT sequence (determined by t_1, t_2, t_3) applied to a specific spin system (determined by ${}^3J^{{}^1\mathrm{H_a},{}^1\mathrm{H_b}}$, ${}^3J^{{}^1\mathrm{H_a},{}^{13}\mathrm{C}}$, ${}^2J^{{}^1\mathrm{H_b},{}^{13}\mathrm{C}}$). Again, the program was verified by comparison with the data published for the molecule HEP: The calculated maximal polarization of

$P = 0.987$

corresponds to the value published by Goldman.
By variation of parameters like J-couplings or flip angles in the simulation, their impact on the hyperpolarization yield can be evaluated (as shown in RESULTS, section 3.4, pp. 77).

Details of the simulations: The product operator formalism for a 3-spin-½ system was used (8D Hilbert space): The density matrix (Eq. 35) was evolved under the time-independent isotropic liquid-state Hamiltonian in the doubly-rotating frame (Eqs. 24, 37). Radio-frequency pulses were implemented as rotations (Eq. 25). Note that the simultaneous 180° pulses on ^{13}C and ^{1}H spins to compensate for B_0 inhomogeneities were not incorporated in the simulations. The programs were written in *python* with the extensions *SciPy*, *NumPy* and *PyLab* [43, 44, 45]. The source code for each program is provided in Appendix I (pp. 118).

Chapter 2: Materials and Methods

This Chapter describes the experimental prerequisites and procedures of the PASADENA experiment: generation of parahydrogen, preparation of chemistry (hydrogenation catalyst and precursor molecules), the construction of a PASADENA polarizer, the development of the experimental workflow, and NMR detection setups for *in vitro* and *in vivo* experiments. A list with all suppliers and parts employed is provided in Appendix II.

2.1 Parahydrogen

Ever since its discovery in the early 1920s [46, 47, 48], parahydrogen (pH_2) was of scientific interest, leading to efficient production methods as a side effect. In the experimental setup used here, commercially available "ultra-pure" (< 1 ppm impurities) hydrogen was catalytically converted to parahydrogen by passage over granular hydrous ferric oxide (IONEX-type O-P catalyst; Molecular Products Inc., Lafayette, CO, USA). After the gas was converted to parahydrogen, it was stored in 7 l aluminium alloy cylinders at room temperature and a pressure of p = 33 bar. Each batch was used within seven days, showing no measurable decrease in the hyperpolarization yield. The parahydrogen production unit is based on the catalyst-bed design as described by Tam and Fajardo [7]. A schematic view of the system used is given in Fig. 6.

The fraction of pH_2 enrichment ($f(pH_2)$) was quantified by ^{1}H NMR. Since parahydrogen does not yield a NMR signal, the pH_2 enrichment was determined measuring the fraction $f(oH_2)$ of residual orthohydrogen: $f(pH_2) = 1 - f(oH_2)$. The following procedure was applied: A glass vial containing air (background), a glass vial containing a reference sample of 75% ortho- and 25% parahydrogen, and a glass vial containing the produced parahydrogen (norm conditions) were prepared. Unlocalized ^{1}H NMR spectra were acquired from each sample, and the background subtracted from the pH_2 and H_2 signal (NEX = 256, TR = 20 ms, MR system No. 2, coil No. 3, section 2.6, p. 56). The ^{1}H NMR signal (S) of the pH_2-enriched gas was compared to the signal of the H_2 reference:

$$f\left(pH_2\right) = 1 - \frac{3}{4}\frac{S\left(pH_2\right)}{S\left(H_2\right)} \tag{59}$$

The parahydrogen enrichment produced was > 90 % (Fig. 7). A list of all parts of the parahydrogen production unit is provided in Tab. 16, pp. 131.

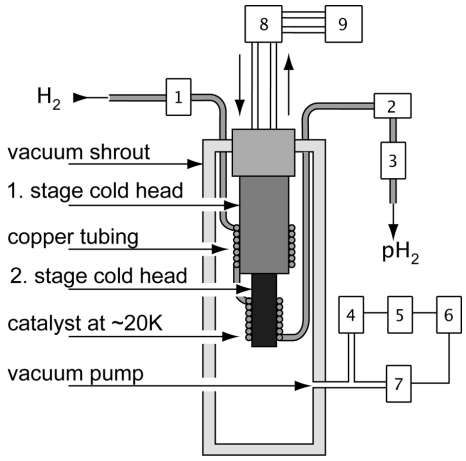

Fig. 6: The parahydrogen production unit.
Commercially available hydrogen gas (25 % parahydrogen, 75 % orthohydrogen, < 1 ppm impurities) is cooled down to T ~ 25 K and passed through a catalyst (granular ferric oxide) for conversion to parahydrogen. The two stages of the cold head are surrounded by copper tubing, filled with the catalyst. (1) Pressure regulator for incoming hydrogen; (2) flow meter; (3) flow controller; (4) pressure gauge; (5) pressure display; (6) relay; (7) vacuum pump; (8) helium compressor; (9) water cooler. A similar setup was published by Tam and Fajardo [7]. Figure taken from [2].

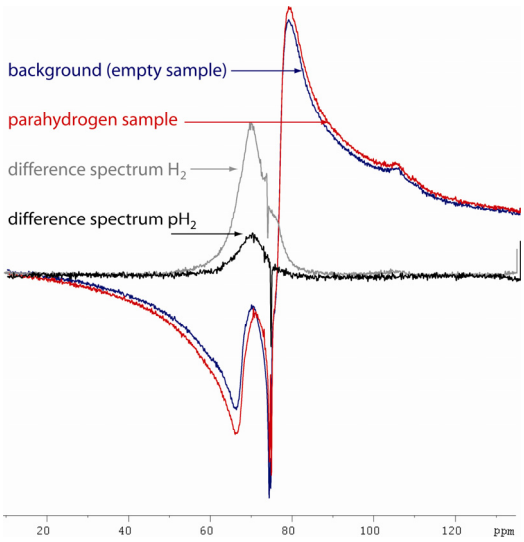

Fig. 7: ^{1}H NMR spectroscopy of gaseous pH_2 for quantification of parahydrogen fraction *f(pH$_2$)*.
^{1}H NMR spectra of air (blue, no phase correction), normal hydrogen (H_2, not shown), and parahydrogen (pH_2, red, no phase correction) in sealed glass vials (1 cm diameter, 10 cm length), were acquired at B_0 = 4.7 T. Subtraction of the background signal provided for the difference spectra of normal H_2 (grey) and pH_2 (black), both phase corrected. The ratio of the H_2 and pH_2 signal intensities allowed for quantification of the parahydrogen fraction (Eq. 59).
Experimental parameters: ^{1}H unlocalized pulse-and-collect sequence, NEX = 256, TR = 20 ms.

2.2 Hydrogenation catalyst

The first step of the PASADENA experiment is the cis-addition of pH_2 to the precursor molecule by homogeneous catalysis.
The catalyst solution [49, 50] was prepared prior to each experimental series (Fig. 8). The bisphosphine ligand, 1,4-bis-((phenyl-3-propane sulfonate) phosphine) butane disodium salt (Q36333, Isotec, OH, USA), was dissolved in H_2O or D_2O to yield 2.0 - 3.0 mmol/L concentration followed by alternating exposure to nitrogen (N_2) and evacuation, to remove oxygen dissolved in the solution. The rhodium (Rh) catalytic moiety was dissolved in ~ 1 ml acetone and added to the bisphosphine solution under N_2 atmosphere (bis(norbornadiene) rhodium (I) tetrafluoroborate, Strem Chemicals, MA, USA). A concentration 5 % smaller than the concentration of bisphosphine was used, to bind all Rh. The resulting solution was vigorously shaken, and acetone was removed by evacuation at room temperature. Typically, batches of 25 – 50 ml were prepared. The solution was kept under N_2 atmosphere until the PASADENA precursor was added and the hyperpolarization experiments were started.

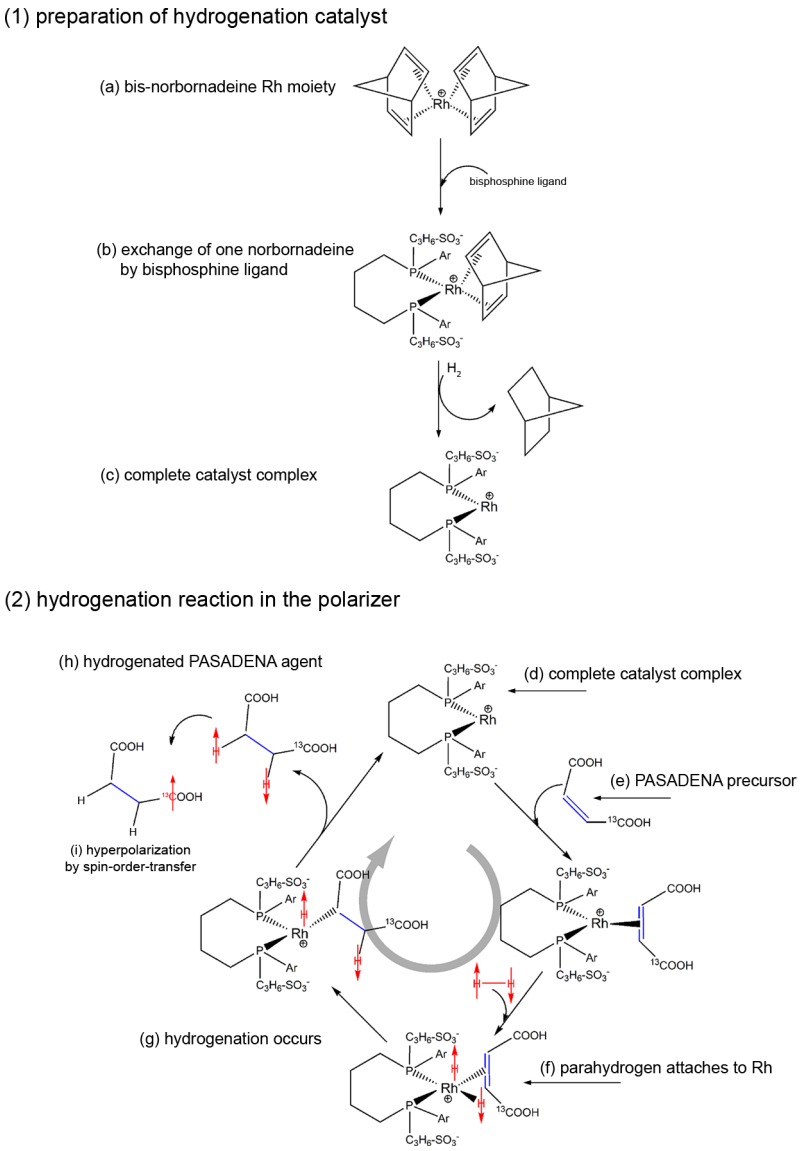

Fig. 8: Preparation of the hydrogenation catalyst (1) and chemical reactions during the PASADENA experiment (2). (1) preparation of the hydrogenation catalyst: bis-norbornadeine Rh moiety is solved in ~ 1 ml acetone and mixed with the bisphosphine ligand in deaerated H_2O / D_2O (25 – 50 ml). In the solution, the ligand and the Rh moiety combine (b, c) to form the complete catalyst complex (d). The solution is kept under protective N_2 atmosphere until it is employed for the PASADENA experiment.
(2) Chemistry of the PASADENA experiment. The unsaturated precursor molecule is added to the catalyst solution (e), and injected into a high-pressure atmosphere of parahydrogen (f). The parahydrogen is added to the precursor molecule by cis-addition to form the PASADENA target molecule (g). Subsequent r.f. spin-order-transfer sequence yields net polarization on the labeled nucleus. Figure modified from [2].

2.3 PASADENA agents

Three molecules were hyperpolarized in this work:

(1) 2-hydroxyethyl 1-^{13}C, 2,3,3-D_3 propionate (HEP),
(2) 2,3,3,3-tetrafluropropyl 1-^{13}C,2,3,3-D_3 propionate (TFPA) and
(3) 1-^{13}C,2,3-D_2 succinic acid (Sum).

The hydrogenation reaction for these molecules is depicted below (Fig. 9), followed by a detailed description of the chemical preparation process and properties of the molecules.
The hydrogenation reaction was deemed to be completed to > 99 % for all molecules, as indicated by ^{13}C NMR spectroscopy measurements (NEX = 1024) of the hydrogenated solution (after the PASADENA experiment): no resonances of the precursor molecules were detected. However, this method does not fully prove that the entire hydrogenation takes place before the spin-order transfer, since the hydrogenation may be carried to completion after the hyperpolarization (with H_2 molecules in solution).

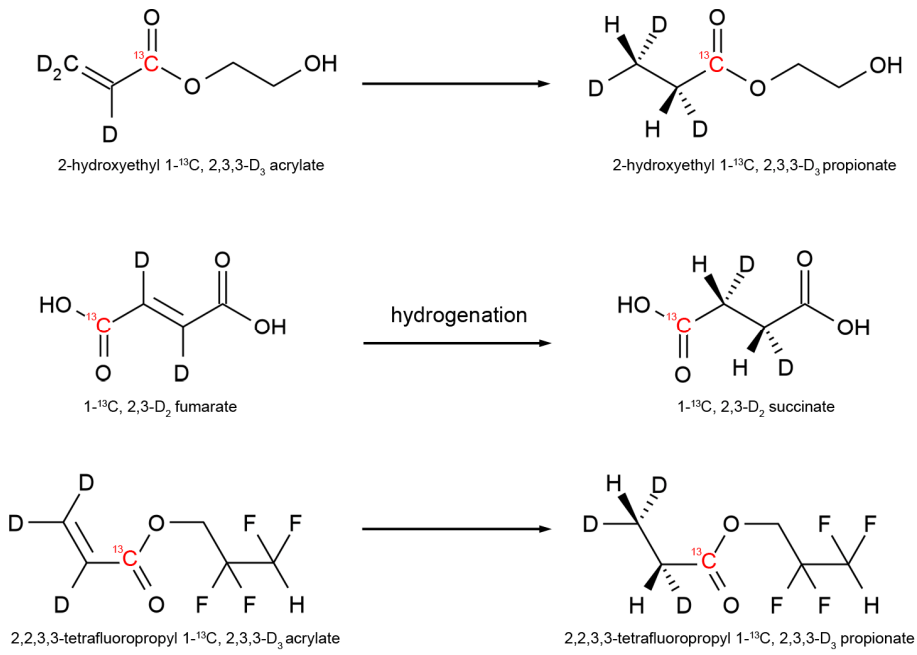

Fig. 9: Stick models of isotopically labeled PASADENA agents and their precursors.
The hydrogenation reaction of HEA to HEP (top), Fum to Suc (middle) and TFPA to TFPP (bottom) are depicted.

2.3.1 2-hydroxyethyl 1-^{13}C, 2,3,3-D3 propionate (HEP).

HEP is the only ^{13}C PASDENA compounds that could be polarized to $P > 0.1$ in aqueous solution previously [37]. The precursor molecule for HEP is 2-hydroxyethyl 1-^{13}C, 2,3,3-D_3 acrylate (HEA, liquid) which was added to the catalyst solution without further preparations (Cambridge Isotope Laboratories (CIL), Andover, MA, USA) [36]. A SOT sequence for HEP was published by Goldman and Johannesson in 2006 [1].

2.3.2 2,3,3,3-tetrafluropropyl 1-^{13}C, 2,3,3-D_3 propionate (TFPP)

In molecular imaging, functional molecules are designed that attach to a specific target. Typically, these molecules are constructed from a receptor-specific moiety (e.g., lipophilic) and a detection moiety (e.g., fluorescence for optical detection, or ^{19}F for NMR).
TFPP is a receptor-specific agent suitable for PASADENA, which was constructed from a PASADENA-, a solubility-, and a lipophilic moiety (P. Bhattacharya, personal communication). It is the first molecule that combines receptor-specificity with the potential of significant signal enhancement owing to PASADENA [51]: the chemical shift of the ^{13}C is a sensitive marker for the binding of the functional moiety to lipid bilayers [52]. Since the PASADENA moiety propionate is the same as in HEP, the SOT sequence as published by Goldman and Johannesson was employed [1].

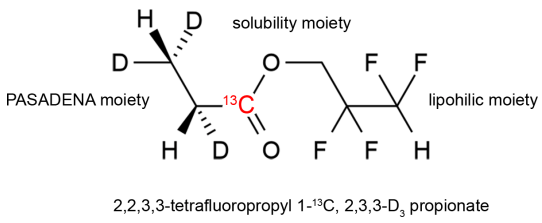

Fig. 10: Chemical structure of 2,2,3,3-tetrafluorropropyl 1-^{13}C, 2,3,3-D_3 propionate (TFPP). TFPP is the first molecule combines target-specificity (here from a lipophilic moiety) with the strong signal enhancement provided by PASADENA. It was constructed such that it comprises a PASADENA moiety, a solubility moiety, and a functional (lipophilic) moiety.

2.3.3 1-^{13}C,2,3-D$_2$ succinate (Suc)

Hyperpolarized biomolecules, e.g. *metabolic tracers*, have demonstrated the feasibility to detect biochemical processes *in vivo* on the time scale of s. 1-^{13}C,2,3-D$_2$ succinate (Fig. 9) is the first biologically relevant molecule which can be hyperpolarized by PASADENA [26] (IUPAC name: butanedioic acid, ethane-1,2-dicarboxylic acid, historically known as *spirit of amber*). The small, symmetric dicarboxylic-acid consists of four carbon, four oxygen, and six hydrogen atoms, of which the two protons at the carboxyl group exchange rapidly in solution ($C_4H_6O_4$, molecular weight (118.09 ± 0.01) u, density (1.56 ± 0.01) g/cm^3). Suc is a compound in the tricarboxylic acid cycle (TCA, Fig. 13).
In earlier studies of this laboratory, acetylene dicarboxylic (ADC) acid was used as a precursor which forms succinate after double hydrogenation. The applicability *in vivo*, however, was limited: A toxic intermediate maleate (Mal) is formed after incomplete hydrogenation, and an inherently short $T_1 \sim 6$ s drastically reduced the time available for signal acquisition (and for the molecule to penetrate the metabolism).
These problems were solved using 1-^{13}C,2,3-D$_2$ fumaric acid as a precursor molecule, which directly forms Suc upon single hydrogenation.

Preparation of precursor solution

The precursor 1-^{13}C,2,3-D$_2$ fumaric acid (Fum, IUPAC: but-2-enedioic acid) was purchased in solid form (custom synthesis by CIL). For mixing with the catalyst solution, the molecule was first dissolved in a small amount of H_2O or D_2O. For reasons described in RESULTS, a buffer was added to the mixture to yield pH 2.9: per 25 ml of catalyst and precursor mix, a phosphate buffer of 1 ml H_3PO_4 and 4 ml H_2PO_4 (both 0.2 mM, in H_2O), or 2.0 ml H_3PO_4, and 0.5 ml H_2PO_4 (both 0.4 mM, in D_2O) was used (Fig. 9). For the PASADENA experiment, the catalyst-precursor solution was drawn into a syringe and connected to the injection port of the PASADENA polarizer.

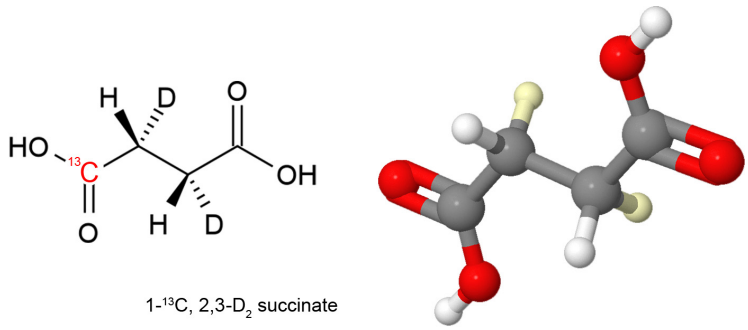

Fig. 11:Chemical structure of 1-^{13}C, 2,3-D$_2$ succinate (Suc), as produced in the PASADENA experiment by hydrogenation of 1-^{13}C, 2,3-D$_2$ fumarate (Fum). ●: oxygen, ●: carbon, ●: hydrogen, ●: deuterium.

Succinate in the TCA cycle

^{13}C NMR allows to investigate the pathways of individual nuclei in metabolic cycles. In previous work with rat hepatocytes, the fate of the ^{13}C succinate labels in the TCA cycle was reported [5]. The use of the 2,3-C label of Suc for biomedical application is limited since the directly attached protons strongly reduce the lifetime of the hyperpolarization (T_1). In contrast, a long T_1 of the order of 50 s was measured for 1,4-C Suc, as demonstrated in RESULTS (section 3.5, pp. 80). The metabolic pathways of the 1,4 labels are shown in Fig. 12.

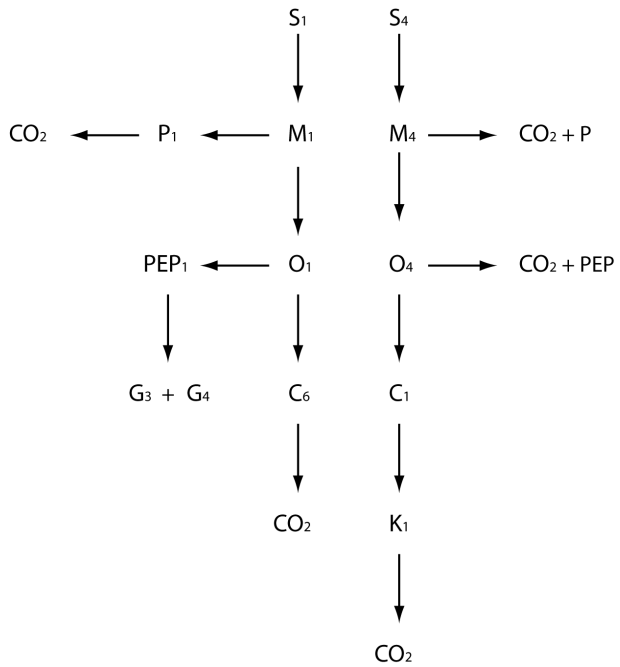

Fig. 12: Fate of the 1,4-^{13}C label (S_1, S_4) of Suc in the TCA cycle.
Schematic view of the metabolic pathway of 1,4-^{13}C Suc in the TCA cycle, derived from rat hepatocytes in [5]. *Abbreviations:* C: citrate, CO_2: carbon dioxide, G: glucose, M: malate, K: 2-ketoglutamate, O: oxaloacetate, P: pyruvate, PEP: phospho-enol-pyruvate. The numbers in subscript indicate the position of the label in the molecule.

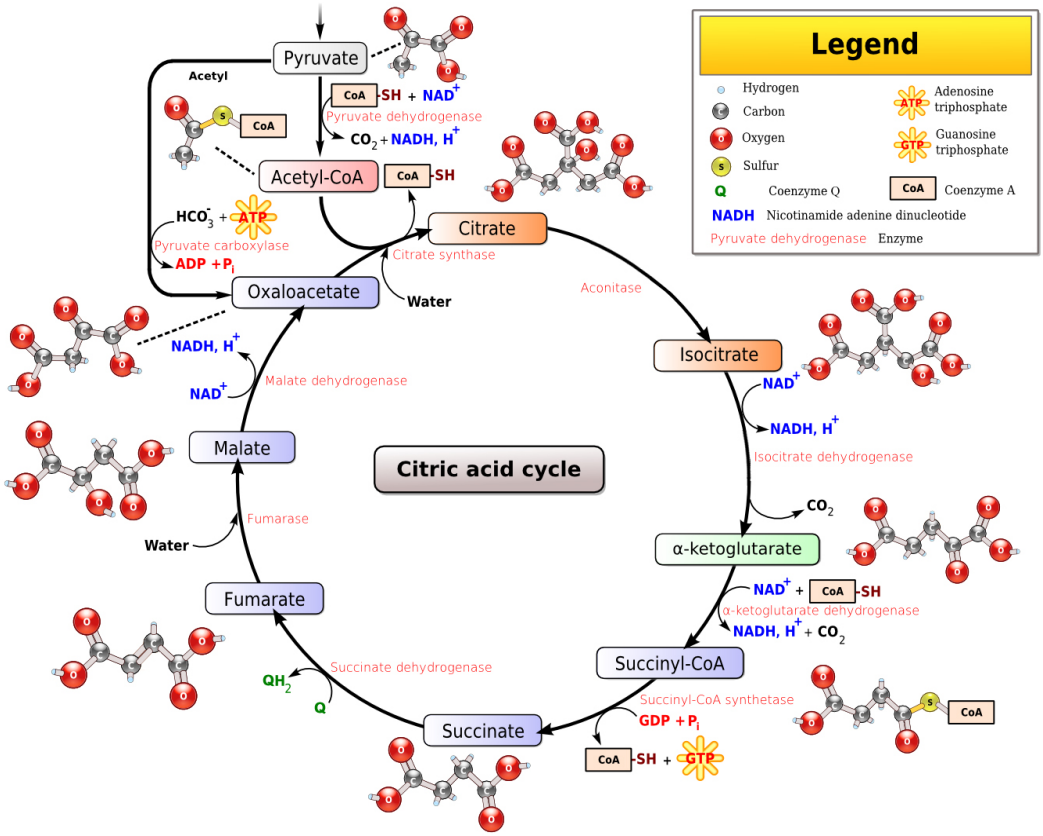

Fig. 13: The tricarboxylic-acid (TCA) cycle (also Krebs cycle or citric-acid cycle), is a closed chain of enzyme-catalysed chemical reactions. It plays a central role in the metabolism of cells. In eukaryotic cells, it takes place in the mitochondrion. Succinate participates in this cycle: it is formed by enzymatic reaction of succinyl – coenzme-A (CoA, catalysed by succinyl-CoA synthethase) and is further metabolized to fumarate (catalysed by succinate dehydrogenase). Figure taken from [53].

Succinate as a marker for brain tumors

In previous experiments of this laboratory in 2006 [4], the uptake and differential metabolism of 1,4-^{13}C Suc in a 9L brain tumor of a rat was investigated: One hour after infusion of ~3 ml of 1,4-^{13}C Suc and maleate (Mal) solution in the jugular vein of a rat, the animal was sacrificed and samples of the tumor and healthy brain were harvested. *Ex-vivo* magic-angle-spinning (MAS) solid-state ^{13}C-NMR spectroscopy was performed with both samples: Resonances of ^{13}C labeled compounds were detected only in a sample taken from the tumor; no ^{13}C resonances was observed in the control sample of healthy brain tissue (1-2 kHz spinning, T = 4 °C, ^{1}H decoupling, spin-echo sequence, NEX = 1024, TR = 5 s). The following conclusions are taken from [4]:

The resonances of Suc and Mal in the NMR spectrum of the tumor tissue indicates the accumulation of these compounds in the tumor, when they are not detectable in normal brain tissue. Since Mal is not a metabolic substrate for glial or neuronal metabolism, the accumulation in tumor tissue is likely to be attributed to a compromised blood-brain barrier. The increased concentration of Suc in the brain tumor may be due to both increased metabolic demand and the compromised blood-brain barrier. Glutamate (Glu) and glutamine (Gln), metabolic products of Suc, may act as specific tumor biomarkers. Abnormalities in tumor TCA-cycle enzymes succinic dehydrogenase and fumarate hydratase were recently linked to known oncogenes [54, 55, 56].

Note the SNR < 20, acquired in 85 min. at B_0 = 11.7 T. Through the > 10.000 fold ^{13}C NMR signal enhancement of hyperpolarization, *in-vivo* ^{13}C detection of the metabolic products of Suc for *in-vivo* detection of brain tumors on much shorter timescales may become feasible.

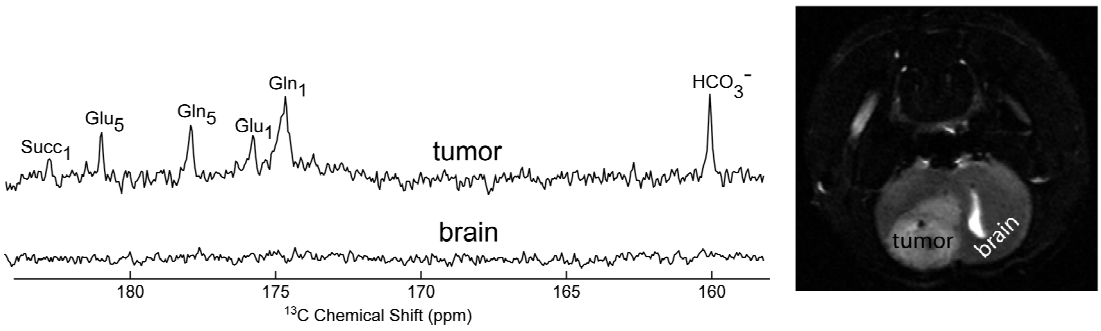

Fig. 14: *Ex vivo* ^{13}C solid-state MAS NMR spectroscopy of tumor and normal brain tissue (left). The regions are indicated in a ^{1}H MR image (right). The resonances of Glutamate (Glu), Glutamine (Gln), and hydrogen carbonate (HCO_3^-) were detected in a 80 mg sample taken from a tumor after infusion of 1,4-^{13}C Suc and Mal in the animal. No ^{13}C resonances were observed in a control sample of healthy brain tissue, as described in the text. Experimental parameters of the MAS measurement: 1-2 kHz spinning, T = 4 °C, ^{1}H decoupling, spin-echo sequence, NEX = 1024, TR = 5 s, B_0 = 11 T. Figure taken from [4].

2.4 The PASADENA polarizer

In this section, the development of a PASADENA polarizer for hyperpolarization of biomolecules in aqueous solution is described. It was designed with the goal to provide for reproducible hyperpolarization of the order of $P \sim 0.1$, within min and in volumes suitable for small-animal research *in vivo* (1 – 5 ml) [3].

The apparatus comprises three major components:

1. fluid-control unit,
2. low-field NMR unit,
3. process-control unit.

Each unit is described in the following sections (2.4.1 – 2.4.3). Since exact adjustments of the low-field NMR unit had proven crucial for optimal hyperpolarization yield, a detailed description of a calibration procedure is provided in section 2.4.4. A complete list of all components and manufactures is given in Appendix II.

While ^{1}H NMR signal enhancement (η) of the order of $\eta = 100$ was already observed in the first PASADENA experiments, it was not until 2001 that $P \sim 0.1$ ($\eta \sim 70{,}000$ at $B_0 = 1.5$ T) was demonstrated on ^{13}C [17]. In these experiments, a dedicated apparatus for hydrogenation and spin-order transfer was used for the first time. One of these prototypes was initially available in the laboratory, and facilitated the development of the next generation of PASADENA polarizers.

2.4.1 Fluid-control unit

The flow of the fluids is controlled by electromagnetic solenoid valves (indicated by V, and 1 in Fig. 15), connected by chemical resistant polytetrafluoroethylene (PTFE) tubing. A new injection cap (see below) and PTFE sleeves added to the valves prevented liquids from contact with metal, allowing the hyperpolarization of liquids in a wide range of pH. The reaction chamber surrounded by the low-field NMR unit was located in a heated compartment (T = 62 °C). A detailed list of the equipment used is given in [3] and in the Appendix II Tab. 12 (pp. 129).
Before the hyperpolarization process, the catalyst-precursor mixture was warmed-up in a PTFE tubing of 5 ml volume in the heated compartment (T = 62 °C). After two min., an automated sequence was started:

(1) the reactor is filled with pH_2 (p = 10 bar, V 1)
(2) injection of catalyst-precursor solution by N_2 (p = 15 bar, V 3, 4)
(3) application of r.f. spin-order-transfer sequence
(4) ejection of hyperpolarized solution (V 5).

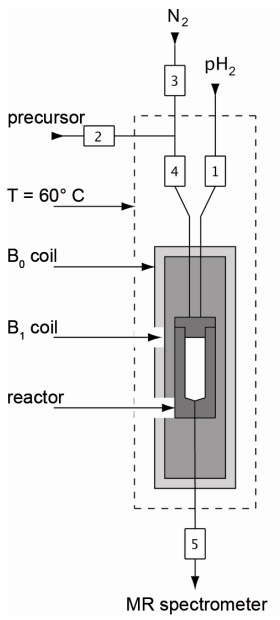

Fig. 15: Scheme of the PASADENA polarizer.
Before the hyperpolarization process, the precursor-catalyst solution is warmed-up for two min to T = 62 °C. Then, an automated sequence is started: (1) the reactor is filled with pH_2 (p = 10 bar), (2) the precursor-catalyst mixture is injected into the reactor by N_2 (p = 15 bar) while ^1H r.f. decoupling pulses (B_1) are applied, followed (3) by the r.f. spin-order-transfer sequence after a reaction time of $t_r = 4$ s. Thereafter, the hyperpolarized agent is expelled through the end cap and delivered to the MR system for *in vitro* or *in vivo* detection. 1 to 5 indicate valves. Figure taken from [3].

Hydrogenation chamber

A completely new construction of the chambers for the hydrogenation reaction (reactor) was accomplished. The reactors were produced by the Physics and Chemistry machine shop of the California Institute of Technology. Polysulfon 1000 (PSE, tensile strength: 800 bar, maximum service temperature: T = 150° C) was chosen to withstand pressure and temperature in excess of p = 15 bar and T = 70° C (Fig. 16).
The reactors consist of three sections, which are screwed into each other and sealed by rubber O-rings. While the prototype reactor (R_1) used a fuel-injector nozzle (stainless steel) for the injection of the catalyst-precursor mixture into the parahydrogen atmosphere, the present design uses a injection cap with a thin bore (0.5 mm diameter) to inject the mixture into the reactor. This cap is disc-shaped with two inlets: one for parahydrogen and one for nitrogen and catalyst-precursor solution (narrowing to 0.5 mm). An outlet at the funnel-shaped end cap allows for the ejection of the hyperpolarized agent. This allowed complete rinsing between each use of the polarizer. The size of the reactors (indicated by R_i , Tab. 2) was reduced from $V(R_1) = (572 \pm 3)$ cm^3 (prototype) to $V(R_2) = (316 \pm 2)$ cm^3 and $V(R_3) = (71 \pm 1)$ cm^3. This permitted hyperpolarization of solution volumes suitable for small-animal studies (1 - 5 ml), and to improve the homogeneity of the B_0 field in the reactor by a factor of 10 (as determined by a B_0 field map, section 2.4.2, pp. 43).

Tab. 2: Chambers for hydrogenation reaction.

No.	inner volume (cm^3)	injection port	material	outer diameter, length (cm)
1	572	fuel injector (stainless steel)	polysulfone	7.6, 27.1
2	316	0.5 mm hole in flat top	polysulfone	7.6, 16.3
3	71	0.5 mm hole in conical top	polysulfone	5.5, 13.0

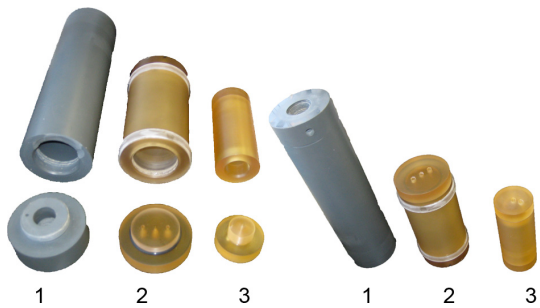

Fig. 16: Reaction chambers for hydrogenation reaction of the PASADENA experiment.
The hydrogenation reaction and subsequent spin-order transfer takes place in the reactor at a temperature of T = 62 °C and a pressure of p = 14 bar. It is placed within the low-field NMR unit (Fig. 17). Reactors No. 2 and No. 3 were newly designed: A non-metallic injection port improved the B_0 homogeneity, provided high chemical resistance and avoided interactions with metal surface and clogging. Reduction in size permitted for hyperpolarization of 1 - 5 ml agent (needed for small-animal studies) and further improved B_0 and B_1 homogeneity over the reaction volume. Technical drawings are provided in Appendix II.

2.4.2 Low-field NMR unit

The purpose of the low-field NMR unit (B_0 ~ 1.7 mT) of the polarizer is the application of ^{1}H decoupling pulses during the hydrogenation period, subsequently followed by the spin-order-transfer (SOT) sequence. Therefore, the coils for the static (B_0) and r.f. (B_1) field enclose the reaction chamber (Fig. 17). Two sets of B_0 and B_1 coils were constructed. Engineering drawings suitable for the construction of the coils, and a list of the equipment used is provided in Appendix II (Tab. 13 and Fig. 52).

Radio frequency transmission (B_1)
The saddle-shaped B_1 coil consists of two loops, each with 6 turns of gauge-22 magnet wire (10 cm x 20 cm), centred on an acrylic tube (outer diameter [O.D.] 11 cm, length 35 cm) connected to the transmitter by a BNC connector on top (based on a design from Promech lab AB, Malmø , Sweden). Two acrylic discs on the inside of the tube hold the reactor at the isocenter of the B_0 coil. The r.f. signal for the ^{1}H-decoupling pulses and SOT sequence was synthesized by a digital-to-analog converter (see section 2.4.3, pp. 46), passed a 150 kHz low-pass filter and was amplified by a broad-band audio amplifier (frequency range 10 Hz – 100 kHz) before it was transmitted to the coil. Since the coil was not tuned, excitation over a broad frequency range was possible.

Static field (B_0)
The B_0 field is generated by a solenoid coil that surrounds the r.f. coil (B_1) and the reactor. It is driven by a precision DC power supply (stability: 20 µV rms, 0.02 % + 1.5 mA ripple and noise). The strength and stability is monitored by a Gauss meter (Hall sensor), located between the B_1 coil and the reaction chamber, near the bottom of the reactor. To improve the axial homogeneity of the coil, the solenoid is divided into three separate circuits (1:2:1 in length) with variable power resistors in parallel, to allow for independent adjustment of the current flow through each section (based on a design by Promech lab AB, Malmø , Sweden). A B_0 field map was acquired to quantify the homogeneity of the static field (Fig. 18). Due to inaccuracies of the positioning of the device, an error of $\Delta x = 2$ mm is assumed. The axial component of the field was found to differ within the volume of the reactor No. 3 by $\Delta B_0 = (0.022 \pm 0.001)$ mT (axial) and $\Delta B_0 = (0.011 \pm 0.001)$ mT (planar), at a field strength of $B_0 \approx 1.8$ mT in the center of the volume (Fig. 20). To avoid a thermal drift of the B_0 field, a minimum of 4 hrs was allowed for the polarizer to reach operational temperature (T = (62 ± 1)° C).

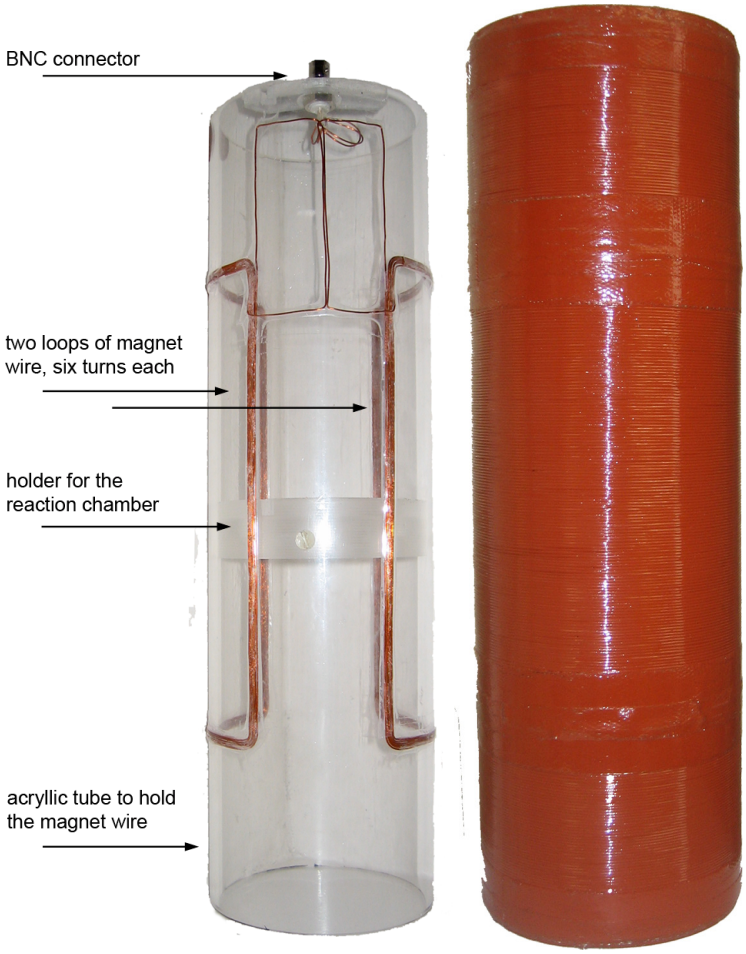

Fig. 17: NMR unit of the PASADENA polarizer.
B_1 coil (left) and B_0 coil (right). Two mountings in the B_1 coil (untuned, saddle-shaped) hold the reaction chamber (Fig. 16) in the isocenter of the assembly. A BNC connector at the top of the B_1 coil connects the cable delivering r.f. The field strength of the surrounding B_0 coil is monitored with a Hall sensor, which is located between B_1 and reactor close to the isocenter. Figure taken from [3].

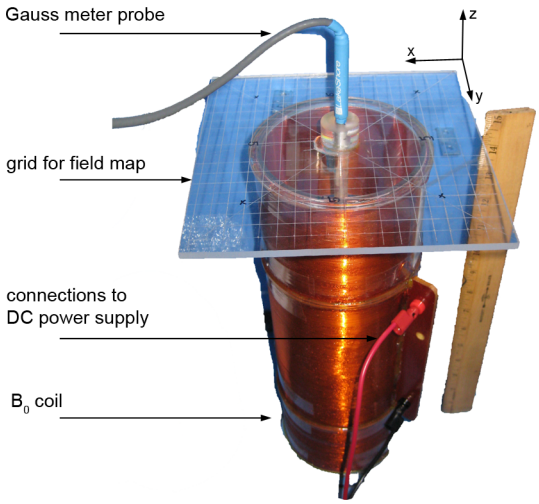

Fig. 18: Setup to map the B_0 field.
A device for the vertical and horizontal alignment of the Gauss meter sensor was constructed to map the B_0 field of the coil. The resulting field map is given in Fig. 20.

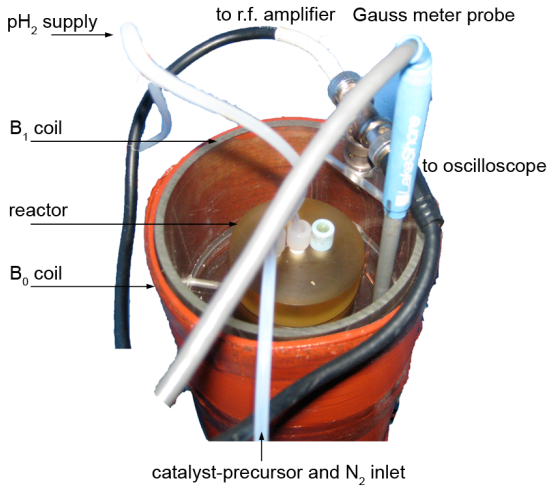

Fig. 19: Assembled low-field NMR unit and reactor. The figure depicts the B_0 and B_1 coil and reaction chamber. Note the coaxial cables connected to the BNC port of the B_1 coil (delivery and monitoring of r.f.), the Gauss meter probe, and the supply lines on top of the reactor (for pH_2 and reagent, see Fig. 15).

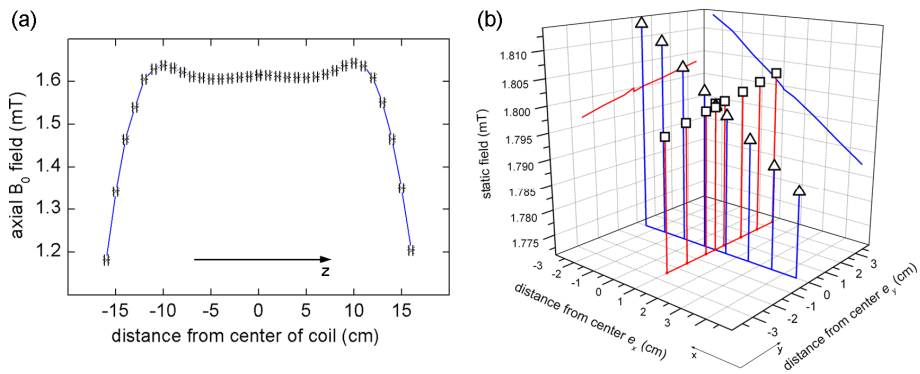

Fig. 20: Axial (a) and planar (b) field map of the B_0 coil.
The z-component of the B_0 field (solenoid coil, Fig. 17) was measured along the z-axis (a) and in the x-y plane at z = 0 (b) with the field-mapping device shown in Fig 18. Within the volume of the reactor No. 3, the field varied by $\Delta B_0 = (0.022 \pm 0.001)$ mT (axial), and $\Delta B_0 = (0.011 \pm 0.001)$ mT (planar): a 10 – fold improvement compared to the prototype polarizer. For definition of the axes, see Fig. 18. The data points in (a) were connected by splines.

2.4.3 Process Control Unit

The PASADENA experiment requires for a precise interplay of opening and closing of valves (e.g. for injection of fluids) and transmission of the r.f. decoupling pulses and SOT sequence. This process is automated and controlled by a central computer. A custom program (Norton, V.A.) based on the LabView platform (National Instruments, USA) controls through hardware-interface cards the valves and transmission of the r.f. pulses to the amplifier. This setup allowed to arrange the individual steps to an accuracy $\Delta t < 1$ ms. The entire sequence of events was saved to a file. A list of the equipment used is provided in Tab. 14 in Appendix II.

Transmitter
The SOT pulse sequence [1, 38] was read from an ASCII-file and synthesized by a digital-to-analog card (DAC) mounted in the polarizer cabinet. The pulses were digitalized at an update frequency of 298.15 kHz, corresponding to four sample points per period at the ^{1}H frequency (74.62 kHz), and >16 samples per period at the ^{13}C frequency (18.76 kHz).

Valves
The digital input/output channels of the DAC card were connected to power relays (12 V, 24 V) to control the electromagnetic solenoid valves of the fluid system (Fig. 21).

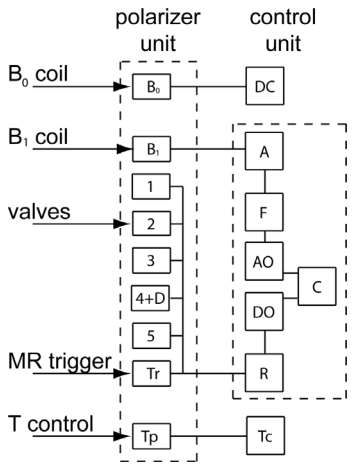

Fig. 21: Scheme of the process control unit of the PASADENA polarizer.
The PASADENA experiment is controlled by a central computer (C): valves for gases and liquids (1-5), r.f. sequence for spin-order-transfer (B_1) and acquisition trigger (Tr). The static field (B_0) and the temperature of the reaction compartment (Tp) are set by separate controllers (DC, Tc).
Abbreviations: A: r.f. amplifier, AO: analog out, D: time-delay relay, DO: digital out, F: 150 kHz low-pass filter, R: relays. Figure taken from [3].

Fig. 22: Picture of the PASADENA polarizer.
The low-field NMR and fluid-control unit of the PASADENA experiment are housed in a heated box (aluminium, T = (62 ± 1) °C), standing on a rack (yellow) holding the central computer and digital-to-analog (DAC) converter. On top are a low-pass filter, r.f. amplifier, Gauss meter and power supply for the B_0 magnet. Next to the setup are parahydrogen (left), nitrogen (right) gas tanks, and an oscilloscope to monitor the r.f. pulses. Figure modified from [3].

2.4.4 Calibration of the low-field NMR system

An initial calibration of the ^{1}H and ^{13}C channels of the low-field NMR system of the polarizer is mandatory to apply accurate decoupling pulses and r.f. spin-order-transfer sequence on the spins of the PASADENA agent in the reactor.
Since the r.f. electronics and B_0 coil were designed for transmission only, an external high-field NMR system was employed for the detection of ^{1}H and ^{13}C NMR signal. The first calibration (shown below) was performed on a 300 MHz NMR spectrometer (No. 3, Tab. 5). For later calibrations, a 4.7 T MR system was used (No. 2).

Center carrier frequency
The resonance condition $\omega_{r.f.} = \omega_{spins}$ was determined by successive ^{13}C NMR experiments at different B_0 strengths and constant carrier frequency (B_0 field sweep). A concentrated 1-^{13}C sodium acetate sample ($CH_3{}^{13}COONa$ dissolved in D_2O) was used in the following procedure:

(1) pre-polarize sample at $B_0 = 7$ T for 3 min.
(2) transport of sample to polarizer (duration: $t_{trans} = (14 \pm 1)$ s)
(3) 180° ^{13}C r.f. excitation pulse in low-field-NMR unit at $B_0 \approx 1.8$ mT
(4) transport of sample back to 7 T NMR spectrometer (duration: $t_{trans} = (14 \pm 1)$ s)
(5) acquisition of ^{13}C signal (pulse-and-collect sequence at $B_0 = 7$ T)

B_0 was incremented by $\Delta B_0 = 0.1$ mT and the experiment repeated eight times (Fig 2). The optimal field was $B_0 = (1.763 \pm 0.001)$ mT, measured close to the isocenter of the coil (position of the Hall sensor of the Gauss meter).

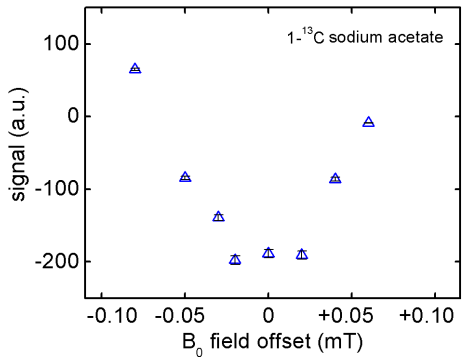

Fig. 23: ^{13}C experiments to adjust the frequency of the low-field NMR unit of the polarizer.
A ^{13}C excitation pulse was applied to a sample (prepolarized at $B_0 = 7$ T) of saturated 1-^{13}C sodium acetate in D_2O in the polarizer, followed by $t_{trans} = (14 \pm 1)$ s transfer to a 7 T NMR spectrometer and detection of ^{13}C NMR signal. This procedure was repeated for eight settings of the B_0 field of the polarizer. The maximum signal was found between $B_0 = (1.743 \pm 0.001)$ mT and $B_0 = (1.783 \pm 0.001)$ mT. The scale of the ordinate refers to the offset from this optimum $B_0 = (1.763 \pm 0.001)$ mT. Figure modified from [2].

Flip angle calibration

For the calibration of the flip angles of the r.f. excitation pulses (B_1) for the decoupling pulses and SOT sequence, the experimental protocol for the B_0 calibration was repeated, only with variation of the ^{13}C or ^{1}H pulse widths ($t_{pulse}^{^{13}\mathrm{C}}$, $t_{pulse}^{^{1}\mathrm{H}}$) instead of B_0 increments. The amplitudes and widths were measured with an oscilloscope (meter-reading uncertainty $\Delta t_{pulse} = \pm 5$ µs and $\Delta U = \pm 0.2$ V). The measured signal as a function of $t_{180°}^{^{13}\mathrm{C}}$ and $t_{180°}^{^{1}\mathrm{H}}$ is shown in Fig 4. A cosine function with correction for T_1 relaxation was applied to fit the data and to extract the widths for the 180 ° pulses:

$t_{180°}^{^{13}\mathrm{C}} = (550 \pm 5)$ µs and

$t_{180°}^{^{1}\mathrm{H}} = (157 \pm 5)$ µs,

at amplitudes of $U^{^{1}\mathrm{H}} = (31.8 \pm 0.2)$ V, $U^{^{13}\mathrm{C}} = (9.6 \pm 0.2)$ V. A more powerful r.f. amplifier allowed for larger B_1 amplitudes ($U^{^{13}\mathrm{C}} = (25 \pm 0.2)$ V, a 2.6 fold increase, and $U^{^{1}\mathrm{H}} = (50 \pm 0.2)$ V, a 1.6 fold increase) and to shorten the pulse widths (increasing the excitation bandwidth). The experiment described above was repeated. Pulse widths for optimal inversion pulses were found to decrease by about the same amount as the amplitudes were increased:

$t_{180°}^{^{13}\mathrm{C}} = (210 \pm 5)$ µs, a 2.6 fold decrease, and

$t_{180°}^{^{1}\mathrm{H}} = (114 \pm 5)$ µs), a 1.4 fold decrease.

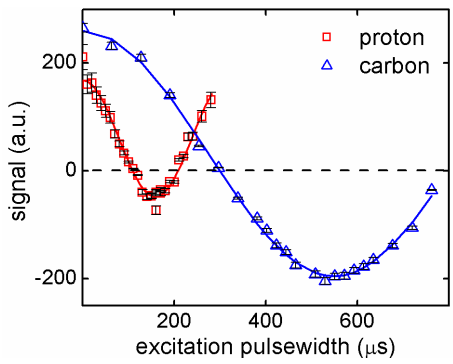

Fig. 24: Flip-angle calibration for ^{13}C and ^{1}H excitation pulses of the low-field MR unit.
In the polarizer, a ^{13}C or ^{1}H rectangular pulse was applied to a prepolarized (at $B_0 = 7$ T) sample of saturated 1-^{13}C sodium acetate in D_2O, followed by $t_{trans} = (14 \pm 1)$ s transport to a 300 MHz NMR spectrometer and detection of ^{1}H or ^{13}C NMR signal. This procedure was repeated with 22 and 31 different pulse widths for ^{13}C, ^{1}H, respectively, at B_1 amplitudes $U^{^{1}\mathrm{H}} = (31.8 \pm 0.2)$ V, $U^{^{13}\mathrm{C}} = (9.6 \pm 0.2)$ V). Inversion pulses were determined to $t_{180°}^{^{13}\mathrm{C}} = (157 \pm 5)$ µs and $t_{180°}^{^{1}\mathrm{H}} = (550 \pm 5)$ µs. Figure taken from [2].

2.5 The PASADENA experiment

Workflow to generate hyperpolarization

The prerequisite for stable yield of ^{13}C hyperpolarization are reproducible experimental conditions and a automated workflow. To achieve this goal, a semi-automated protocol for entire PASADENA experiment was developed, which is described in this section.

The central features of the PASADENA experiment, the hydrogenation and spin-order transfer, as well as the agent delivery and detection of ^{13}C NMR signal for *in vitro* experiments were programmed into the polarizer's process-control unit. The task of the experimenter was reduced to the supply of the precursor solution, start the polarization process, and flushing of the lines after each experiment: The apparatus finally allowed operation of the entire PASADENA experiment by one experimenter, as compared to a staff of four required before.

The following steps take place in the automated process:

(1) the reactor is filled with parahydrogen (p = 10 bar),
(2) the precursor molecule is injected through the injection cap, and
(3) the r.f. spin-order-transfer sequence is applied after a reaction time of 4 s.

(4) For application *in vivo*, the hyperpolarized agent was drawn into a syringe at the outlet of the polarizer, and then administered to the animal.
For *in vitro* experiments, after the spin-order transfer was finished, the hyperpolarized sample was pushed (N_2) through polyethylene tubing into a glass Pasteur pipette, placed in dual-tune $^{1}H/^{13}C$ solenoid coil No. 1 in MR No. 2 (Fig. 27, Tab. 5). 10 s were allowed for the sample to settle down, before the detection of ^{13}C signal is triggered by the polarizer (unlocalized pulse-and-collect sequence No. 4).

The individual steps and timings of the PASADENA experiment are listed in Tab. 4. The whole procedure provided a stable hyperpolarization yield. A checklist for the experiment is provided in Tab. 3.

Start-up and shut-down procedure

In order to obtain stationary conditions for the PASADENA experiment, the heater for the reaction compartment, power supply for the B_0 magnet, Gauss meter, amplifier and low-pass filter were turned on two hours before the beginning of the experiment. The fluid lines and reactor were flushed repeatedly with deionised water and N_2 gas to assure clean lines before the experiment was started. If needed, the system was flushed with D_2O or appropriate buffer solutions to remove residual water from moistened surfaces and adjust the pH for the following experiments. Before the first hyperpolarization experiment, a blank run without precursor solutions but with N_2 and pH_2 was carried out, to guarantee fresh pH_2 and N_2 in the reactor and fluid lines.

Tab. 3: Checklist for the PASADENA experiment.

No.	parameter	value
1	N_2 pressure	p = 14 bar
2	pH_2 pressure	p = 10 bar
3	B_0 field	as calibrated
4	B_1 pulses	as calibrated
5	detection coil	empty
6	detection sequence	standby for trigger signal
7	temperature	T = 62 °C
8	valve sequence	loaded
9	SOT r.f. sequence	loaded
10	precursor	1 - 5 ml injected
11	amplifier, filter, Gauss meter, DAC cards, B_0 magnet power supply	on

Tab. 4: Workflow of the PASADENA experiment.
Manual cleaning and preheating (1) is followed by an automated procedure (2). The curved brackets denote events and valves (Fig. 15). From the time point of its generation, the spin hyperpolarization decays exponentially with life time T_1: The time-sensitive steps (6 – 8) are marked in red. The braces indicate the number and state of the valves: O: open, C: closed.

(a) step	(b) time point	(c) process	(d) duration
1. manual preparation			
(a)	0 s	clean polarizer: flush lines and reactor with 14 bar N_2 gas. Valves {V2 O}, {V3 O}, {V4 O}, {V5 O}.	10 s
(b)	10 s	preheat precursor solution: transfer 3.5 ml of precursor into the injection line {V2 O}.	120 s
total duration of manual preparations: 130 s			
2. automated procedure			
(1)	0 s	hydrogenation and spin-order-transfer fill reaction chamber with parahydrogen {V1 O}.	4 s
(2)	4 s	fill reaction chamber with parahydrogen {V1 O}, pressurize precursor solution {V3 O}	2 s
(3)	6 s	close parahydrogen {V1 C} pressurize precursor solution {V3 O} start r.f. decouplings sequence {r.f. on}	>1 s
(4)	6 s	inject precursor solution {V3, V4 O} start r.f. SOT sequence {r.f. on}	4 s
(5)	10 s	end r.f. SOT sequence {r..f. off} eject hyperpolarized agent {V3, V4, V5 O}	1 s
(6)	11 s	delivery and detection deliver agent to scanner {V3, V4, V5 O}, or manually transport to animal (the automated sequence ends here)	20 s
(7)	31 s	stop delivery {V3, V4, V5 C} settle down of agent {wait}	10 s
(8)	41 s	send trigger signal {trigger on}	3 s
total duration of hyperpolarization, delivery, and detection: 37 s			

2.5.1 Methods for *in-vivo* experiments

Cell experiments

The NMR detection of metabolic products through the enhanced sensitivity of hyperpolarization may allow for characterizing differential metabolism of cancer and control cell lines, potentially allowing systematic screening and classification. In this work, human pancreatic cancer cells and Human embryonic kidney cells 293 (HEK) were exposed to hyperpolarized succinate during acquisition of ^{13}C NMR signal, as described in RESULTS (section 3.6.3, pp. 94). The cells were grown and prepared by Mr. L. Barrios and Dr. Ingram at HMRI. Two MR-compatible incubators for cell cultures were developed to permit hyperpolarization experiments.

MR incubator No. 1
Thirteen ml suspension of cells and media were injected into a truncated 30 ml syringe and transferred to coil No. 2 (Fig. 28). A mechanic permitted rotation of the syringe throughout the experiment within the coil. The entire setup was placed in an atmospheric chamber with a controlled temperature at T = 37 °C (Fig. 26). An injection catheter at the tip of the syringe was fed through a tubing to the outside of the magnet's bore. This permitted injection of agents and signal acquisition while during sample rotation. The motion to rotate the sample was transfered from a geared motor through a driveshaft of 3 m length. Constructions supporting the drive shaft and holding the motor were placed in front of the bore. A phantom containing the cell-growth medium and 10 mM 1-^{13}C glucose was prepared for calibration of the coil (tune, match, flip-angle calibration). A gas-permeable bioreactor was designed to replace the modified syringe as sample holder, but was not manufactured in time.

MR incubator No. 2
To allow for gas exchange of the cell culture during the NMR experiment, a surface coil (No. 5, Figs. 26, 27) was constructed to fit the bioreactor bags used to grow speroids (Fig. 25). The hyperpolarized agent was injected through a catheter reaching outside of the magnet's bore. This setup did not allow for rotation of the bioreactor. Two phantoms were prepared for calibration containing vegetable oil and cell-growth medium with 10 mM 1-^{13}C glucose.

Preparation of cell cultures
The cells were proliferated first as mono layers in flasks before they were transferred to a so-called 'zero-gravity' incubator (which names rotating bioreactors, so that the cells are constantly falling through the solution), to form three dimensional clusters (spheroids) for up to 48 hrs. Spheroids do attach less to surfaces, and allow better contact with the hyperpolarized nutrient in solution, as compared to many superposed layers of individual cells.

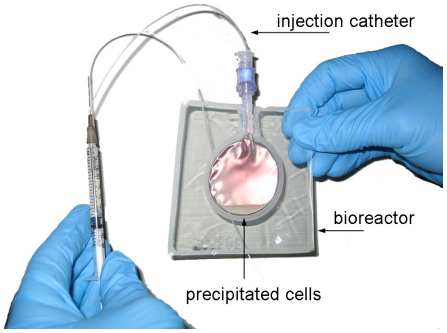

Fig. 25: Bioreactor, delivery line and HEK cells in nutrition media.
The permeable membrane of the bioreactor allows for gas exchange of the cell culture with the surrounding atmosphere. A valve permitted the injection and extraction of small amounts of liquid through a catheter. This reactor was used to form speroids and in MR incubator No. 2. Note the precipitation of the cells at the bottom of the reactor (white).

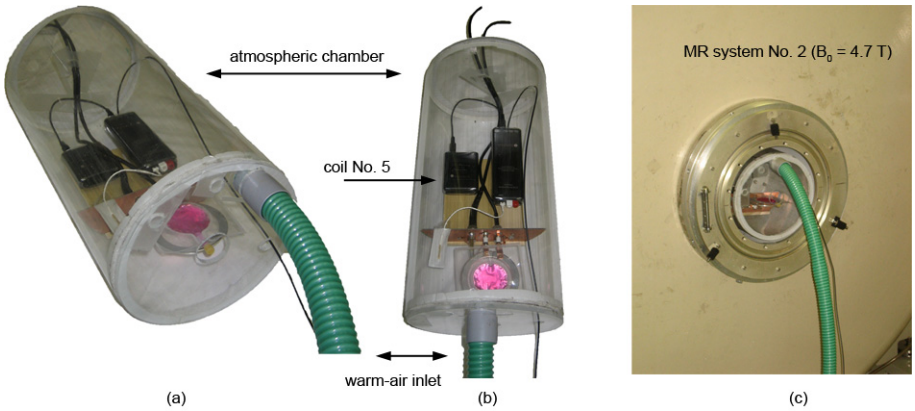

Fig. 26: Atmospheric chamber and coil No. 5 for NMR on cell cultures (MR incubator No. 2)
(a) and (b): closable compartment (acrylic) with temperature control unit and MR antenna No. 8. The chamber was constructed to provide a controlled temperature T = 37 °C for *in vivo* experiments at MR No. 2 (c). Openings permitted feed-through of an injection catheter for application of hyperpolarized samples and a drive shaft (for rotation of the sample within the coil). Warmed air was provided through a hose (green).

Animal experiments

A catheter for the injection of hyperpolarized agents was implanted in the tail vein or carotid artery of a rat (Sprague Dawney) by a surgeon. The rat was anesthetized with isoflurane, placed in the MR antenna (No. 2 or 6), and inserted in the magnet (MR 1 or MR 2). Radio frequency and B_0 adjustments were performed, and ^{1}H reference images were acquired. The hyperpolarized solution was produced, transported to the MR system and injected through the catheter. Subsequently the MR pulse sequence for detection of ^{13}C signal was started.
The protocol for the animal experiments (preparations, surgery, anaesthesia, monitoring of vital signs during the experiment) were approved and performed by trained animal surgeons (Dr. K. Kanamori and Dr. H. Chang).

2.6 Detection methods

Several high-resolution NMR spectrometers ($v_0(^1H) = 300$, 500, 600 MHz), an animal MR imager ($B_0 = 4.7$ T) and a clinical whole-body MR tomograph ($B_0 = 1.5$ T) were employed for ^1H and ^{13}C spectroscopy and imaging. The MR systems, probes, and sequences are described in the following.

2.6.1 MR systems

The PASADENA polarizer was located in proximity of two MR tomographs: A $B_0 = 4.7$ T Bruker horizontal-bore (20 cm diameter) imaging spectrometer with two transmit and receive channels at a distance of d = (7.6 ± 0.1) m, and a $B_0 = 1.5$ T clinical whole-body MR tomograph at d ~ 20 m.
High-resolution NMR spectrometers with proton frequencies of 300, 500, and 600 MHz ($B_0 = 7$ T, 11 T, 14 T) for 5 mm sample tubes were available at the California Institute of Technology (Tab. 5).

Tab. 5: MR systems used.

No.	B_0 / $\nu_0(^1H)$	manufacturer	description
1	1.5 T	GE[1]	clinical whole-body MR tomograph
2	4.7 T	Bruker[2]	Paravision 3.02 and XwinNMR software.
3	300 MHz	Varian[3]	300 MHz (^1H) Varian Mercury high resolution NMR spectrometer
4	500 MHz	Varian	500 MHZ (^1H) Varian high resolution NMR spectrometer (5 mm probe, ^1H, ^{13}C)
5	600 MHz	Varian	600 MHz (^1H) Varian high resolution NMR spectrometer

— *Abbreviations:* [1]General Electric, Milwaukee, WI, USA. [2]Bruker, Karlsruhe, Germany. [3]VARIAN, Palo Alto, CA, USA.

2.6.2 MR antennas

Tables 6 lists the antenna systems employed at the MR No. 1 and No. 2. Coils No. 1, 2, 5 and 6 were build in the laboratory. The schematic of antennas No. 1 and 5 is given in Fig. 27 c [6].

Coil No. 1 was used for the quantification of the degree of polarization (Fig. 27 a). Prior to each NMR experiment, the coil was filled with a sample of the solution to be detected, centred in the bore, and fully calibrated (match, tune, shim, and flip-angle calibration). A T-connector on top of the pipette allowed for delivery of hyperpolarized agents and release of overpressure through a line connected to an overflow reservoir, preventing spilling on the coil electronics. The pipette tip was connected to a PE tubing to withdraw the solution after detection, allowing successive experiments without coil repositioning or additional hardware calibration. The copper wire was tightly wound around the lower third of the pipette at a total length of L = 1.2 cm (sensitive region of the coil). Injection of sample solution exceeding the sensitive region guaranteed a constant filling-factor (~ 72%) for all experiments.
Coil No. 2 was build for NMR of ^{129}Xe gas, therefore only of limited use for ^{13}C animal imaging (matching, tuning and flip angle calibration under load were not possible).

Tab. 6: List of r.f antennas for MR systems No. 1 and No. 2.

No.	B_0 (T)	tune	description
1	4.7	^{13}C, ^{1}H	dual-tune solenoid coil, holding a Pasteur pipette for detection and quantification of hyperpolarized signal (Fig. 27),.D = 7 mm, L = 1.2 cm (EYC) (Fig. 27 a).
2	4.7	^{1}H, ^{13}C	dual-tune volume coil (modified bird-cage design), D = 5 cm, L = 20 cm (EYC).
3	4.7	^{1}H	volume coil (two legged bird cage modification) for detection of hydrogen gas samples (DPW), D = 1.2 cm, L = 3 cm.
4	4.7	^{1}H, ^{13}C	dual-tune solenoid coil for mice and cell cultures (Advanced Imaging Research inc., Cleveland, OH, USA).
5	4.7	^{13}C, ^{1}H	dual-tune surface coil for NMR of bioreactors (Fig. 27), D = 7.5 cm (JBH) (Fig. 27 b).
6	1.5	^{13}C	two-loop surface coil for ^{13}C MRS of human head, D = 15 cm (KH).
7	1.5	^{1}H	body resonator

— *Abbreviations:* D: inner diameter, L: length. Initials indicate the constructor of the coil. EYC: Dr. E. Y. Chekmenev, JBH: Jan-Bernd Hövener, KH: Dr. K. Harris, DPW: Dr. D. P. Weitekamp.

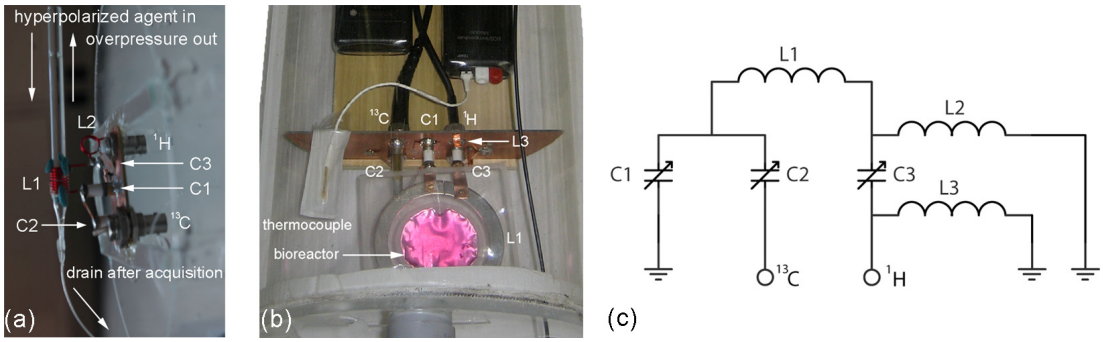

Fig. 27: ^{13}C and ^{1}H dual-tune r.f. antennas No. 1 (a) and Nr 5 (b). The corresponding schematic is depicted in (c). A construction in coil No. 1 allowed automated transportation and filling with the hyperpolarized agent (a). Coil No. 2 was employed for *in-vivo* experiments with human cells exposed to hyperpolarized Suc. The-dual tune circuit (c) allowed for individual tune and match of the frequency bands (^{13}C ~ 50 MHz, ^{1}H ~ 200 MHz). The following components were used (for the solenoid and surface coil, respectively): Transmit and receive antenna (L1): 10 turns magnet wire (D 1.2 mm) around Pasteur pipette (O.D. 7.0 mm, I.D. 6.0 mm, active volume (475 ± 60) mm^3, sample volume (343 ± 44) mm^3, filling factor 72 %) (a), and a silver plated copper ring (O.D 9.5 cm, I.D. 7.5 cm, thickness 2 mm, L = 120 nH) (b). L2: 1.75 turns (same wire and diameter as L1). L3: ~2 · 0.3 cm^2 copper foil. C1, C2, C3: variable capacitors (max. C = 2 – 120 pF) [6].

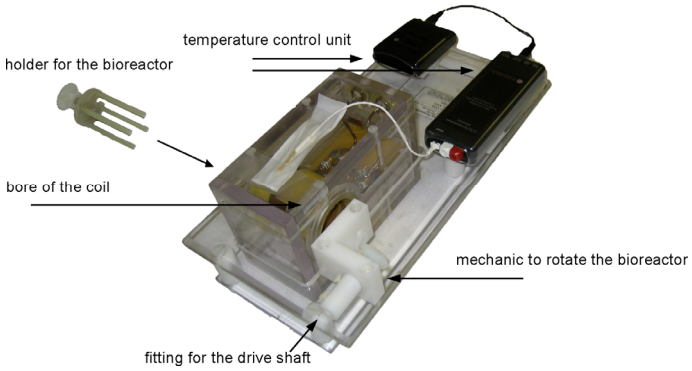

Fig. 28: ^{13}C and ^{1}H dual-tune r.f. antenna No. 4 for NMR on cell cultures (MR incubator No. 1).
A mechanic was added to coil No. 4 to permit rotation of the cell-bioreactor inside the coil during administration of the hyperpolarized agent. Furthermore, a temperature monitoring device was installed, including controller, thermocouple, and battery pack. For cell experiments, the entire setup was placed in the atmospheric chamber (Fig. 26).

2.6.3 MR sequences

The MRI and NMR sequences of MR systems No. 1 and 2 are listed in below (Tab. 7).

Sequence No. 3 was modified to receive an external trigger signal submitted by the polarizer. Sequence No. 4 was developed for the purpose of imaging of hyperpolarized ^{13}C solution [3].

Tab. 7: List of r.f. pulse sequences employed.

No.	MR system No.	coil No.	nucleus	description
1	1	7	^{1}H	fast gradient echo sequence (for morphological imaging)
2	1	6	^{13}C	3D FISP
3	2	1, 2, 4	^{1}H, ^{13}C	pulse-and-acquisition sequence, 64 consecutive single acquisitions (NEX = 1), used TR's = 200 ms, 5 s, 20 s, 30 s.
4	2	2, 4	^{1}H, ^{13}C	FISP for ^{1}H and hyperpolarized ^{13}C MRI
5	3, 4, 5	*	^{1}H, ^{13}C	pulse-and-collect sequence (for high-resolution NMR: lock, decoupling optional).

— *Abbreviations:* FISP: Fast Imaging with Steady State Precession. * coils provided by the manufacturers of the spectrometers.

2.6.4 Quantification of the degree of hyperpolarization

The ^{13}C signal of the hyperpolarized samples $S_{hyp}^{t_a}$ was detected a period t_a after the samples were produced. The enhancement $\eta^{t=t_a}$ of the signal was quantified in respect to the signal S_{ref} of a thermally polarized sample of ethanol (ETOH):

$$\eta^{t=t_a} = \frac{S_{hyp}^{t=t_a}}{S_{ref}} \cdot \frac{c_{ref}}{c_{hyp}} = \frac{P_{hyp}^{t=t_a}}{P_B}, \tag{60}$$

where c_{hyp} and c_{ref} are the molar concentrations of the hyperpolarized and reference sample (the concentration of ^{13}C in ETOH at natural abundance is $c_{ref} = 188.5$ mM). The signal intensities were determined by numerical integration (XwinNMR, Bruker, Karlsruhe, Germany). The reference signal was acquired prior to the hyperpolarization experiments under identical acquisition parameters, coil position and hardware calibrations (shim, e.g.). This permits to calculate the polarization degree:

$$P_{hyp}^{t=t_a} = \eta^{t=t_a} \cdot P_B . \tag{61}$$

In the moment of detection, the degree of polarization has already decayed for t_a owing to longitudinal relaxation. If the decay constant T_1 is known, the signal enhancement $\eta^{t=0}$ and degree of polarization $P_{hyp}^{t=0}$ at $t_a = 0$ can be estimated:

$$\begin{aligned} \eta^{t=0} &= \eta^{t=t_a} \cdot \exp\left(\frac{t_a}{T_1}\right) \\ P_{hyp}^{t=0} &= \eta^{t=0} \cdot P_B \end{aligned} \tag{62}$$

In the automated workflow described before, the interval between production and detection of hyperpolarization was $t_a = (33.0 \pm 0.1)$ s (including hyperpolarization, transportation, acquisition trigger). For manual transportation of the hyperpolarized sample, e.g. to MR 1, t_a was measured with a stopwatch.

2.6.5 Measurement of T_1

The T_1 values for the PASADENA agents were measured directly on the hyperpolarized samples: A series of small angle ($\alpha \approx 8°$) pulse-and-collect experiments was applied to probe the decay of the magnetization (small-excitation-angle approximation, SEA). The T_1 values were extracted by fitting an exponential decay function to the data, taking into account the loss of magnetization caused by the excitation pulses (Eq. 63, Origin 7.5 and 8.0, Origin labs, USA).

$$S(t) = S_0 \cdot e^{-\left(\frac{t}{T_1}\right)} \cdot e^{-\left(\frac{(1-\cos(\alpha))t}{TR}\right)} \tag{63}$$

Chapter 3: Results

The RESULTS chapter consists of six sections:

The performance of the new PASADENA polarizer is evaluated in the section 3.1: Spin hyperpolarization $P \sim 0.1$ was achieved using 2-hydroxyethyl 1-^{13}C, 2,3,3-D_3 propionate (HEP) and TFPP. The new equipment required only one operator, and allowed to produce hyperpolarized samples of 1 - 5 ml in intervals of three min. [3, 57].

In the second section (3.2), the steps leading to the hyperpolarization of the PASADENA biomolecule 1-^{13}C 2,3-D_2 succinate (Suc) are presented. This involves the identification and synthesis of the precursor molecule, the determination of its J-couplings, and calculation of the spin-order-transfer sequence.

The reproducibility of the hyperpolarization of ^{13}C in Suc is investigated in section 3.3: A total of 28 hyperpolarization experiments were performed on subsequent days. In average, a polarization of $\overline{P}_{hyp}^{t=33s} = 0.064 \pm 0.002$ was detected $t_a = (33.0 \pm 0.5)$ s after the production of hyperpolarization. The polarization at $t_a = 0$ is estimated to $\overline{P}_{hyp}^{t=0} = 0.148 \pm 0.005$ [26].

The impact of suboptimal r.f. pulses of the spin-order-transfer (SOT) sequence on the hyperpolarization yield is investigated in theory and experiments the fourth section 3.4 [2].

The effect of pH, field strength, and deuteration of solvent and molecular sites on the lifetime T_1

of the ^{13}C hyperpolarization of Suc, TFPP and HEP is examined next (3.5). Maximal $T_1 = (59.7 \pm 3.2)$ s for Suc, $T_1 = (73.6 \pm 1.6)$ s for HEP, and $T_1 = (48 \pm 5)$ s for TFPP were achieved in D_2O solution, at pH 7.0 ± 0.1 and $B_0 = 4.7$ T [58].
The results of sections 3.1 – 3.5 permitted the application of hyperpolarized 1-^{13}C 2,3-D_2 Suc and HEP *in vivo:* ^{13}C MR images (MRI) and spectra (MRS) were acquired after injection of hyp-Suc and hyp-HEP in rats and cell cultures. Strong signal enhancement was observed in all experiments (3.6).

3.1 Performance of the PASADENA polarizer

The individual techniques described in METHODS were combined to a semi-automated ^{13}C PASADENA hyperpolarization experiment (Fig. 30). The following experimental procedure was developed and employed in all further experiments:

A	preparation of parahydrogen (section 2.1, p. 30).
B	start-up sequence for polarizer (section 2.5, p. 50).
C	preparation of MR detection system: Match, tune, and shim, acquisition of ^{13}C reference spectrum for quantification of polarization degree. Setup of detection sequence for remote trigger (section 2.6, p. 56).
D	preparation of catalyst-precursor mixture (in aqueous or D_2O solution), connection to injection port of the polarizer (section (section 2.5, p. 50).
E	injection of catalyst-precursor mixture, and start of automated PASADENA sequence: hydrogenation, spin-order transfer and formation of net polarization (section 0, p. 50).
F	transport of the hyperpolarized sample to a high-field detection system (B_0 = 1.5 T, 4.7 T, 7 T).
G	trigger of acquisition for ^{13}C NMR spectroscopy and imaging (section 2.6, p. 56).
H	cleaning and preparation for the next experiment (section 2.5, p. 50).
I	shut-down of polarizer (section 2.5, p. 50).

The entire cycle (E – H), including preheating (120 s), hyperpolarization, MR signal detection, rinsing, and reloading the polarizer with precursor lasts only $t_{cycle} \sim 180$ s (Tab. 4).
The performance of the PASADENA polarizer was examined using HEP. A degree of polarization $P = 0.09 \pm 0.01$ was observed $t_a = (33.0 \pm 0.5)$ s after the production of the sample. The polarization at $t_a = 0$ was estimated to $P = 0.18 \pm 0.02$, assuming a $T_1 = (50.7 \pm 0.3)$ s. At $B_0 = 4.7$ T, this corresponds to a ^{13}C signal enhancement (η) of $\eta(t_a = 33\ s) > 2.2 \cdot 10^4$ or $\eta(t_a=0) > 4.4 \cdot 10^4$. Figure 29 shows the spectrum of a sample of hyp-HEP (c = 2.5 mM), and the spectrum of pure ethanol used for quantification of the polarization degree (ETOH, 100 vol. % anhydrous, spectrum 512 fold enlarged, ^{13}C concentration at nat. abundance: 188 mM).

The stability of the new polarizer was much improved: The coefficient of variance (c_v) of the polarization yield was $c_v = 0.05$ (n = 3), while experiments with the prototype setup yielded $c_v = 1.09$ (n = 10) (Appendix III, p. 133).

Hyperpolarization of TFPP

Since the PASADENA moiety propionate in TFPP is the same as in HEP, the SOT sequence as published by Goldman and Johannesson was employed(section 1.4, pp. 27). Hyperpolarization $P > 0.1$ was achieved.

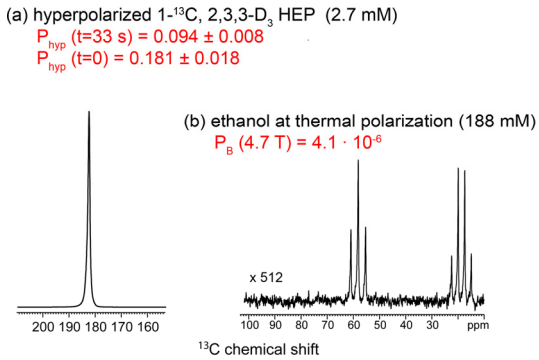

Fig. 29: PASADENA hyperpolarization using the new polarizer.
(a) ^{13}C spectrum of 2.7 mM hyperpolarized 1-^{13}C 2,3,3-D_3 hydroxyethyl propionate (hyp-HEP), produced with the new polarizer. The degree of polarization was quantified to $P_{hyp}^{t_a=33s} = 0.094 \pm 0.008$ at detection of ^{13}C signal, $t_a = (33.0 \pm 0.5)$ s after its generation. The polarization at $t_a = 0$ is estimated to $P_{hyp}^{t_a=0} = 0.181 \pm 0.018$, assuming a $T_1 = (50.7 \pm 0.3)$ s. (b) ^{13}C spectrum of ethanol used to quantify the degree of hyperpolarization (100 vol. %, concentration of ^{13}C = 188 mM at natural abundance, spectrum 512 fold enlarged).
Experimental parameters: unlocalized ^{13}C pulse-and-collect sequence No. 3, NEX = 1, MR system No. 2, coil No. 1

Fig. 30: Setup for the PASADENA experiment.
The polarizer cabinet (left) is located in d = (7.6 ± 0.1) m distance to an unshielded B_0 = 4.7 T MR-system (No. 2). The stray field of the magnet was measured to be B_{stray} = 0.1 mT at the polarizer. A detailed description of the polarizer is given in Fig. 22.

3.2 PASADENA hyperpolarization of ^{13}C in succinate

The following steps were identified to achieve PASADENA hyperpolarization of a new molecule:

(1) Identification and synthesis of a precursor molecule
(2) Determination of the J-couplings among parahydrogens and to be polarized nucleus
(3) Calculation of the spin-order-transfer sequence.

The details leading to the hyperpolarization of succinate (Suc) are described in the following sections.

(1) Precursor molecule

The requirements for a precursor molecule are

- the ability to accommodate the parahydrogen moiety,
- a ^{13}C label, preferably at a site that provides long T_1, and
- a molecular structure, such that the added protons are not magnetically equivalent.

In earlier experiments of this laboratory, the precursor molecule acetylenedicarboxylic (ADC) acid was employed for hyperpolarization of Suc (ADC forms Suc after double hydrogenation) [4]. However, ADC did not prove suitable for biomedical application due to the relatively short T_1 (~ 6 s) and toxic intermediate maleate (formed after single hydrogenation). Both problems were solved using the precursor 1-^{13}C, 2,3-D_2 fumaric acid (Fum): Suc is formed directly after a single hydrogenation (Figs. 9, 31), and the T_1 of 1-^{13}C is significantly prolonged (~10 fold since the protons at 2,3-C are exchanged by deuterons) [26]. In order to break the magnetic equivalence and simplify the spin dynamics, the ^{13}C label is confined to only one carboxyl site (1-C) in the otherwise symmetric molecule. The molecule was synthesised by Cambridge Isotopes Laboratories (CIL), USA.

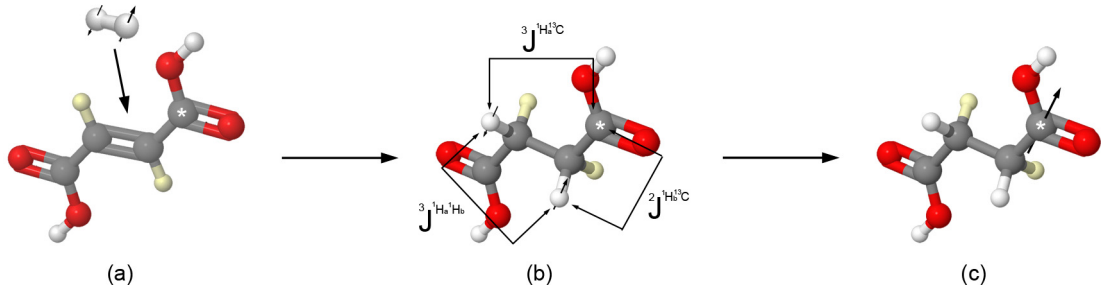

Fig. 31: Scheme of PASADENA hyperpolarization process for 1-^{13}C 2,3-D_2 succinate.
(a) Molecular parahydrogen ( ) is added to 1-^{13}C 2,3-D_2 fumarate by catalytic hydrogenation. (b) A spin-order-transfer sequence is applied (using the J-couplings) to transfer the spin order and form net-polarization on the labeled carbon site (c). : deuterium, : oxygen, : hydrogen, : carbon. The asterisk indicates the ^{13}C label.

(2) Determination of J-couplings of succinate

In order to calculate the r.f. spin-order-transfer (SOT) sequence for Suc (section 1.3.3, p. 17), the J-couplings between the nuclei involved must be known. The involved nuclei are the protons originating from the parahydrogen molecule, ^1H_a and ^1H_b, and the to be polarized nucleus, here ^{13}C. The corresponding J-couplings are ${}^3J^{^1H_a,^{13}C}$ (^1H_a to ^{13}C, across three bonds) ${}^2J^{^1H_b,^{13}C}$ (^1H_b to ^{13}C, across two bonds) and ${}^3J^{^1H_a,^1H_b}$ (^1H_a to ^1H_b, across three bonds). The coupling constants were extracted from high-resolution NMR spectra of succinic acid (natural abundance of nuclear isotopes), obtained at B_0 = 14 T (MR No. 6, pp. 56) [26]. The pH value proved to be crucial for the resolution of the line splittings (Fig. 31): This effect is attributed to the pH dependent chemical exchange of the protons of the molecule. To obtain resolved resonances, pH 3 was chosen for all further experiments.

To obtain the coupling constants, the spectrum of the PASADENA spin system (^1H_a, ^1H_b, ^{13}C, section 1.3.3, p. 17) was simulated in GAMMA [59]. The J-couplings (${}^3J^{^1H_a,^{13}C}$, ${}^2J^{^1H_b,^{13}C}$, ${}^3J^{^1H_a,^1H_b}$) of the system were varied until the resulting spectrum matched to the experimentally acquired spectrum [26]. The best match was found at

$$\begin{aligned} {}^3J^{^1H_a,^{13}C} &= 5.82 \text{ Hz}, \\ {}^2J^{^1H_b,^{13}C} &= -7.15 \text{ Hz and} \\ {}^3J^{^1H_a,^1H_b} &= 7.41 \text{ Hz}, \end{aligned} \tag{64}$$

optimized with a Levenberg-Marquart algorithm (MATLAB, Mathworks, USA. V.A. Norton, personal communication). The maximal error is estimated to $\Delta J = \pm 20$ %.

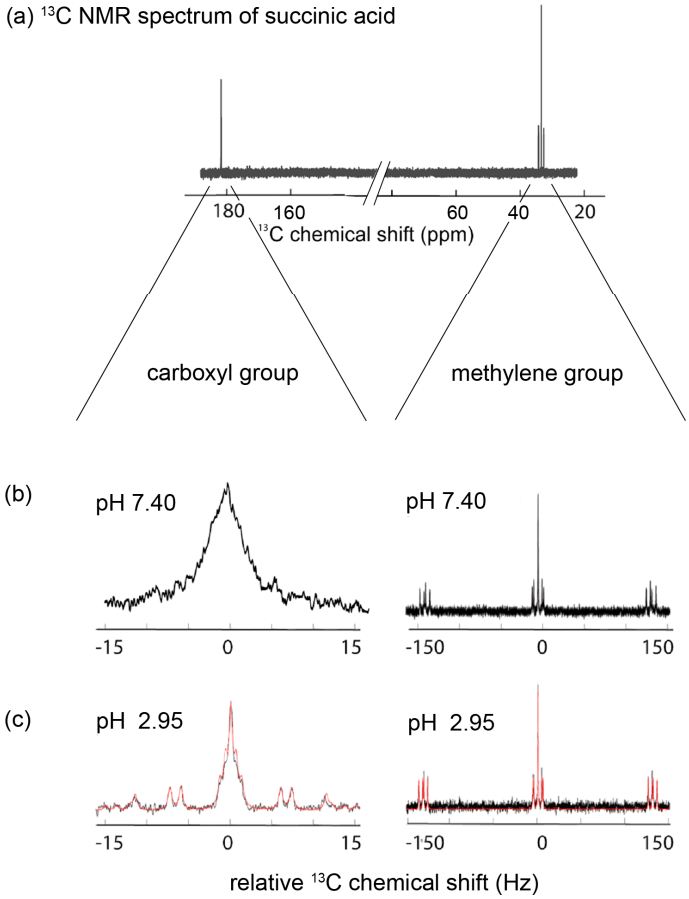

Fig. 32: ^{13}C-NMR spectra of succinate (black, nat. abundance) and fit (red) to determine the J-couplings.
(a) The ^{13}C NMR spectrum of succinic acid exhibits two resonances of the carboxyl-carbon (1,4-^{3}C) at δ ~ 185 ppm, and the methylene-carbon (2,3-^{13}C) at δ ~ 35 ppm. (b) Enlarged representation of the carboxyl-carbon and methylene-carbon spectra (pH 7.4). Note the broad line shape of the carboxyl carbon. (c) ^{13}C-NMR spectra (black) and simulations (red) of the same resonances at pH 2.95. Note the improved resolution of line splittings of the carboxyl resonances. The J-couplings extracted from the simulated spectrum were ${}^{3}J^{{}^{1}H_a,{}^{13}C} = 5.82$ Hz, ${}^{2}J^{{}^{1}H_b,{}^{13}C} = -7.15$ Hz and ${}^{3}J^{{}^{1}H_a,{}^{1}H_b} = 7.41$ Hz. These values were employed to calculate the spin-order-transfer sequence for Suc.
Experimental parameters: unlocalized ^{13}C pulse-and-collect sequence, NEX = 256, no decoupling, 600 MHz Varian high-resolution spectrometer No. 5 (pp. 59). Figure modified from [2].

(3) Adaptation of SOT sequence to succinate

The SOT sequence (Fig. 5) for Suc was calculated using the program presented in THEORY (section 1.4, pp. 27). For the measured J-couplings of Suc:

$$\begin{aligned} &{}^{3}J^{H_aC} = 5.82 \text{ Hz}, \\ &{}^{2}J^{H_bC} = -7.15 \text{ Hz and} \\ &{}^{3}J^{H_aH_b} = 7.41 \text{ Hz}, \end{aligned} \tag{64}$$

the following values for the free-evolution intervals (for the SOT) were obtained (θ = 47.22°):

$$\begin{aligned} t_1^{Suc} &= 27.87 \text{ ms}, \\ t_2^{Suc} &= 37.04 \text{ ms}, \\ t_3^{Suc} &= 50.78 \text{ ms}. \end{aligned} \tag{65}$$

These are in good agreement with the following intervals, which were calculated using a different approach (GAMMA [59], V.A. Norton, personal communication):

$$\begin{aligned} t_1^{Suc} &= 27.84 \text{ ms}, \\ t_2^{Suc} &= 36.84 \text{ ms}, \\ t_3^{Suc} &= 50.76 \text{ ms}. \end{aligned} \tag{66}$$

In both cases, the predicted maximal polarization for Suc is

$$P = 0.991.$$

It is instructive to consider the theoretical impact of inaccurately known J-couplings on the efficacy of the SOT sequence: Figure 33 shows the theoretical hyperpolarization yield achieved with the SOT sequence for Suc (Eq. 65) in dependence of the J-couplings of the simulated spin system (Eq. 64). When the heteronuclear couplings (${}^{3}J^{{}^{1}H_a,{}^{13}C}$, ${}^{2}J^{{}^{1}H_b,{}^{13}C}$) were set ±20 % off the value used to calculate the SOT sequence (Eq. 64), the simulated hyperpolarization yield decreased to $P \approx 0.95$. The homonuclear proton-proton coupling (${}^{3}J^{{}^{1}H_a,{}^{1}H_b}$) had a stronger impact: ±20 % off led to $P = 0.76$.

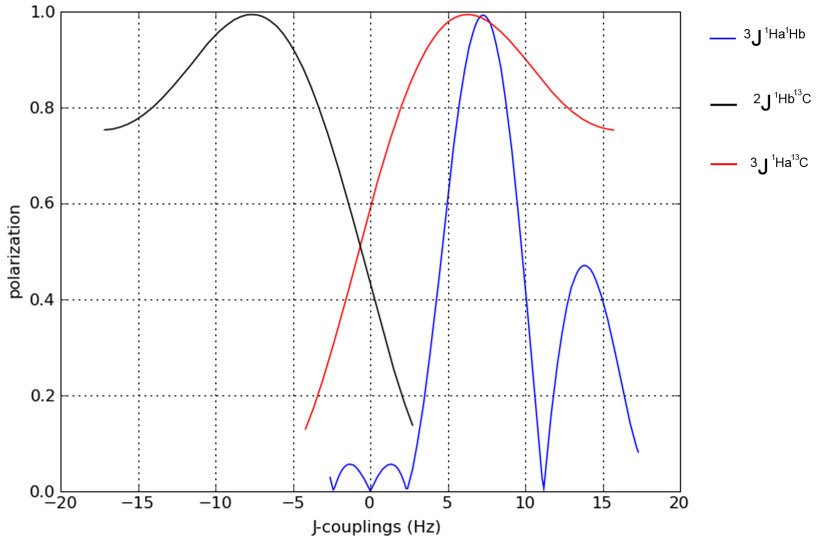

Fig. 33: Simulation: Dependence of the hyperpolarization yield on the J-couplings in the case of succinate.
The effect of a SOT sequence based on inaccurate J-couplings was simulated. First, a SOT sequence was calculated for Suc (Eq. 65) and applied in a simulation to the succinate spin system ($^{3}J^{^{1}H_a,^{1}H_b}$ = 7.41 Hz, $^{3}J^{^{1}H_a,^{13}C}$ = 5.82 Hz, $^{2}J^{^{1}H_b,^{13}C}$ = -7.15 Hz, Eq. 64). A polarization of $P = 0.991$ was calculated. In the next step, each coupling constant of the spin system was varied ±10 Hz in steps of 0.1 Hz around the values in Eq. 64. For each setting, the PASADENA experiment was simulated using the SOT sequence calculated before (Eq. 65). The resulting hyperpolarization yield was plotted against values of the coupling constants.
Simulation parameters: 3-spin-½ system, isotropic liquid-state Hamiltonian in doubly rotating frame (^{13}C and ^{1}H), ideal pulses, no relaxation. Source code provided in Appendix I (pp. 114).

Hyperpolarization of succinate

The SOT sequence was written to an ASCII file (MATLAB) and loaded into the polarizer. A catalyst-precursor solution containing 1-^{13}C, 2,3-D_2 Fum (c = 1.95 mM) was prepared as described in METHODS (section 2.3.3, pp. 36). A sample of hyperpolarized succinate (volume (3.0 ±0.5) ml) was produced, automatically transported to the MR system in t_a = (33.0 ± 0.5) s and detected (Mr. No. 2, coil No. 1, sequence No. 3). The polarization degree was quantified to $P_{hyp}^{t_a=33s}$ = (0.084 ± 0.007) with respect to thermally polarized ETOH (Fig. 34). The hyperpolarization at t = 0 was estimated to $P_{hyp}^{t_a=0}$ = 0.192 ± 0.019, assuming T_1 = (39.6 ± 0.6) s (pp. 79). For details of the calculation of $P^{t=0}$, see section 2.6.4, pp. 60.

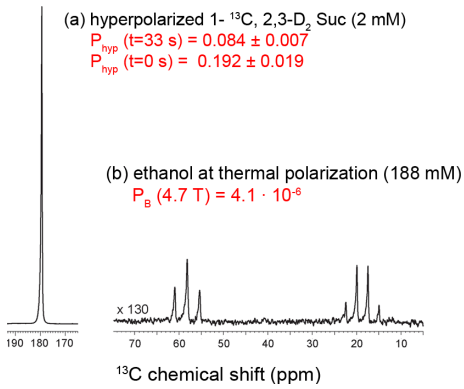

Fig. 34: Hyperpolarization of 1-^{13}C, 2,3-D_2 succinate.
(a) ^{13}C hyperpolarization of $P_{hyp}^{t_a=33s}$ = 0.084 ± 0.007 was measured t_a = (33.0 ± 0.5) s after the generation. The polarization at t_a = 0 was estimated to $P_{hyp}^{t_a=0}$ = (0.192 ± 0.019). (b) The degree of polarization was quantified with respect to the ^{13}C NMR signal of thermally polarized ethanol ($P_B = 4.1 \cdot 10^{-6}$, c = 188 mM per ^{13}C site at natural abundance).
Experimental parameters: ^{13}C pulse-and-collect sequence No. 3, NEX = 1, MR No. 2, coil No. 1 (pp. 59).

3.3 Reproducibility of succinate hyperpolarization

To quantify the stability of Suc hyperpolarization, serial hyperpolarization experiments were performed on four days. For every series of experiments, the catalyst-precursor mixture was prepared (section 2.2, pp. 32) with a precursor concentration (Fum) in the range of c(Fum) = 0.96 – 2.93 mM.

For ^{13}C signal detection, the setup described in the previous section was used (MR No. 2, coil No. 1, sequence No. 3). Including data processing, evaluation and documentation, the experiments were carried out in intervals of ca. 10 min. The mean values and statistical errors (standard deviation (SD) and standard error (SE)) of the polarization degree were determined [2].

In average,

$$\overline{P}_{hyp}^{t_a=33s} = 0.\ 064 \pm 0.002 \text{ (SD = 0.008), n = 16}$$

was detected $t_a = (33.0 \pm 0.5)$ s after the production of the sample (in D_2O, Tab. 8) This corresponds to a relative signal enhancement by a factor of $\eta(t_a = 33\ s) \sim 15{,}900$ at $B_0 = 4.7$ T. The "intra-day" variability was found to be

$$\overline{P}_{hyp}^{t_a=33s} = 0.069 \pm 0.008 \text{ (SD = 0.013), n = 3,}$$

$$\overline{P}_{hyp}^{t_a=33s} = 0.071 \pm 0.002 \text{ (SD = 0.003), n = 4,}$$

$$\overline{P}_{hyp}^{t_a=33s} = 0.065 \pm 0.001 \text{ (SD = 0.003), n = 5,}$$

$$\overline{P}_{hyp}^{t_a=33s} = 0.062 \pm 0.004 \text{ (SD = 0.023), n = 4.}$$

Assuming a lifetime of the ^{13}C polarization of $\overline{T}_1 = (39.6 \pm 0.6)$ s (in D_2O, measured in section 3.5, pp. 80), the nascent polarization at $t_a = 0$ was estimated to:

$$\overline{P}_{hyp}^{t_a=0} = 0.148 \pm 0.005 \text{ (SD = 0.01).}$$

This corresponds to a signal enhancement of $\eta^{t=33s} \sim 37{,}400$ at $B_0 = 4.7$ T and T = 293.15 K (see section 2.6.4, p. 60).

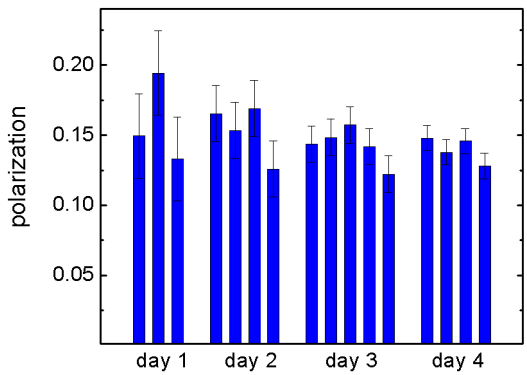

Fig. 15: Reproducibility of hyperpolarization yield in 1-^{13}C, 2,3-D_2 Suc.
An average of $\overline{P}_{hyp}^{t_a=33s}$ = 0.064 ± 0.002 was achieved in n = 16 hyperpolarization experiments in D_2O, performed on successive days (Tab. 8). The polarization in the moment of generation ($t_a = 0$) was estimated to $\overline{P}_{hyp}^{t=0}$ = 0.148 ± 0.005, assuming an exponential decay under T_1 = (39.6 ± 0.2) s for (33.0 ± 0.5) s (shown above). Figure modified from [2].

Although it is assumed that injection of small amounts of D_2O in animals is harmless [60], hyperpolarization was also determined in aqueous solution (Tab. 9). The average ^{13}C polarization obtained in H_2O was

$$\overline{P}_{hyp}^{t=33s} = 0.054 \pm 0.004 \text{ (SD = 0.013), and}$$

$$\overline{P}_{hyp}^{t=0} = 0.128 \pm 0.009 \text{ (SD = 0.031), n = 12.}$$

No influence of the concentration of Suc on the degree of polarization was found in the range c(Suc) = [0.96 – 2.93] mM in D_2O (Tab. 8) and c(Suc) = [1.65 – 2.89] mM in water (Tab. 9).

Tab. 8: List of serial hyperpolarization experiments using 1-^{13}C, 2,3-D_2 Suc in D_2O (Fig. 15).
The reproducibility of PASADENA hyperpolarization of 1-^{13}C, 2,3-D_2 Suc solved in D_2O was determined in n = 16 experiments on four days. The standard error and standard deviation is given.

(a) No.	(b) $P_{hyp}^{t_a=0}$	(c) $P_{hyp}^{t_s=33s}$	(d) c (Suc) (mM)	(e) c (Rh) (mM)
1	0.149	0.065	1.71	2.2
2	0.194	0.084	1.71	2.2
3	0.133	0.058	1.71	2.2
mean ± SE	0.159 ± 0.018	0.069 ± 0.008	SD = 0.033 (t_a = 0), 0.013 (t_a = 33 s)	
4	0.165	0.072	1.40	2.2
5	0.153	0.067	1.40	2.2
6	0.169	0.073	1.40	2.2
7	0.126	0.055	0.96	2.2
mean ± SE	0.153 ± 0.010	0.067 ± 0.004	SD = 0.020 (t_a = 0), 0.003 (t_a = 33 s)	
8	0.144	0.062	2.93	2.1
9	0.148	0.064	2.93	2.1
10	0.157	0.068	1.24	2.2
11	0.142	0.062	1.24	2.2
12	0.122	0.053	1.24	2.2
mean ± SE	0.143 ± 0.006	0.062 ± 0.003	SD = 0.013 (t_a = 0), 0.006 (t_a = 33 s)	
13	0.148	0.064	1.59	2.2
14	0.138	0.060	1.95	2.2
15	0.146	0.063	1.59	2.2
16	0.128	0.056	2.07	2.2
mean ± SE	0.140 ± 0.005	0.061 ± 0.002	SD = 0.009 (t_a = 0), 0.002 (t_a = 33 s)	
total (n = 16)	0.148 ± 0.005	0.064 ± 0.002	SD = 0.018 (t_a = 0), 0.008 (t_a = 33 s)	

— *Abbreviations:* (a) number of experiment; (b) estimated degree of polarization at $t_a = 0$ assuming a $T_1 = (39.6 \pm 0.6)$ s; (c) degree of polarization at detection, $t_a = (33.0 \pm 0.5)$ s after sample production; (d) concentration of Suc in mM; (e) concentration of Rh-catalyst complex in mM.

Tab. 9: List of serial Suc hyperpolarization experiment using 1-^{13}C, 2,3-D_2 Suc H_2O.
The reproducibility of PASADENA hyperpolarization of 1-^{13}C, 2,3-D_2 Suc in H_2O was determined in n = 12 experiments on three days. The standard error (SE) and standard deviation (SD) is given.

(a) No.	(b) $P_{hyp}^{t_a=0}$	(c) $P_{hyp}^{t_s=33s}$	(d) c (Suc) (mM)	(e) c (Rh) (mM)
1	0.162	0.068	1.85	2.2
2	0.190	0.080	1.85	2.2
3	0.175	0.073	1.85	2.2
mean ± SE	0.176 ± 0.008	0.074 ± 0.004	SD = 0.014 (t_a = 0), 0.006 (t_a = 33 s)	
4	0.101	0.042	2.89	2.2
5	0.131	0.055	2.89	2.2
6	0.124	0.052	2.89	2.2
7	0.122	0.051	2.89	2.2
mean ± SE	0.120 ± 0.007	0.050 ± 0.003	SD = 0.013 (t_a = 0), 0.006 (t_a = 33 s)	
8	0.098	0.041	1.65	2.2
9	0.102	0.043	1.65	2.2
10	0.116	0.049	1.65	2.2
11	0.118	0.050	1.65	2.2
12	0.106	0.044	1.65	2.2
mean ± SE	0.108 ± 0.004	0.045 ± 0.002	SD = 0.009 (t_a = 0), 0.004 (t_a = 33 s)	
total (n = 12)	0.129 ± 0.009	0.054 ± 0.004	SD = 0.031, 0.013, for t = 0, t = 33 s	

— *Abbreviations:* (a) number of experiment; (b) estimated degree of polarization at $t_a = 0$ assuming a $T_1 = (27.3 \pm 1.8)$ s (c) degree of polarization at detection, $t_a = (33.0 \pm 0.5)$ s after sample production; (d) concentration of Suc in mM; (e) concentration of Rh-catalyst complex in mM.

3.4 Stability of the PASADENA hyperpolarization

Suboptimal ^{13}C and ^{1}H r.f. pulses in the SOT sequence, e.g. caused by experimental imperfections of B_0 or B_1, reduce the hyperpolarization yield. These effects were investigated in experiments and simulations:

Dependence of hyperpolarization on B_1

The simulation of the PASADENA experiment (section 1.4, pp. 27) was employed to investigate the effect of suboptimal r.f. pulses on the hyperpolarization yield. The flip angles of the ^{13}C and ^{1}H r.f. pulses in the Suc SOT sequence (Eq. 65) were varied individually in the range of 0 - 200 %. For each setting, the PASADENA experiment was simulated, and the degree of polarization calculated. The hyperpolarization yield was relatively robust: Using a flip angle offset of ±50 % (for ^{13}C or ^{1}H pulses), the theoretical polarization was still half of the maximal value ($P = 0.991$) (Fig. 35).

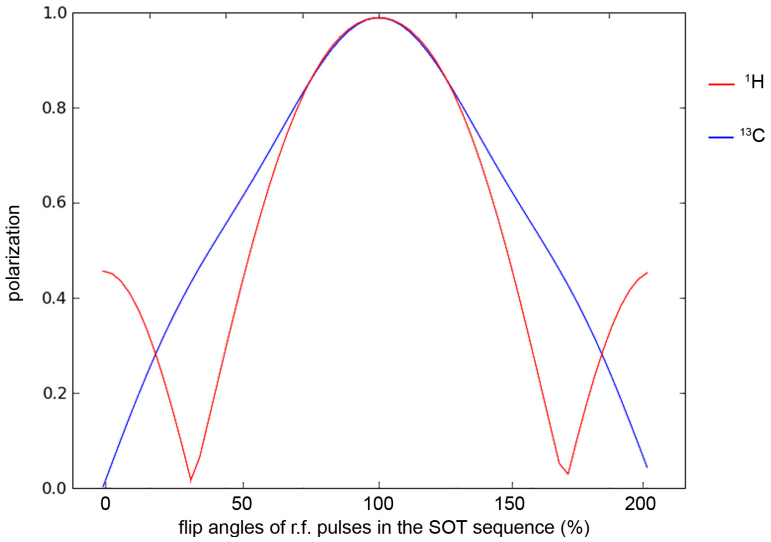

Fig. 35: Simulations: Dependence of the hyperpolarization yield on the flip angles of the SOT sequence in the case of Suc. The hyperpolarization yield was simulated for Suc for different of flip angles of the ^{1}H and ^{13}C excitation pulses in the SOT sequence. First, a SOT sequence was calculated for Suc (Eq. 65) and applied in a simulation to the succinate spin system (Eq. 64): A polarization of $P = 0.991$ was obtained. In the next step, the flip angles for ^{13}C or ^{1}H excitation pulses in the SOT sequence were varied from 0 – 200 % (see sequence in Fig. 5). For each setting, the PASADENA experiment and the hyperpolarization yield was simulated.
Simulation parameters: 3-spin-½ system in Hilbert space, isotropic liquid-state Hamiltonian in doubly rotating frame (^{13}C and ^{1}H), ideal pulses, no relaxation. Source code provided in Appendix I (pp. 114).

The effect of poorly calibrated B_1 pulses in the SOT sequence was as well investigated experimentally. The hyperpolarization yield was recorded as a function of the ^{13}C and ^{1}H pulse widths in the SOT sequence ($t^{^1\mathrm{H}}$ and $t^{^{13}\mathrm{C}}$), beginning with the previously calibrated values $t^{^1\mathrm{H}}_{calibrated} = (114 \pm 5)$ µs and $t^{^{13}\mathrm{C}}_{calibrated} = (210 \pm 5)$ µs (section 2.4.4, pp. 48). For each setting (of $t^{^{13}\mathrm{C}}$ and $t^{^1\mathrm{H}}$), a SOT sequence was calculated and a PASADENA experiment performed (the amplitudes of the r.f. pulses were kept constant).

As expected from the simulations, the hyperpolarization was quite robust and did not vanish in the broad range of pulse widths applied: $t^{^{13}\mathrm{C}} \in [87.3 - 134.0]$ ms and $t^{^1\mathrm{H}} \in [127.0 - 300.0]$ ms. For ^{1}H, maximum polarization was observed at $t^{^1\mathrm{H}}_{180°} = (114 \pm 1)$ µs, which corresponds to the value obtained from the calibrations (r.f. pulse amplitude $U^{^1\mathrm{H}}_{pulse} = (50.0 \pm 0.2)$ V). For ^{13}C, maximal polarization was observed at $t^{^{13}C}_{180°} = 1.1 \cdot t^{^{13}C}_{calibrated} = (230 \pm 23)$ µs (r.f. pulse amplitude $U^{^{13}\mathrm{C}}_{pulse} = (25.0 \pm 0.2)$ V). The experimental data and simulations are superposed in Fig. 36 (the y-axis of the simulations was scaled to the maximal polarization observed in the experiments): The ^{13}C simulations and experiments are in good agreement. For ^{1}H, though, the decrease of polarization in the experiment is stronger than expected from theory (Fig. 36 a and b). For ^{13}C, though, the maximal polarization was found at a pulse width of $t^{^{13}C} = 1.1 \cdot t^{^{13}C}_{calibrated}$.

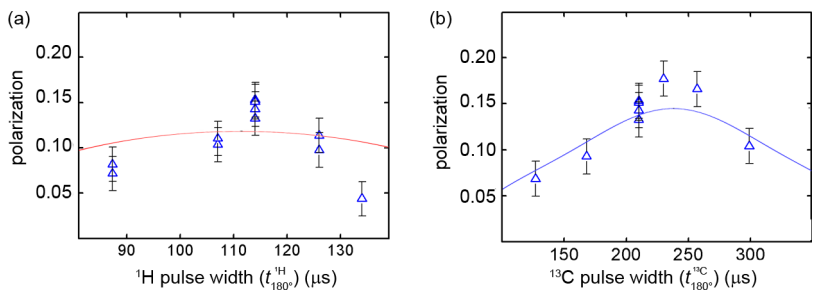

Fig. 36: Dependence of hyperpolarization yield on ^{1}H (a) and ^{13}C (b) pulse widths of the SOT sequence. The PASADENA experiment was conducted with different settings for the ^{1}H and ^{13}C pulse widths of the SOT sequence. For ^{1}H, maximum polarization was observed at $t^{^1\mathrm{H}}_{180°} = (115 \pm 12)$ µs (r.f. pulse amplitude $U^{^1\mathrm{H}}_{pulse} = (50.0 \pm 0.2)$ V). For ^{13}C, maximal polarization was observed at $t^{^{13}C}_{180°} = (230 \pm 23)$ µs (r.f. pulse amplitude $U^{^{13}\mathrm{C}}_{pulse} = (25.0 \pm 0.2)$ V). The hyperpolarization yield in dependence of the flip angles was simulated and superposed (scaled to the maximal polarization): For ^{13}C, the loss in polarization observed in the experiment is stronger than predicted by the simulations (a) (red line). For ^{1}H, the simulations are in good agreement with the experimental data (blue line) (b).

Dependence of hyperpolarization on B_0

The dependence of the polarization degree on the setting of the B_0 field (of the low-field unit of the polarizer) was investigated experimentally. The PASADENA experiment was performed with different values of the B_0 field, set by the B_0 power supply and measured with a Gauss meter (section 2.4.2, pp. 43).

As expected, the polarization degree decreased when B_0 was detuned from the previously calibrated value B_0^{cal} (section 2.4.4, pp. 48). A Gaussian fit was performed to estimate the full-width-at-half-maximum: FWHM = 0.062 ± 0.010 mT. At $B_0 = B_0^{cal} \pm 0.15$ mT, no detectable hyperpolarization was produced (Fig. 37 a). The r.f. amplifier allowed for maximum pulse amplitudes of $U_{pulse}^{^{13}C} = (25.0 \pm 0.2)$ V and $U_{pulse}^{^{1}H} = (50.0 \pm 0.2)$ V, respectively.

When the experiment was repeated with the prototype polarizer, the FWHM decreased (Fig. 37 b). This was attributed to the less powerful and stable r.f. hardware: The maximal amplitudes of the pulses $U_{pulse}^{^{13}C} = (25.0 \pm 0.2)$ V and $U_{pulse}^{^{1}H} = (16.0 \pm 0.2)$ V required longer pulse widths, which also reduced the excitation bandwidth in the frequency domain. This was reflected in an increased dependence of the polarization degree to the B_0 setting: The width of the distribution decreased by a factor of 3.4 to a FWHM = (0.018 ± 0.001) mT when the pulses were 3.1 times longer. At $B_0 = B_0^{cal} \pm 0.04$ mT, no enhanced ^{13}C signal was detected. Because of the large variability, two outliers were omitted for the fit of the data in Fig. 37 b.

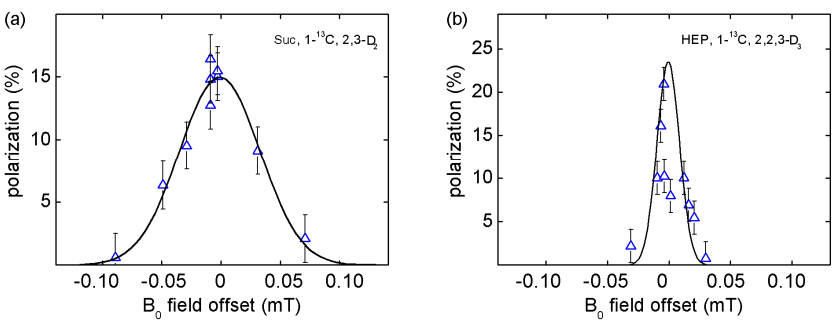

Fig. 37: Hyperpolarization yield as a function of B_0 and B_1-bandwidth in the new (a) and prototype polarizer (b). As expected, the polarization degree decreased when B_0 was detuned from the previously calibrated value B_0^{cal}. (a) More powerful r.f. pulses in the new polarizer reduced the impact of off-resonant B_0 on the hyperpolarization yield. At a setting $B_0 = B_0^{cal} \pm 0.03$ mT, the degree of polarization was reduced to ~ 50 % of the polarization obtained at $B_0 = B_0^{cal}$ (r.f. amplitudes $U_{pulse}^{^{1}H} = (50.0 \pm 0.2)$ V, $U_{pulse}^{^{13}C} = (25.0 \pm 0.2)$ V). (b) At the same offset, no hyperpolarization was obtained with the prototype polarizer (r.f. amplitudes $U_{pulse}^{^{1}H} = (16.0 \pm 0.2)$ V, $U_{pulse}^{^{13}C} = (25.0 \pm 0.2)$ V). The fluctuations in (b) demonstrate the instability of the prototype polarizer. Two outliers were omitted for the Gaussian fit.

3.5 T_1 of hyperpolarized agents

A major challenge for the application of hyperpolarized metabolic tracers *in vivo* is the lifetime of the polarization: A significant fraction has already decayed in the moment of signal detection. Furthermore, the long relaxation time (T_1) should be extended as much as possible to allow a substantial penetration of biochemical pathways by the hyperpolarized ^{13}C label.
It is instructive to consider the major sources for longitudinal spin-relaxation in liquid-state NMR: the interactions of magnetic-dipole moments of the spins and the chemical-shift anisotropy (CSA).
Protons possess the largest magnetic-dipole moment and are the most abundant spins in molecule; hence, their contribution to spin relaxation is significant. The substitution of protons in the solvent and molecule by an atom with smaller nuclear dipole moment can reduce the relaxation rates. Deuterium (D) is a common proton substitute with a gyromagnetic ratio smaller than that of ^1H: $\gamma(^1H) \approx 6.5 \cdot \gamma(D)$. Furthermore, to a certain extent, D is tolerated in living systems: the substitution of the non-exchanging protons by deuterons in 1-^{13}C, 2,3-D_2 Suc (1-^{13}C to 1-^{13}C, 2,3-D_2) had no detectable effect on the metabolism of cells [26], and deuterium oxide (D_2O) is generally tolerated by organisms in small amounts [60].
The use of D_2O instead of water reduces the dipolar relaxation caused by chemical exchange and intermolecular collisions with solvent molecules. To reduce dipolar relaxation caused by atoms on non-exchangeable sites, however, custom synthesized molecules need to be purchased (1-^{13}C, 2,3-D_2 Suc, for example).
The relaxation caused by chemical shift anisotropy depends on B_0^2. In our experiments, the hyperpolarized sample first experiences a $B_0 \sim 1.7$ mT in the polarizer, followed by field drop to $B_0 \sim 0.1$ mT during transport, and an increase to $B_0 = 4.7$ T when the magnet of the MR system is approached.
The dependence of the longitudinal relaxation T_1 on the B_0 field was descried phenomenological by [61, 62]:

$$T_1 \approx A\nu^B, \tag{67}$$

where A and B are empirical parameters, and ν is the resonance frequency. T_1 is expected to decrease at lower B_0 fields. Since the T_1 values were obtained at $B_0 = 4.7$ T, the estimated degree of polarization at $t = 0$ is assumed to be a lower limit.

In the following, the impact of pH, B_0, deuteration of solvent and target molecule on the longitudinal relaxation of PASADENA agents is discussed [58]. The T_1 values were determined experimentally with the SEA method (section 2.6.5, pp. 61): The decaying polarization of a sample was probed with ^{13}C low-angle pulse-and-collect experiments with a TR = 20 – 40 s. For

details on the calculation of the measurement uncertainties, see Appendix III, pp. 133. An overview of all measured T_1 values is given in Tab. 10.

Effect of deuteration of molecular sites

The spin-lattice relaxation time of 1-^{13}C in hyperpolarized deuterated succinate (1-^{13}C,2,3-D_2) in H_2O was measured to $T_1 = (56.8 \pm 2.9)$ ms at pH 7 and $B_0 = 4.7$ T (Fig. 38, ○). For comparison, the T_1 of non-hyperpolarized protonated 1-^{13}C Suc at $B_0 = 7$ T and pH 7.1 was measured with inversion recovery to $T_1 = (6 \pm 1)$ s (pH 7.1, Bhattacharya P., personal communication).
The deuteration of the non-exchanging sites prolongs T_1 significantly.

Effect of solvent deuteration

In deuterium oxide solution, $T_1 = (39.6 \pm 0.6)$ s of 1-^{13}C, 2,3-D_2 Suc (Fig. 38, □) was measured, as compared to $T_1 = (27.6 \pm 1.8)$ s for the same molecule in H_2O (both at pH 3, Fig. 38, △). Similarly, T_1 of HEP at pH 7 increased from $T_1 = (50.7 \pm 0.3)$ s in H_2O (Fig. 39, □) to $T_1 = (73.6 \pm 1.6)$ s in D_2O (Fig. 39, △).

Effect of pH and field strength

For reasons described in section 3.2, pp. 67, the hyperpolarization of Suc requires for pH 3. At this pH, a $T_1 = (27.6 \pm 1.8)$ s is measured for 1-^{13}C, 2,3-D_2 Suc in H_2O at $B_0 = 4.7$ T (Fig. 38, △). A strong increase to $T_1 = (56.8 \pm 2.9)$ s (Fig. 38, ○), was observed when the sample was buffered to pH 7 at $B_0 = 4.7$ T (concentrated phosphate buffer). Preliminary results indicate that solvent deuteration (D_2O) at pH 7 has no significant impact on the T_1 observed. The dependence of T_1 on pH is attributed to the dependence of the rate of chemical exchange on pH.

Interestingly, no signal was observed, when the hyperpolarized sample was buffered to pH 7 at the outlet of the polarizer in $B_0 \sim 1$ mT stray field of MR No. 2 ($B_0 =$ 4.7 T): By the time the ^{13}C signal was detected (20 – 30 s later), no hyperpolarization was observed. Since $T_1 = 56$ s at pH 7 in $B_0 = 4.7$ T, the signal loss is assumed to occur during the buffering and transport of the sample through low-field. The experiment was repeated with different configurations of the experimental setup to exclude effects other than pH and B_0 (Tab 11).

Tab. 10: T_1 values of ^{13}C PASADENA agents determined by low-angle pulse-and-collect experiments (except No. 1) as a function of molecular deuteration (No. 1, 2), solvent deuteration (2, 3 and 6, 7), pH (3, 4) and B_0 (4, 5).

No.	molecule	Fig.	B_0 (T)	solvent	method	pH	T_1 (s)	n
1	1-^{13}C, 2,3-$^{1}H_2$ Suc	–	7	H_2O	IR	7.1 ± 0.1	6 ± 1	1
2	1-^{13}C,2,3-D_2 Suc	38	4.7	H_2O	SEA	3.0 ± 0.1	27.3 ± 1.8	3
3	1-^{13}C,2,3-D_2 Suc	38	4.7	D_2O	SEA	3.0 ± 0.1	39.6 ± 0.6	4
4	1-^{13}C,2,3-D_2 Suc	38	4.7	D_2O/H_2O	SEA	7.0 ± 0.1	59.7 ± 3.2 *	1
5	1-^{13}C,2,3-D_2 Suc	–	10^{-3} – 4.7	D_2O/H_2O	SEA	7.0 ± 0.1	< 5	3
6	1-^{13}C, 2,3,3-D_3 HEP	39	4.7	H_2O	SEA	7.0 ± 0.1	50.7 ± 0.3 *	1
7	1-^{13}C,2,3,3-D_3 HEP	39	4.7	D_2O	SEA	7.0 ± 0.1	73.6 ± 1.6 *	1
8	1-^{13}C,2,3-D_2 Suc	49	4.7	H_2O	SEA	6.3 ± 0.1	55.8 ± 1.5 *	1
9	TFPP	–	4.7	H_2O	SEA	7.0 ± 0.1	48 ± 5 *	1

— *Abbreviations:* IR: inversion recovery, SEA: small-excitation-angle approximation. * error was determined by the exponential fit.

Tab. 11: Experiments to determine the effect of pH and field strength on the relaxation time of hyperpolarized 1-^{13}C, 2,3-D_2 succinate.

No.	signal	buffered at	detection technique	coil No.
1	no	polarizer outlet, B_0 ~ 0.1 mT	SEA, 15°, TR = 5 s	4
2	no	polarizer outlet, B_0 ~ 0.1 mT	90° pulse-and-collect	4
3	yes	no buffer	90° pulse-and-collect, TR = 100 ms, std. protocol	1
4	no	polarizer outlet, B_0 ~ 0.1 mT	90° pulse-and-collect, TR = 100 ms, std. protocol	1
5	yes	in coil at B_0 = 4.7 T	90° pulse-and-collect, TR = 100 ms, manual delivery	1
6	yes	in coil at B_0 = 4.7 T	SEA, 15°, TR = 5 s	4

— *Abbreviations*: SEA: small-excitation-angle approximation, TR: repetition time, std protocol: automated standard protocol of the PASADENA experiment (hyperpolarization, sample transport, detection, section 2.5, pp 50).

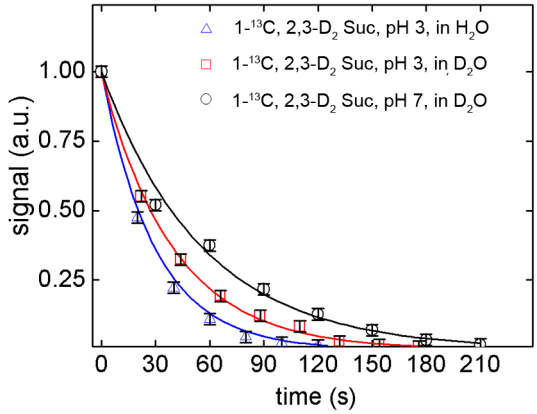

Fig. 38: Lifetime of hyperpolarized succinate at $B_0 = 4.7$ T.
The decay of the ^{13}C signal of hyperpolarized 1-^{13}C, 2,3-D_2 Suc was sampled at $B_0 = 4.7$ T (section 2.6.5, pp. 59). ^{13}C-T_1 was determined for the molecule in solution in H_2O, pH 3: $T_1 = (27.3 \pm 1.8)$ s, △), in D_2O, pH 3: $T_1 = (39.6 \pm 0.6)$ s, □) and in D_2O, pH 7 $T_1 = (59.7 \pm 3.2)$ s, ○).

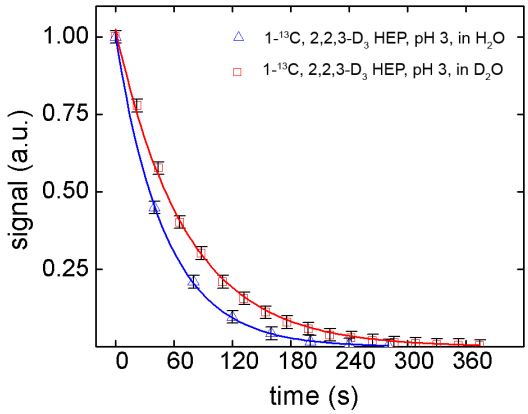

Fig. 39: Lifetime of hyperpolarized HEP at $B_0 = 4.7$ T.
The decay of the ^{13}C signal of hyperpolarized 1-^{13}C, 2,3,3-D_3 HEP in H_2O and D_2O was measured at $B_0 = 4.7$ T (section 2.6.5, pp. 59). ^{13}C-T_1 was determined to $T_1 = (50.7 \pm 0.3)$ s in H_2O (△), and $T_1 = (73.6 \pm 1.6)$ s in D_2O (□).

3.6 ^{13}C NMR experiments with hyperpolarized agents *in vivo*

^{13}C MR imaging (MRI) and spectroscopy (MRS) experiments were performed to monitor the disposition of hyperpolarized Suc and HEP *in vivo*. Details of the experimental setup employed are given in METHODS.

At the time of the *in vivo* studies, the available detection system, in particular the r.f. antennas and pulse sequences, was not optimized. Coil No. 2, build for xenon gas NMR, did not allow for proper match and tune when loaded with a rat; as a consequence, the ^{13}C excitation pulses could not be calibrated. Despite these limitations, strongly enhanced ^{13}C signal was detected in all experiments, thus establishing proof-of-principle of the detection of PASADENA hyperpolarized biomolecules *in vivo*.

3.6.1 Application of hyperpolarized HEP in a rat

A catheter was implanted in the carotid artery or tail vein of rats (Sprague Dawley, Harlan SD) for injection of hyperpolarized HEP (MR system No. 2, coil No. 2, pp. 56). For each experiment, a morphological ^{1}H MR image was acquired to permit anatomical correlation with the ^{13}C MR images. A sphere containing 1-^{13}C acetate (c = 1 M, δ = 184 ppm) was placed in proximity to the rat.

Estimation of polarization degree *in vivo*

The degree of polarization in the moment of injection (t_a = (30 ± 2) s) was estimated be similar as observed in previous *in-vitro* experiments: $P_{hyp}^{t_a=30s} \sim 0.1$. The T_1 of hyperpolarized HEP *in vivo* was assumed to be on the same order as measured *in vitro* at pH 7 (T_1 = (50.7 ± 0.3) s). Therefore, the degree of polarization in the MRI images acquired within 5 s after injection can be estimated to $P_{in\ vivo}^{t=35\ s} > 0.05$.

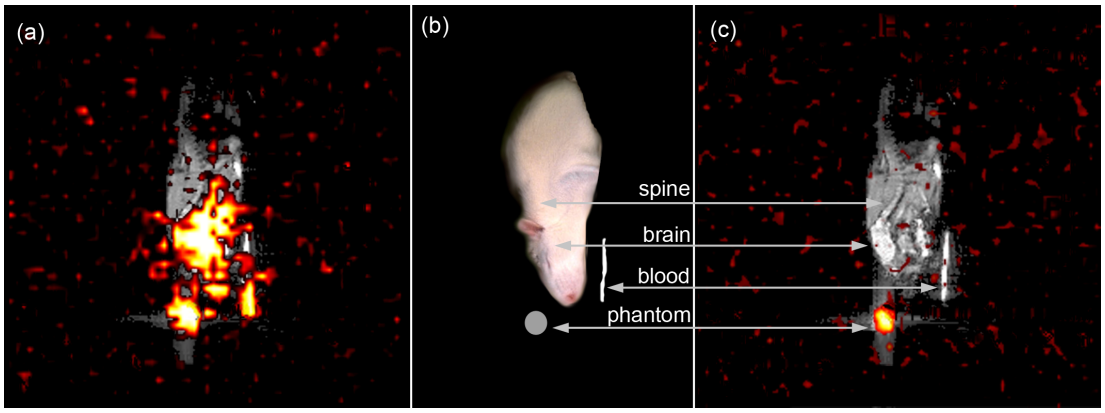

Fig. 40: Sagittal *in vivo* ^{13}C and ^{1}H MRI after injection of hyp-HEP in the carotid artery of a rat.
(a) Sagittal ^{13}C MRI (color) acquired after injection of hyp-HEP (acquisition time 0.15 s), overlaid on ^{1}H MRI (gray). Strong ^{13}C signal was observed after the injection of ~ 1 ml of hyperpolarized solution in the carotid artery. (c) After the decay of the hyperpolarization, the only ^{13}C signal originates from the model solution (1 M ^{13}C acetate). (b) Picture of a rat for anatomical reference. Note the brain, spine and pooled blood from the incision in the ^{1}H image (c).
Experimental parameters: ^{13}C 2D Fast Imaging with Steady State Precession (FISP) projection, in-plane resolution $(4 \cdot 4)$ mm^2, TR = 3.2 ms, TE = 1.6 ms, measurement time 154 ms per slice. ^{1}H 3D FISP, $(1.2 \cdot 1.2 \cdot 5)$ mm^3, TR = 10 ms, TE = 5 ms, measurement time 1.6 s per slice.

First experiment: Injection in carotid artery.

A volume of V ≈ 1 ml of hyp-HEP (c = 30 mM) was injected in the carotid artery of rat No. 1 (Fig. 40). Enhanced ^{13}C NMR signal was detected in the region of the head with a 2D FISP sequence (Fast Imaging with Steady State Precession, projection, in-plane resolution $(4 \cdot 4)$ mm^2, TR = 3.2 ms, TE = 1.6 ms). This demonstrates the feasibility to detect ^{13}C signal of hyperpolarized HEP *in vivo*, despite the suboptimal equipment. A ^{1}H MR image was acquired afterwards for anatomical correlation (3D FISP, resolution $(1.2 \cdot 1.2 \cdot 5)$ mm^3, TR = 10 ms, TE = 5 ms).

Second experiment: Injection in tail vein

Two ml of hyperpolarized HEP was injected in the tail vein of rat No. 2 (Fig. 41). ^{13}C images were acquired and overlaid on ^{1}H proton images (^{13}C 2D projection FISP, TE = 1.6 ms, TR = 3.2 ms, in-plane resolution: $(3 \cdot 3)$ mm^2, ^{1}H 3D FISP, resolution $(0.9 \cdot 0.9 \cdot 4)$ mm^3, TR = 10 ms, TE = 5 ms).

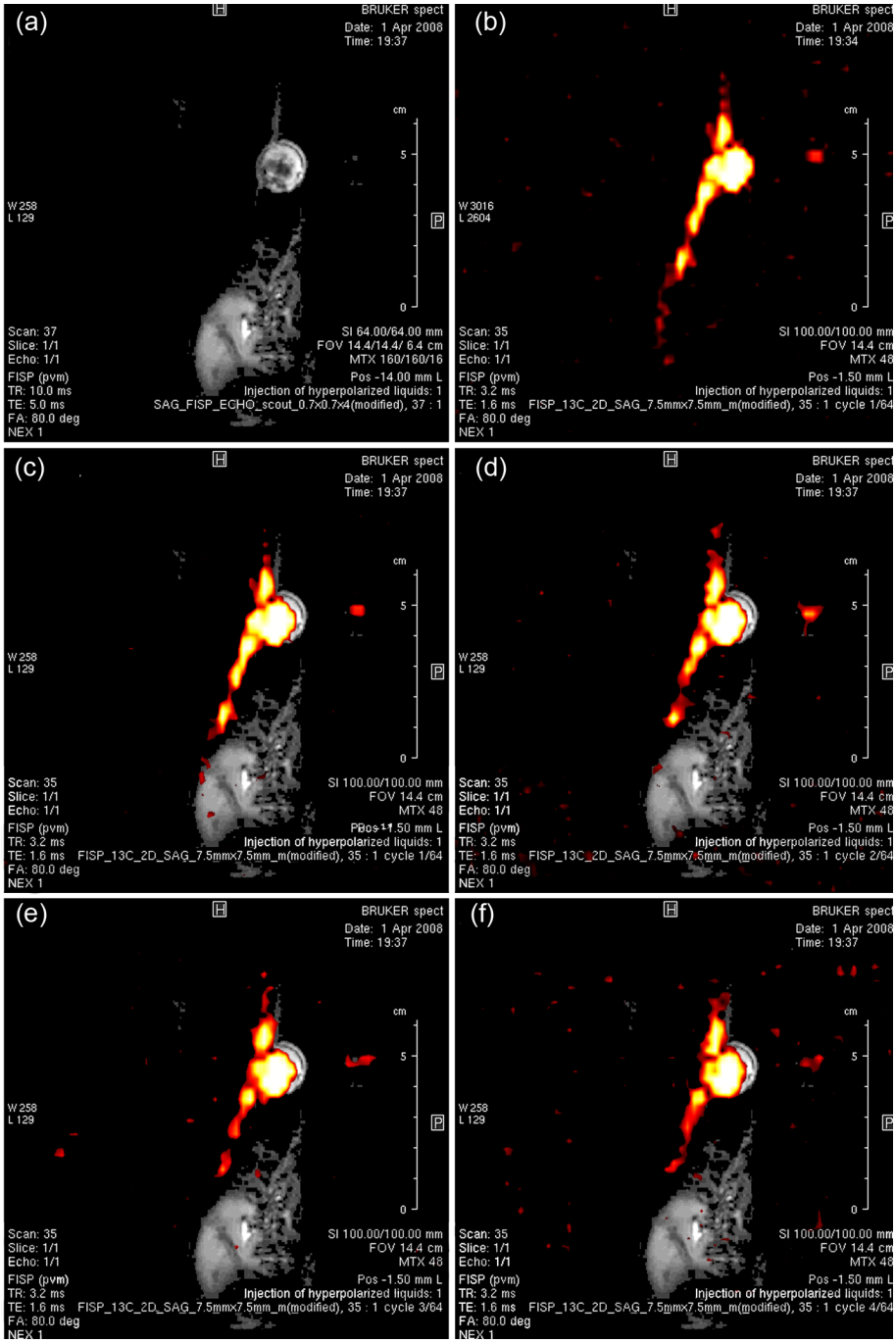

Fig. 41: Sagittal *in vivo* ^{13}C and ^{1}H MRI after injection of hyp-HEP in the tail vein of a rat.
(a) Morphological ^{1}H MRI (grey) of rat and spherical phantom (1 M ^{13}C acetate), acquired prior to the injection of the hyperpolarized agent, (b) ^{13}C image (color) acquired after administration of ~2 ml hyp-HEP in (acquisition time 0.15 s). (c) – (f) Overlay of ^{1}H and ^{13}C images, acquired in intervals of 0.15 s. Note the increase in ^{13}C noise as receiver gain is automatically adjusted to compensate the signal loss.
Experimental parameters: ^{13}C 2D Fast Imaging with Steady State Precession (FISP) projection, in-plane resolution $(3 \cdot 3)$ mm, TR = 3.2 ms, TE = 1.6 ms, measurement time 154 ms per slice. ^{1}H 3D FISP, resolution $(0.9 \cdot 0.9 \cdot 4)$ mm^3, TR = 10 ms, TE = 5 ms, measurement time 1.6 s per slice.

3.6.2 ^{13}C NMR experiments with hyperpolarized succinate in rats *in vivo*

^{13}C MR imaging experiments

Subsecond ^{13}C MRI (0.3 s per slice) was performed 9 s after close arterial injection of 1 ml of of hyperpolarized Suc (c = 25 mM) in a rat (Sprague Dawley, Fig. 42). The experiments were performed on a clinical B_0 = 1.5 T whole-body MR system. A coronal ^{13}C image was acquired and overlaid on a ^{1}H morphological image for anatomical reference (^{13}C 3D FIESTA, TR = 6.3 ms, TE = 3.1 ms, (5 · 5 · 5) mm^3 spatial resolution, FOV = 220 mm / 320 mm, 44 phase encoding steps / 64 readout points. MR No. 1, ^{13}C surface coil No. 6 and ^{1}H body resonator, section 2.6, 2.6.2, pp. 56).

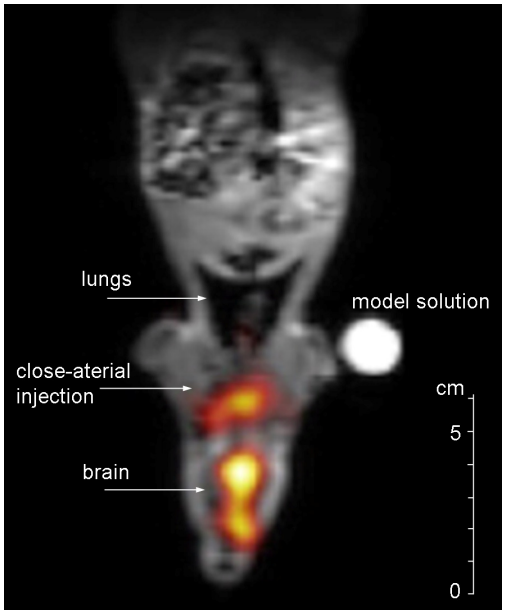

Fig. 42: Coronal *in vivo* ^{13}C and 1H MRI after close arterial injection of hyperpolarized succinate in a rat, overlaid on an anatomical ^{1}H MRI.
Subsecond coronal ^{13}C MRI image acquired 9 s after close-arterial injection of 1 ml hyperpolarized Suc (c = 25 mM, in color). The ^{13}C image was overlaid on a coronal ^{1}H fast gradient echo image with matching field-of-view (FOV) and slice location acquired prior to infusion to provide anatomical correlation (grey).
Experimental parameters: ^{13}C MRI sequence: 3D FIESTA, TR = 6.3 ms, TE = 3.1 ms, measurement time = 0.3 s per slice, (5 · 5 · 5) mm^3 spatial resolution, FOV = 220 mm / 320 mm, 44 phase encoding steps / 64 readout points, respectively. ^{1}H MRI sequence: fast gradient echo. Figure taken from [2].

^{13}C-MR spectroscopy experiments

A rat (Sprague Dawley) was prepared as described in the previous experiments. A volume of ~1 ml of hyp-Suc (c = 50 mM) was injected through a catheter in the carotid artery and monitored by unlocalized ^{13}C-MR spectroscopy (B_0 = 4.7 T, MR system No. 2, coil No. 2). A sphere containing 1-^{13}C acetate (c = 1 M, δ ≈ 184 ppm [63]) was placed next to the head within the sensitive region of the coil.

First experiment

Enhanced ^{13}C NMR signal was observed by serial unlocalized low-angle spectroscopy in intervals of TR = 5 s (t_{pulse}^{13C} = 200 µs, Figs. 43, 44, 45, 46)

^{13}C signal increase is observed for a total time of 55 s (corresponding to 20 spectra, Fig. 43). An increase of ^{13}C signal is observed in the first ten spectra, followed by a decay with exponential character (spectra 11 – 20, Fig. 44). The signals were quantified using a fitting routine [8, 9].

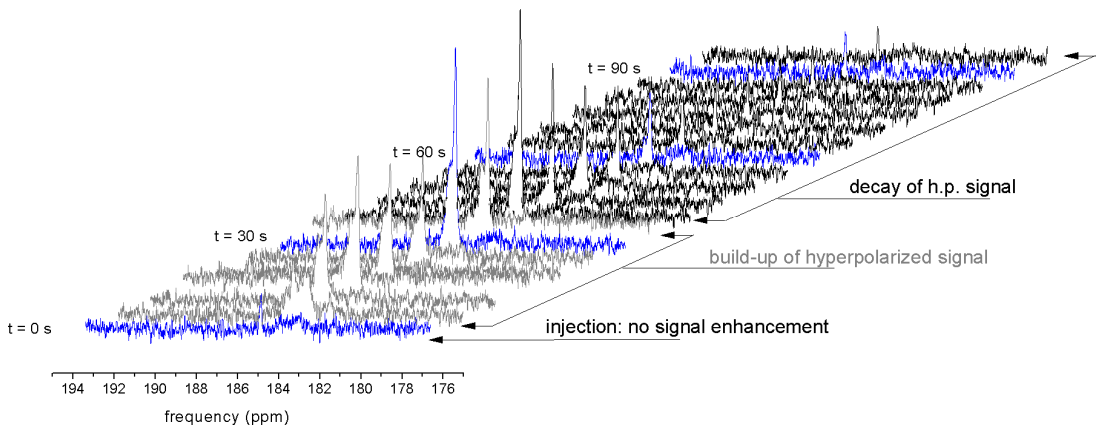

Fig. 43: Unlocalized serial *in-vivo* ^{13}C-NMR spectroscopy of a rat head after injection of hyperpolarized succinate in the carotid artery.
In vivo ^{13}C NMR spectra were acquired every 5 s for a total duration of 95 s after the injection of ~1 ml hyp-Suc (c = 50 mM) in the carotid artery of a rat. The head of the rat was in the sensitive region of the coil. The hyperpolarized ^{13}C signal is observed in 12 of 20 spectra (60 s).
Experimental parameters: ^{13}C pulse-and-collect sequence, NEX = 1, TR = 5 s, 15 Hz line broadening was applied prior to Fourier transform.

In order increase the SNR to identify potential metabolites (e.g. fumarate at $\delta = 177$ ppm), eleven spectra with enhanced ^{13}C signal and the same number of spectra without enhanced signal were averaged (Fig. 45). Small resonances are observed and are currently under investigation.

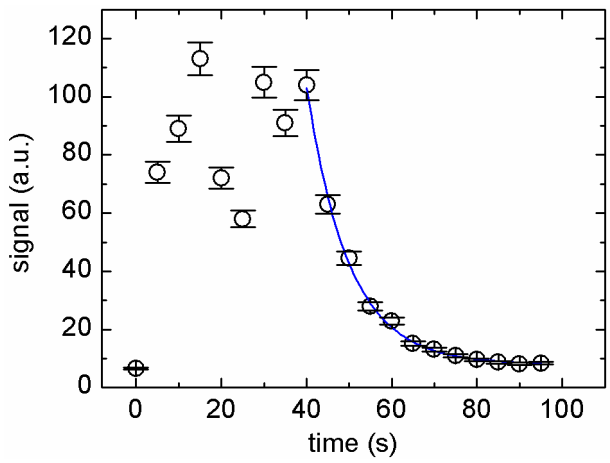

Fig. 44: Signal intensities of serial *in vivo* ^{13}C MR spectroscopy of hyp-Suc in a rat.
The intensities of hyp-Suc in spectra No. 9 to 20 (Fig. 44) decreased exponentially under the effect of relaxation, dilution, and continuous excitation (mono exponential fit: lifetime = 10 s).
Experimental parameters: 10 Hz line broadening was applied before Fourier transform. Quantification was performed with [8, 9].

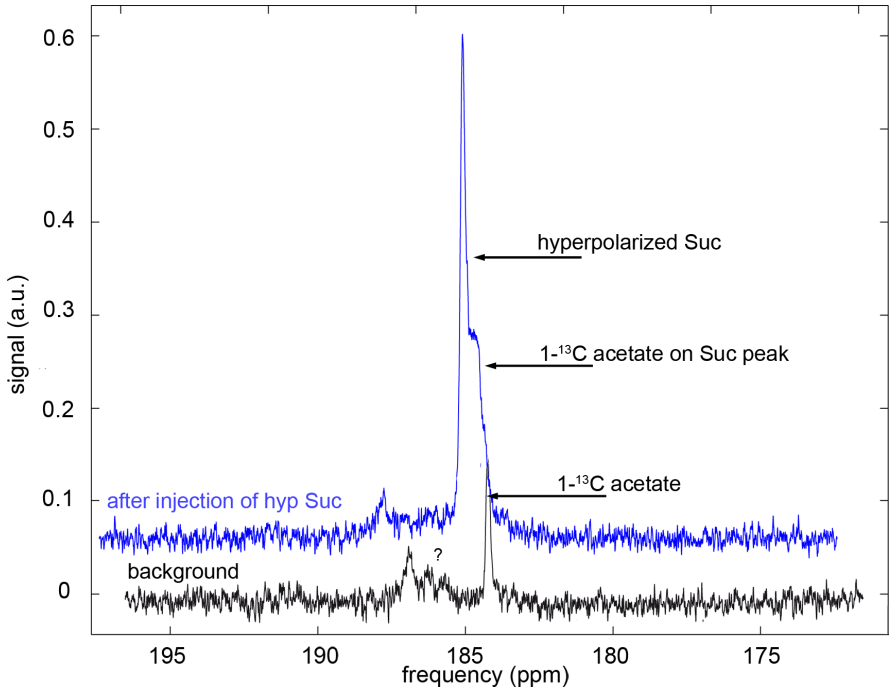

Fig. 45: Unlocalized *in vivo* ^{13}C MR spectroscopy of a rat head, acquired after injection of hyp-Suc in the carotid artery (blue) and background (black). Average of eleven spectra.
Unlocalized ^{13}C pulse-and-collect spectra were acquired every 5 s after the injection of ~1 ml hyp-Suc (c = 50 mM, Fig. 45). Increased ^{13}C signals was observed for 55 s (top, blue, average of 11 spectra). After the decay of the hyperpolarized signal, the background signal was acquired (bottom, black, average of 11 spectra), exhibiting the resonance of a 1 M acetate phantom (δ = 184 ppm), which is expected ~ 1 ppm lower frequency (right side) of the Suc (δ = 185 ppm) peak. The spectra were aligned to match the frequency assignments of Suc and acetate.
Experimental parameters: ^{13}C pulse-and-collect sequence, NEX = 1, TR = 5 s, 15 Hz line broadening was applied prior to Fourier transform. Average of 11 spectra shown. The spectra were aligned to match the frequency assignments of Suc and acetate.

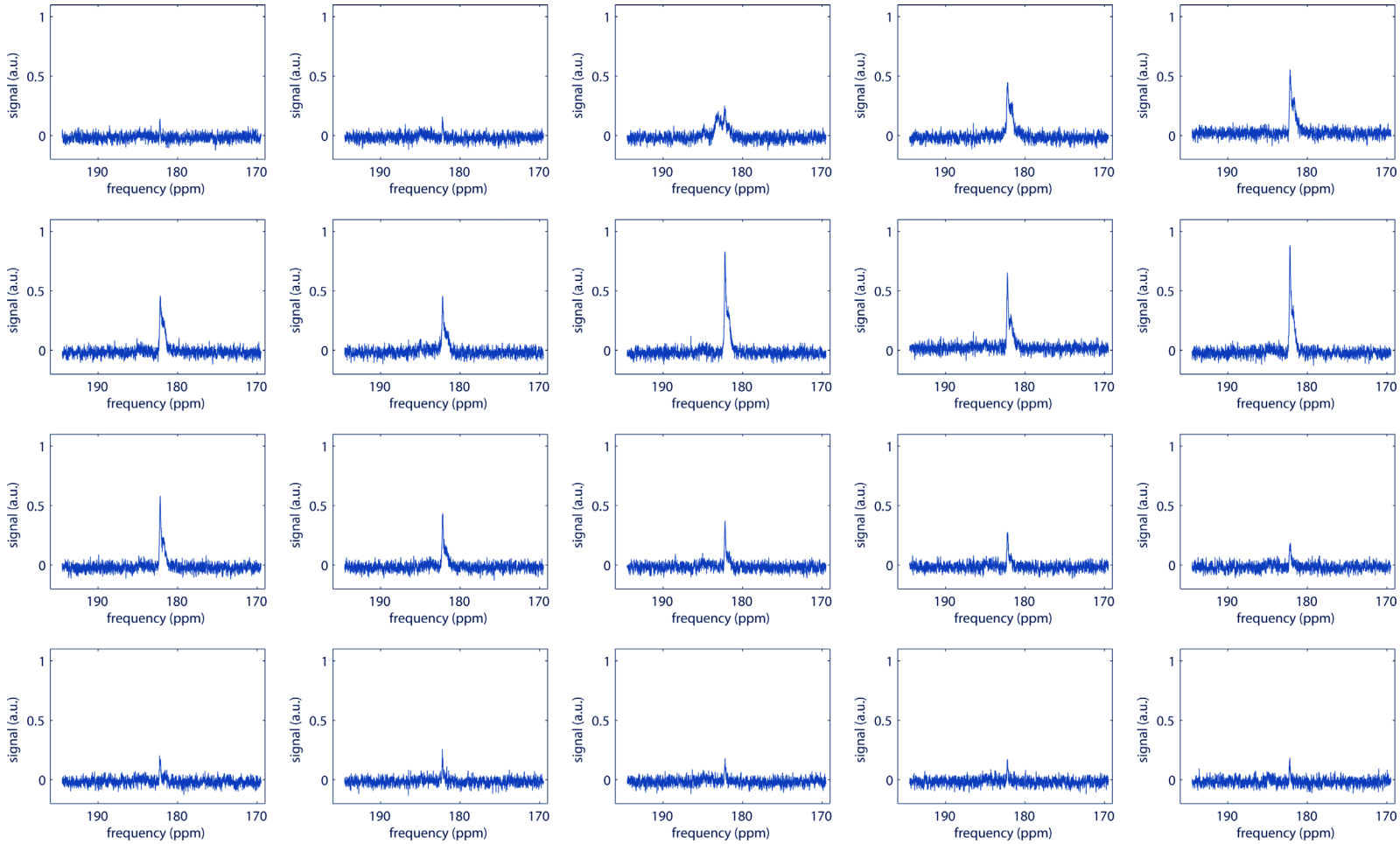

Fig. 46: Unlocalized serial *in vivo* ^{13}C MR spectroscopy of a rat head after injection of ~1 ml hyp-Suc (c = 50 mM) in the carotid artery. Individual spectra of Fig. 45. The peak of the acetate phantom lies on top of the increasing resonance oh hyp-Suc, e.g. in the third spectrum of the top row. *Experimental parameters:* ^{13}C pulse-and-collect sequence, NEX = 1, TR = 5 s, 15 Hz line broadening.

Second experiment

^{13}C signal acquisition was started $t = (30 \pm 2)$ s after the injection of hyp-Suc ($t_{pulse}^{13C} = 2$ ms, TR = 30 s). Enhanced ^{13}C signal was detected in the first 4 – 5 spectra (Fig. 48). While no peaks of metabolic products of hyp-Suc were clearly identified, there may be a resonance at the chemical shift of fumarate (δ = 177 ppm), which is the expected metabolic product of succinate in the TCA cycle (section 2.3.3, pp. 36, Fig. 47).

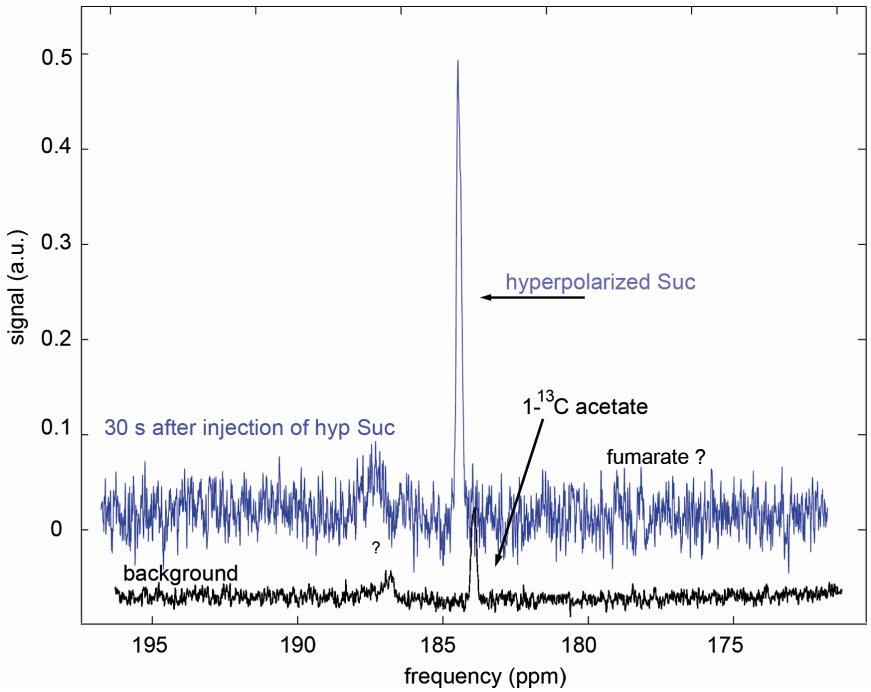

Fig. 47: Unlocalized *in vivo* ^{13}C MR spectroscopy of a rat head, acquired $t = (30 \pm 2)$ s after injection of hyperpolarized succinate in the carotid artery (blue) and background (black).
Acquisition of serial unlocalized ^{13}C spectra was started (30 ± 2) s after injection of hyp-Suc in a rat (TR = 30 s, pulse width $t_{pulse}^{13C} = 2$ ms). Enhanced ^{13}C signal was detected in the first four spectra, of which the first is shown above (blue). After decay of the signal, the background was acquired (black). There may be traces of hyperpolarized fumarate at ~177 ppm, the expected chemical shift of fumarate.
Experimental parameters: ^{13}C pulse-and-collect sequence, NEX = 1, TR = 30 s, 15 Hz line broadening. The ^{13}C excitation pulse width could not be calibrated for reasons described at the beginning of this chapter. The spectra were aligned to match the frequency assignments of Suc and acetate.

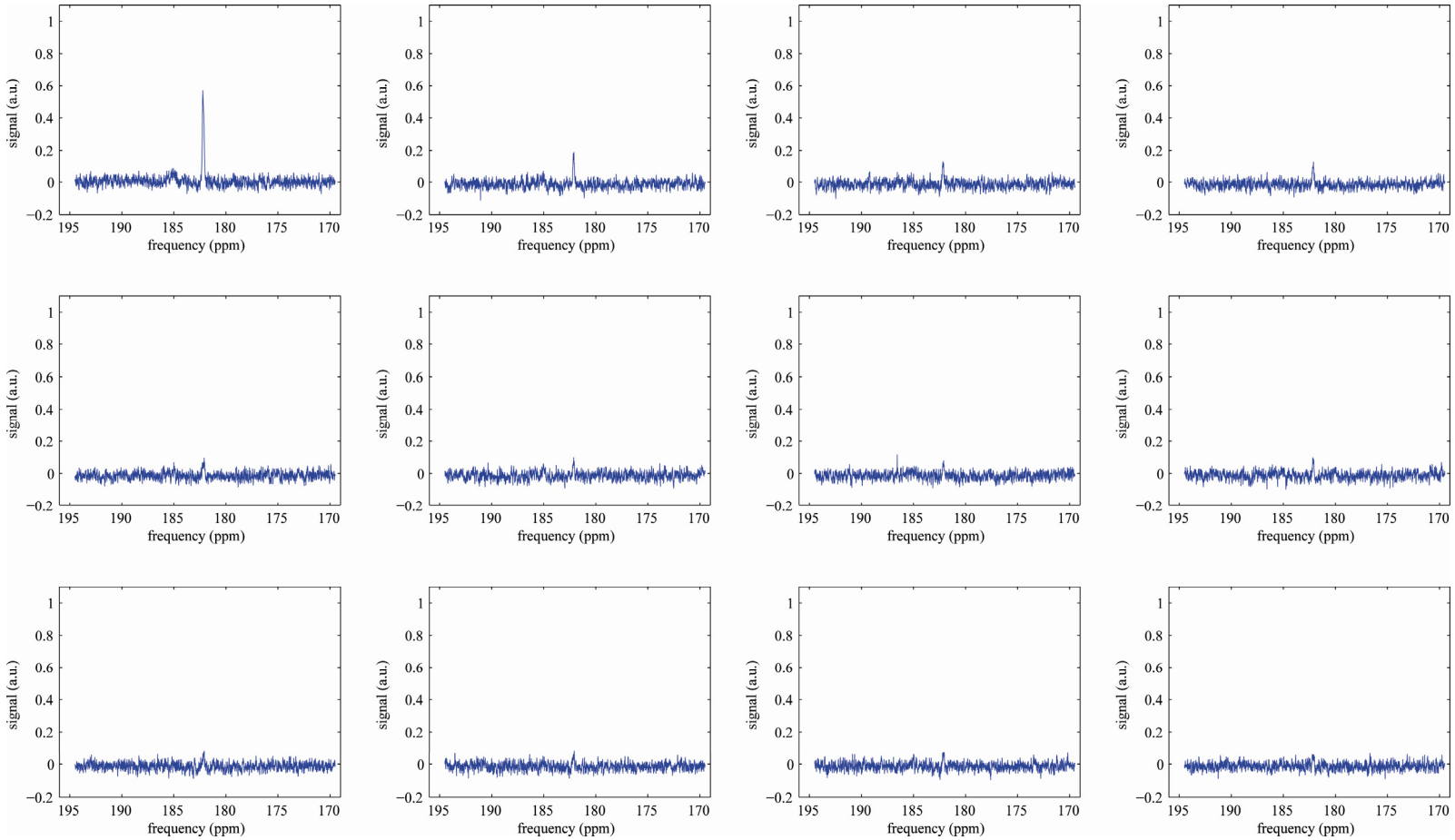

Fig. 48: Unlocalized *in-vivo* ^{13}C-MR spectroscopy of a rat head, acquired (30 ± 2) s after injection of hyperpolarized succinate in the carotid artery
Unlocalized ^{13}C spectra were acquired in intervals of 30 s starting (30 ±2) s after ~1 ml hyp-Suc (c = 50 mM) was injected into the carotid artery of a rat. Hyperpolarized signal is observed in the first 4 – 5 spectra.
Experimental parameters: ^{13}C pulse-and-collect sequence, NEX = 1, TR = 30 s, 15 Hz line broadening was applied prior to Fourier transform. The ^{13}C excitation pulse width could not be calibrated for reasons described at the beginning of this chapter. The spectra were aligned to match the frequency assignments of Suc and acetate.

3.6.3 Application of hyperpolarized Suc in cell cultures

The detection of metabolic products through the enhanced sensitivity of hyperpolarization may permit to characterize differential metabolism of cancer and control cell lines, potentially allowing systematic screening and classification. The feasibility of hyperpolarized MR of cell cultures was investigated in three steps:

(1) The detection of metabolic products of cell lines exposed to 1-^{13}C glucose and succinate was demonstrated with high resolution ^{13}C NMR spectroscopy (MR 6).

(2) These experiments were repeated for pancreatic cancer cells and human embryonic kidney cells 293 (HEK) in an MR compatible incubator developed for hyperpolarization experiments (MR system 2). Six hrs after exposure to 1-^{13}C glucose or succinate, the resonances of lactate, a marker for anaerobic metabolism, were detected by unlocalized ^{13}C spectroscopy (NEX = 8192, TR = 2.5 s, B_0 = 4.7 T). This proved the viability of the cells in the MR incubator.

(3) NMR acquisition was performed while the cells were exposed to hyperpolarized succinate. These results are presented in the following.

Experimental procedure

12 ml nutrient - free solution containing spheroids of ~ $20 \cdot 10^6$ HEK cells were filled into the bioreactor of MR incubator No. 1 (MR system No. 2). 1 ml of saturated pH 7 phosphate buffer was added, to maintain a neutral pH after injection of succinate. A volume of 2 ml of hyperpolarized succinate (c = 30 mM, pH 3) was injected into the rotating bioreactor, and an unlocalized ^{13}C low-angle pulse-and-collect sequence was started (TR = 5 s, $\alpha \sim 10°$, no rotation during acquisition). Strong ^{13}C signal enhancement was observed. The individual spectra are shown in Fig. 49 and Fig. 51. The average of the first ten spectra is provided in Fig. 50. An exponential fit (Eq. 63) of the signal intensities yielded the lifetime of the polarization: $T_1 = (55.8 \pm 1.5)$ s (Fig. 49 b, Tab. 10). After the experiment, pH 6.7 was measured in the sample.

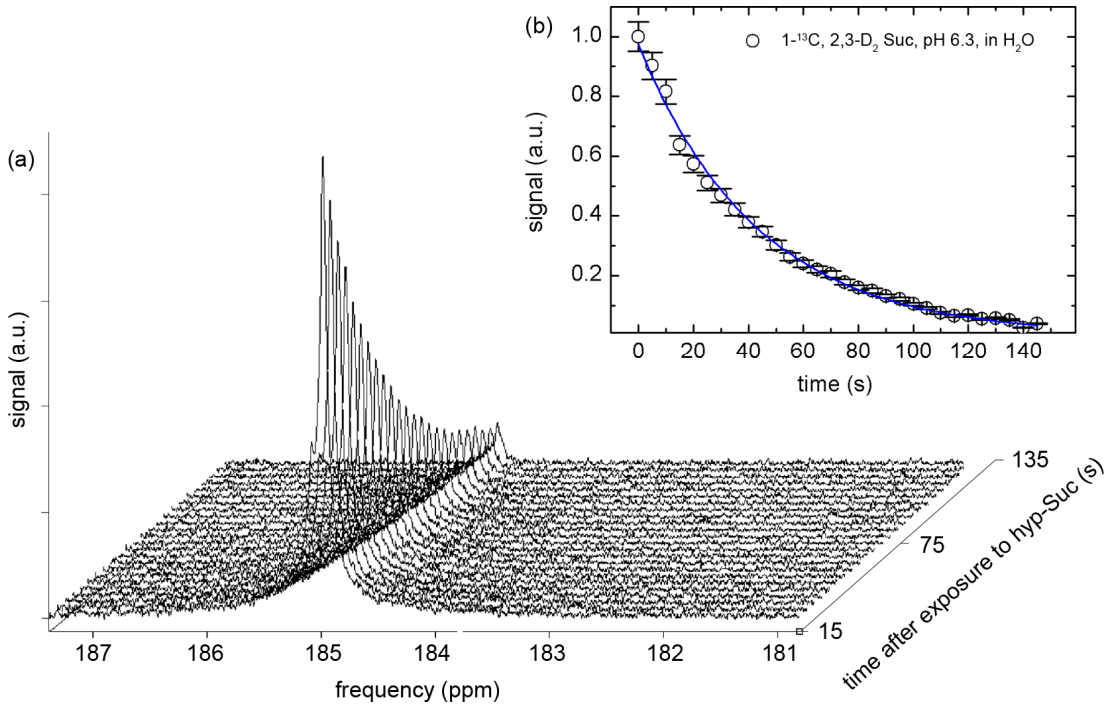

Fig. 49: Unlocalized serial *in vivo* ^{13}C MR spectroscopy of hyp-Suc in cell culture.
(a) ~1 ml hyperpolarized (c = 30 mM) 1-^{13}C, 2,3-D_2 succinate was administered to spheroids formed by ~$2 \cdot 10^6$ Human Embryonic Kidney cells (HEK 293). 15 s after administration of hyp-Suc, ^{13}C NMR spectra were acquired in intervals of TR = 5 s for a total duration of 120 s. Strong ^{13}C signal enhancement is observed. The individual spectra are shown in Fig. 51.
(b) An exponential function (Eq. 63) was fitted to the normalized signal intensities of (a): The lifetime of the polarization was calculated to T_1 = (55.8 ± 1.5) s (Tab. 10).
Experimental parameters: ^{13}C unlocalized low-angle (α ~ 10°) pulse-and-collect sequence, TR = 5 s, 1 Hz line broadening. MR incubator No. 1 in MR system No. 2. Temperature of the cells: T = (37.0 ± 0.5) °C. Rotation of the bioreactor was off during acquisition.

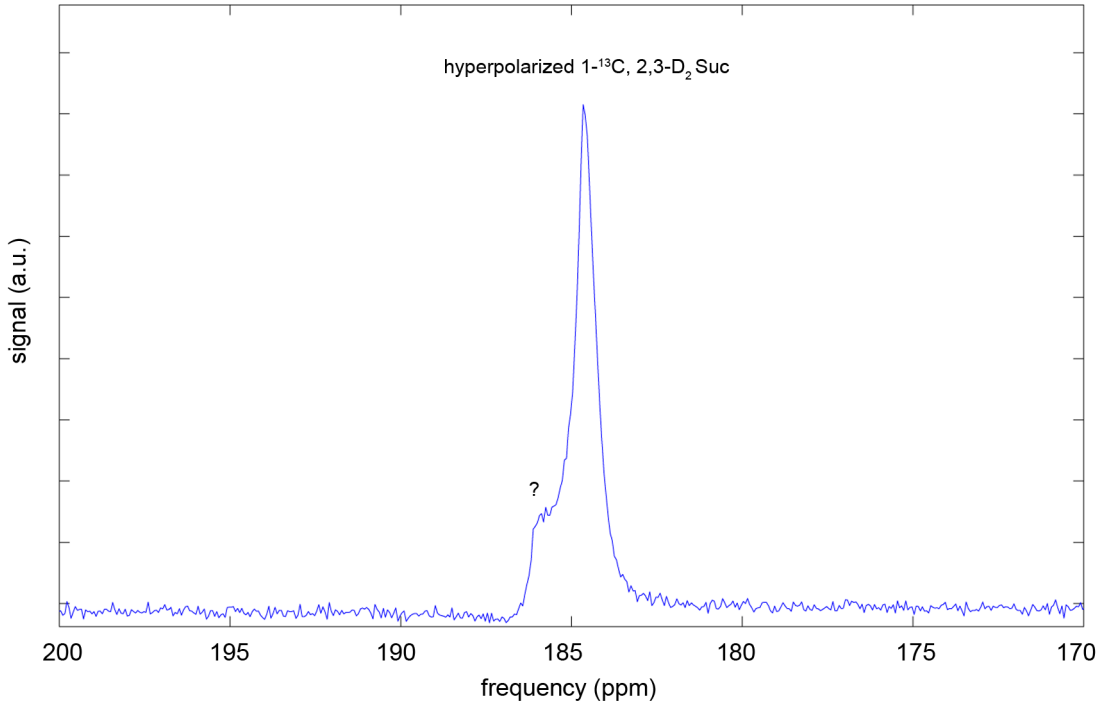

Fig. 50: Unlocalized *in vivo* ^{13}C MR spectroscopy of hyp-Suc in cell culture, average of 10 spectra. Hyperpolarized 1-^{13}C, 2,3-D_2 succinate (~1 ml, c = 30 mM) was administered to ~ $20 \cdot 10^6$ spheroids of Human Embryonic Kidney cells (HEK 293). 15 s after administration of hyp-Suc, ^{13}C NMR spectra were acquired in intervals of TR = 5 s for a total duration of 120 s. The average of the first ten spectra is shown here.
Experimental parameters: unlocalized low angle (α ~10°) pulse-and-collect sequence, 1 Hz line broadening. MR incubator No. 1 in MR system No. 2. Temperature of the cells: T = (37.0 ± 0.5) °C. Rotation of the bioreactor was off during acquisition.

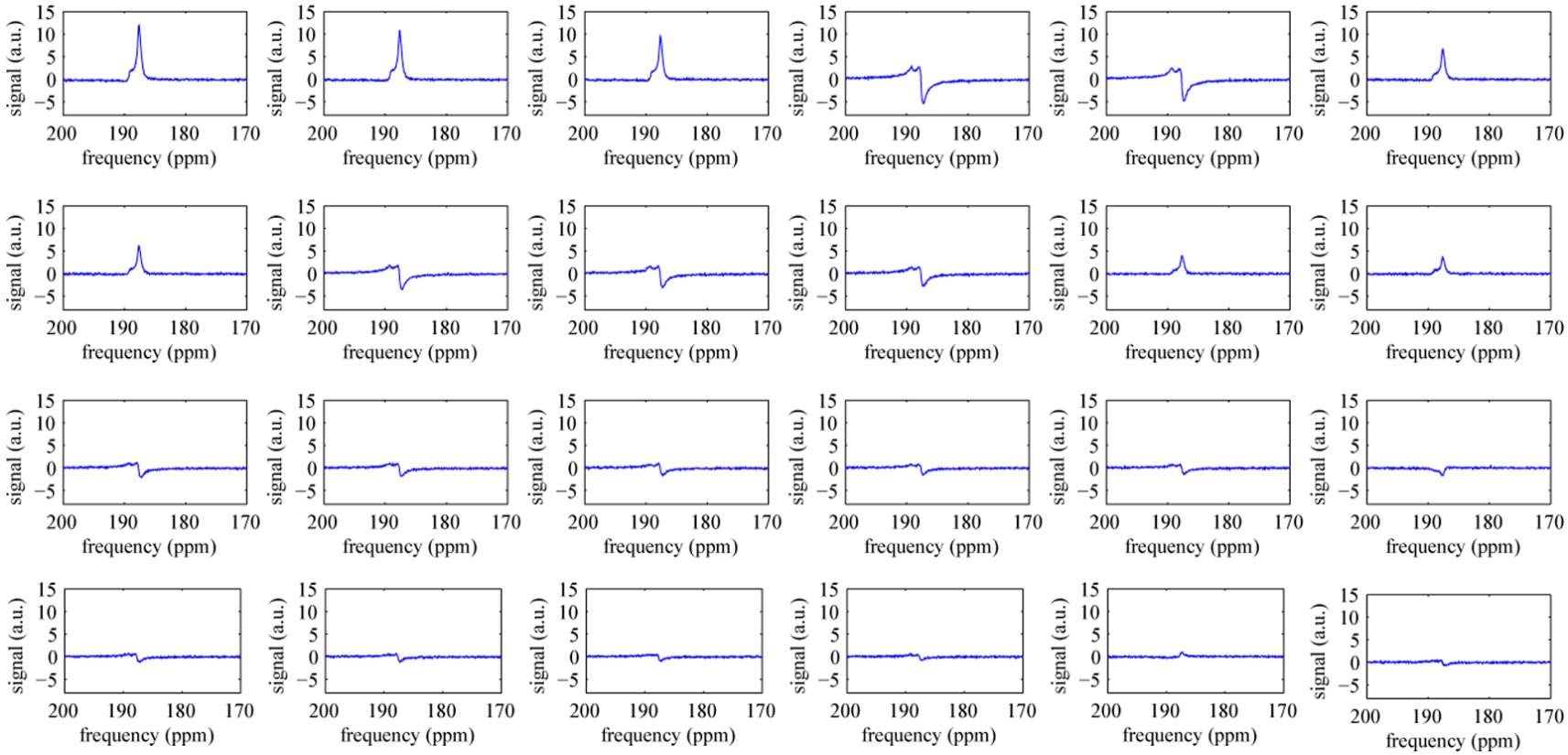

Fig. 51: Unlocalized serial *in-vivo* ^{13}C-NMR spectroscopy of hyp-Suc in cell culture.
Hyperpolarized 1-^{13}C, 2,3-D_2 succinate (~1 ml, 30 mM) was administered to ~ $20 \cdot 10^6$ spheroids of Human Embryonic Kidney cells (HEK 293). 15 s after administration of hyp-Suc, ^{13}C NMR spectra were acquired in intervals of TR = 5 s for a total duration of 120 s. The reason for the phase jumps is unknown.
Experimental parameters: Unlocalized low angle (~10°) pulse-and-collect sequence, 1 Hz line broadening. MR incubator No. 1 in MR system No. 2. Temperature of the cells: T = 37 °C. Rotation of the bioreactor was off during acquisition.

Chapter 4: Summary and Discussion

To integrate the present work into the scientific context, this chapter starts with a brief overview of spin hyperpolarization in biomedical research, together with a short summary. A detailed discussion of the key results of this work is given in the following three sections, namely (1) the PASADENA polarizer, (2) new biologically relevant molecules, and (3) the *in vivo* application of hyperpolarized PASADENA agents.

PASADENA hyperpolarization in biomedical research.

A general perspective and summary of the present work.

Nuclear Magnetic Resonance (NMR) is extensively applied in diagnostic imaging and for studies of biochemistry *in vivo*. The major limitation of NMR is the low sensitivity, which is a consequence of low thermal polarization (caused by the extremely small nuclear magnetic moments): For example, only about one ppm of all ^{1}H spins in the detection volume contribute to the NMR signal (at $B_0 = 1.5$ T and room temperature). Therefore, *in vivo* ^{1}H MR spectroscopy (MRS) is limited to a chemical, spatial and temporal resolution of the order of *mM*, cm^3 and *min*.
Several promising methods aiming at an improved sensitivity of NMR, like magnetization transfer sequences or higher field strengths of B_0, operate within the constraints of thermal nuclear spin polarization and therefore provide only moderate increase of the signal to noise ratio (SNR) of the order of 2 – 10 fold.

Hyperpolarization techniques for gases, molecules in solid-state and in solution have demonstrated signal enhancement of several orders of magnitude by generation of large non-equilibrium nuclear polarization of the order of unity [16, 17, 64]. The resulting signal amplification will enable new applications, like imaging of metabolic processes *in vivo*. Even real-time biochemical information about the molecular basis of diseases could be obtained in the future by hyperpolarization of magnetic biomolecular tracers.

PASADENA ("Parahydrogen And Synthesis Allow Dramatically Enhanced Nuclear Alignment") [23] is unique in its ability to achieve hyperpolarization on the order of unity in liquid state within seconds. The technique employs the spin order of parahydrogen to produce large non-equilibrium hyperpolarization on ^{1}H or X nuclei, for example ^{15}N, ^{19}F, ^{31}P or ^{13}C (used here). The method employed in this work consists of two major steps: (a) the catalytic addition of parahydrogen to an unsaturated bond of a precursor molecule and (b) the application of an r.f. spin-order-transfer (SOT) sequence to generate hyperpolarization on the dedicated nucleus.

Contrary to other Dynamic Nuclear Polarization (DNP) techniques, PASADENA achieves hyperpolarization at T = 60 °C within seconds (DNP: solid-state, hours at T ~ 10 K). Also, PASADENA is less expensive since no superconducting magnet, microwave source and liquid-He cryostat is required as for DNP.
On the other hand, while DNP polarizers are commercially available and used by an increasing number of laboratories, PASADENA is presently installed only in very few places (<5). The instrumentation for PASADENA is neither commercially available nor published in scientific literature. Thus, the design of a suitable instrumentation setup was the purpose of the first part of this work:

> A polarizer for the PASADENA hyperpolarization of ^{13}C labeled molecules in solution was developed. The design is based on a prototype which was initially available in the

laboratory. High non-equilibrium polarization $P > 0.1$ was achieved repeatedly in intervals of three min, using HEP[1] in 1 – 5 ml aqueous solution [3].

Evidence of the utility of hyperpolarization techniques for *in vivo* research was demonstrated first in mid-1990s by hyp-^{3}He MRI of the airways in humans [64]. *In vivo* angiography in animals using PASADENA hyperpolarized ^{13}C was done before with HEP and MDE[2] (in acetone solution), both toxic and without metabolic relevance [17, 35, 36]. Thus, in the second part of this work, new biologically relevant molecules were introduced to the PASADENA technique:

^{13}C PASADENA hyperpolarization $P \sim 0.1$ of 1-^{13}C, 2,3-D_2 succinate (Suc) [26] and the functional molecule 2,2,3,3-tetrafluoropropyl, 1-^{13}C 2,3,3-D_3 propionate (TFPP) [51] was achieved reproducibly [2]. Toxic intermediates present in earlier experiments [4] were avoided. Moreover, the lifetime of Suc polarization, which is crucial for application *in vivo*, could be increased ten-fold to $T_1 = (60 \pm 3)$ s. A proposition for the further extension of the pool of possible PASADENA agents, including a method to calculate the dynamics of the spin system exposed to the spin-order-transfer sequence, is provided.

The new instrument, methods and molecules permitted the demonstration of the utility of PASADENA for *in vivo* applications, were studied in the third part of this work:

The disposition of the hyperpolarized agents Suc and HEP was detected by ^{13}C MR imaging (MRI) and spectroscopy (MRS) in animals (rats) *in vivo* and cell cultures. In all experiments, strong ^{13}C NMR signal enhancement was observed. The proof-of-principle for the feasibility of PASADENA hyperpolarization of biologically relevant molecules *in vivo* was established.

Parts of this work were published in [26] and submitted in the manuscripts [2, 3, 27, 51], respectively.

[1] 2-hydroxyethyl 1-^{13}C, 2,3,3-D_3 propionate
[2] maleic acid dimethyl ester

The PASADENA polarizer

Summary

A polarizer for PASADENA spin hyperpolarization of biologically relevant ^{13}C molecules in aqueous solution was developed [3]. The design was based on a prototype built by the group of Goldman *et al.* in Malmø, Sweden, which transferred to HMRI in 2005 and was employed in the beginning of this work.
High ^{13}C spin-polarization of the order of $P = 0.1$ was achieved regularly on molecules in aqueous solution. Volumes of 1 - 5 ml were produced in intervals of 3 min (section 3.1, pp. 65) [2, 66]. Compared to the NMR signal from a thermally polarized ^{13}C sample at room temperature (293 K) and $B_0 = 1$ T ($P = 8.7 \cdot 10^{-7}$), this corresponds to a signal enhancement (η) of the order of $\eta = 10^5$. There is a distinct advantage in production time at comparable hyperpolarization yield compared to other methods (e.g. DNP). The apparatus has been in continuous use in the laboratory, providing hundreds of hyperpolarized samples with several different ^{13}C enriched agents.

The main features of the polarizer are:

Fluid control unit. Chemically resistant components permitted the use of solutions in a broad pH range, which is needed for biologically relevant PASADENA agents [26]. The hydrogenation reactor was completely redesigned to reduce the reaction volume and allow for a higher reaction pressure. A metallic nozzle, which sprayed reagent and parahydrogen into the reactor, was replaced by a newly developed port to avoid metal and also to improve the injection process. All other metal parts in the fluid lines were replaced by non-metallic components, avoiding the contact of metal to pH_2 and catalyst-precursor solution and providing enhanced reproducibility (section 2.4.1, pp. 41).

Low-field NMR unit. The homogeneity of the B_0 (shim) was markedly improved (10-fold) by reduction of the reactor size, the implementation of a precision DC power supply, and the removal of the injection nozzle. Also, a new pulse-amplifier allowed for more stable and stronger r.f. pulses. Altogether, these modifications improved the performance of the low-field NMR unit strongly, resulting in a much more robust polarization yield (compare the coefficient of variance (c_v) of the polarization yield of the developed setup $c_v = 0.05$ (n = 3) to $c_v = 1.09$ of the prototype, section 2.4.2, pp. 43).

Process control unit. An experimental workflow for the PASADENA experiment was developed. Complete automation of hydrogenation, spin-order transfer, sample delivery and NMR acquisition trigger removes the need for a group of collaborating operators during the hyperpolarization experiment. The instrument now yields 1 – 5 ml of hyperpolarized 1-^{13}C succinate in intervals of three min with only one operator working at the apparatus (section 2.4.3, pp. 46).

Progress was also made in the chemistry of PASADENA. Mixing of reagents under nitrogen atmosphere and the preparation of the catalyst for each series of experiments removed a serious source of instability. While earlier works employed pure acetone as solvent [35], only ~1 vol. % of acetone were needed for the preparation of the catalyst-precursor solution. This fraction was further reduced by evacuation before the solution was hyperpolarized and administered *in vivo*. Now, the acetone content which is very low does no longer prevent *in vivo* application of PASADENA agents.

Limitations and future improvements

80 % of the theoretically possible signal enhancement by hyperpolarization were readily achieved with the new device. Thus, future improvements are in the order of a factor of ten. Besides further signal enhancement, measures to improve the reliability and handling of the entire PASADENA experiment are crucial for routine application of PASADENA.

Mainly three factors have an impact on reproducibility and outcome of PASADENA hyperpolarization:

(a) The primary source of spin order: parahydrogen,
(b) the hydrogenation of the precursor molecule,
(c) the spin-order-transfer (SOT) sequence.

A review and discussion of these steps is given in the following.

(a) parahydrogen.
The maximal possible hyperpolarization ($P = 1$) depends on the purity of parahydrogen (pH_2 fraction $f(pH_2)$):

$$P\left(pH_2\right) = f\left(pH_2\right) - \tfrac{1}{3} f\left(oH_2\right) \tag{68}$$

where $f(pH_2) + f(oH_2) = 1$ (section 1.3.1, pp. 12 and [67]).
The equipment employed in this work provides a pH_2 fraction $f(pH_2) > 0.9$ (section 2.1, pp. 30). This corresponds to a maximal possible hyperpolarization degree of $P(pH_2) > 0.86$ (with $f(pH_2) > 0.9$ in Eq. 68). Purities $f(pH_2) > 0.99$ were obtained by other investigators (not related to PASADENA) [7], yet the resulting gain of P is only moderate (e.g. by implementation of an exact temperature control of the ortho – para conversion chamber).

A significant advancement would be a device that continuously monitors the pH_2 fraction prior to each PASADENA experiment, to avoid unexpected loss of pH_2 enrichment. This can be realized by measuring the difference of the specific heat of the pH_2 and oH_2 fraction within the polarizer: This measure could markedly improve the reliability for routine application of PASADENA.

(b) hydrogenation reaction.
The hydrogenation reaction transfers the spin order of the parahydrogen to the molecule. Only molecules, which are hydrogenated in the reaction time (t_r) before the spin-order-transfer sequence is applied, will be hyperpolarized (here $t_r = 4$ s). Therefore, the performance of the hydrogenation catalyst is crucial for the hyperpolarization yield.
Under the actual conditions, the hydrogenation reaction was deemed to be complete within the reaction time $t_r = 4$ s (at p = 10 bar pH_2 and T = 62 °C, and a catalyst-substrate ratio ~1). This is supported by the fact that no precursor signal was resolved by ^{13}C NMR spectroscopy of the hydrogenated sample (NEX = 1024, $B_0 = 4.7$ T).
A decrease in polarization yield was observed if the catalyst-precursor solution was older than ten hours or extensively exposed to air: This is explained by the sensitivity of the Rhodium (Rh)-based catalyst to oxygen and moisture. Individual preparation of the catalyst solution for each experimental series under protective atmosphere (e.g. N_2) avoided this effect.

For future experiments, faster hydrogenation as the consequence of another catalyst, higher reaction temperature and pressure, may lead to improvements of the hydrogenation efficacy and the degree of polarization. The main advancement, however, is expected by a complete automation of the preparation process. This would further reduce the exposure of the Rhodium catalyst to atmospheric oxygen, accelerate the process and reduce experimental variability (currently under development in this laboratory). The benefits of a solid-supported catalyst are discussed on page 109.

(c) spin-order transfer.
The spin-order transfer (SOT) from pH_2 to a labeled nucleus (here ^{13}C) is the essential step of PASADENA hyperpolarisation. It is achieved by a r.f. SOT sequence, which is adapted to the J-couplings of the hyperpolarized molecule. Thus, loss of polarization will occur by (1) a spin-order-transfer sequence based on inaccurate J-couplings, and (2) imperfect pulses.

> **Calculation of the SOT sequence.** To determine the effect of a SOT sequence calculated with inaccurate J-couplings, a simulation of the PASADENA experiment was performed (section 1.4, pp. 26). For $\Delta J = \pm 20$ %, the maximum depleteion of the polarization was 25 %. Thus, the hyperpolarization yield may be further improved through more accurately known coupling constants.
>
> **Application of the SOT sequence.** Obviously, the quality of the B_0 (homogeneity and stability) and B_1 (r.f. pulses) fields is pivotal for the effectiveness of the SOT and the hyperpolarization yield. It was shown experimentally that a B_0 offset by $\Delta B_0 = \pm 0.04$ mT caused ~ 50 % loss of polarization. This is already a significant improvement: using the prototype polarizer, no hyperpolarization was observed when the same offset was applied (section 3.4, pp. 77). This is proves the effectiveness of the new apparatus.

The following factors were identified to decrease the polarization yield:
The static field of the $B_0 = 4.7$ T MR unit perturbs the low-field NMR unit of the polarizer. In numbers, at a distance of (7.6 ± 0.1) m, the stray field of the unshielded magnet adds a horizontal component of ~ 0.1 mT to the vertical $B_0 \approx 1.7$ mT of the polarizer. Thus, the r.f. pulses are not perpendicular to the B_0 field, therefore suboptimal: This is manifested in a

complete loss of hyperpolarisation if the polarizer is moved to close proximity of the magnet. A shorter distance would decrease the delivery time of the hyperpolarized sample, and therefore increase the effective hyperpolarization available at the time of detection. Active (field compensation gradients) or passive shielding for the PASADENA polarizer are potential solutions under investigation in our laboratory.
Furthermore, the frequency difference between ^{13}C and ^{1}H is only $\Delta\nu = 54$ kHz at $B_0 = 1.7$ mT. Thus the r.f. pulses applied at the frequency of one spin species may also affect the other. Simulations suggest that the interactions between the ^{13}C and ^{1}H channels can be as large as 9 % under the conditions of the present study (V.A. Norton, personal communication). This problem can be solved by performing the hyperpolarization experiment at a higher field (e.g. $B_0 = \sim 10$ mT) and by designing small-band excitation pulses (currently under investigation) [68].

Altogether, it is assumed that the spin-order transfer process holds the largest potential to access the last remaining order of magnitude of polarization (e.g., shielding of the low-field NMR unit, or more accurate determination of the J-couplings).

New PASADENA agents

Summary

Spin hyperpolarization $P > 0.1$ by PASADENA was previously demonstrated only on the toxic molecule HEP and MDE [17, 25, 35]. For the first time, significant PASADENA hyperpolarization of a functional and biologically relevant molecule was achieved in this work:

> **1-^{13}C, 2,3-D$_2$ succinate** (Suc) is a promising PASADENA agent with the possible future application to the diagnostics of brain tumors (section 2.3.3, pp. 36) [4]. In contrast to earlier attempts by this laboratory [4], the lifetime of the hyperpolarization was significantly prolonged (10 – fold) [58], and toxic side-products were avoided (section 3.2, pp. 67) [26, 51].
>
> **2,2,3,3 tetrafluorropropyl 1-^{13}C, 2,3,3-D$_3$ propionate** (TFPP) is the first molecule to combine the functionality of a target-specific moiety (here: lipophilic) with the significantly increased MR signal of PASADENA. This opens the door for MR imaging of specific targets (e.g. plaque), harnessing the enhanced sensitivity of hyperpolarization (section 2.3.2, pp. 35) [51, 52].

Hyperpolarization of Suc was achieved repeatedly: A mean polarization $\overline{P}^{t=33s} = 0.064 \pm 0.002$ (n = 16, in D_2O) and $\overline{P}^{t=33s} = 0.054 \pm 0.004$ (n = 12, in H_2O) was detected in serial experiments, at the time $t_a = (33.0 \pm 0.5)$ s after the hyperpolarization was produced [3, 57]. Similar polarization was observed for TFPP (section 3.2, pp. 67). Based on the lifetimes of the polarization determined at $B_0 = 4.7$ T, the mean polarization for Suc at $t = 0$ was estimated to $\overline{P}^{t=33s} = 0.148 \pm 0.005$ (in D_2O) and $\overline{P}^{t=33s} = 0.129 \pm 0.009$ (in H_2O) (section 3.3, pp. 73) [2]. A simulation was developed to calculate Goldman's SOT sequence for new molecules (i.e. a given set of J-couplings).

Limitations and future improvements

The major hindrance for application of PASADENA polarized compounds *in vivo* – the lack of biologically relevant agents – has been resolved [26]. The biomedical or diagnostic value of PASADENA agents Suc and TFPP must now be explored. The extension of the pool of biologically relevant PASADENA agents is a major task:

(a) Precursor molecule
A major challenge is the identification of a stable precursor molecule, which can be hydrogenated rapidly. A suitable precursor will not exist for all molecules. Even if a precursor is identified, the synthesis of the isotopically labeled molecule is complex and expensive. This is the major restriction to the PASADENA technique.

(b) J-couplings
To generate an efficient spin-order-transfer sequence for a new molecule, the J-couplings in the compound pH_2-metabolite must be known. This is not considered a severe limitation to PASADENA since J-couplings can be measured accurately in liquid-state NMR.

(c) Spin-order transfer
The theories developed by Goldman and Johannesson [1] and Norton and Weitekamp [38] enable the calculation of efficient SOT sequences for any molecule. However, the programming of the SOT sequence is complex. Thus, the theoretical spin physics of the SOT sequence is not restricting the versatility of PASADENA.

Molecules currently under investigation in our laboratory are discussed in OUTLOOK (pp. 111).

Detection of ^{13}C hyperpolarization *in vivo*

Summary

The design of the polarizer [2, 3] and the functional and biologically relevant molecules [26, 51] represent an advancement of the PASADENA hyperpolarization technique towards biomedical application. The proof-of-principle of *in vivo* ^{13}C MRI and MRS using biologically relevant agents was established in the third part of this work:

> Strongly enhanced ^{13}C signal was detected after injection of hyperpolarized Suc and HEP in rats and cell lines *in vivo*: First MR images and spectra form 1-^{13}C, 2,3-D_2 Suc were obtained. Studies are in progress to identify the metabolic products of succinate in real-time hyperpolarization experiments (section 3.6, pp. 84).

Limitations and further improvements

The following improvements are envisaged for the routine application of PASADENA agents *in vivo*:

Minimization of polarization loss
The available *in vivo* NMR signal is reduced by the decay of hyperpolarization (time constant: T_1) during the time between production and injection of the hyperpolarized sample in the animal. Additionally, effects like dilution and relaxation in the tissue *in vivo* further reduce the detectable signal. Possible countermeasures are (a) prolongation of the lifetime T_1 and (b) shortening of time for transport of the sample.

> **(a) Strategies to prolong the T_1** [58]. A strong dependence of the hyperpolarization lifetime T_1 on pH and B_0 was observed. Transported of hyperpolarized Suc through low field (mT – T) in solution of H_2O or D_2O at pH 3 and neutralization prior to injection *in vivo* proved most efficient. After ~ 20 s of transportation through low field, a polarization degree of the order of $P \sim 0.1$ was observed, which was sufficient for the subsequent experiments.
>
> **(b) Shortening of the transportation time.** Deployment and operation of the polarizer in the proximity of the 4.7 T spectrometer to decrease the transportation time was already discussed in the beginning of this chapter. PASADENA hyperpolarization within the high field of the MR imager would not only minimize the delivery time, but also reduce the required PASADENA equipment significantly. However, the current theories for the SOT require a low magnetic field such that the chemical-shift between the protons are negligible. Therefore, to generate polarization by PASADENA within the B_0 magnet of a clinical MR scanner, a new theoretical approach is needed first.

Catalyst removal.
PASADENA, unlike other DNP techniques which use an electron donor in form of toxic radical initiators, requires a hydrogenation catalyst. Ideally, the catalyst would be removed at the completion of hydrogenation, and before r.f. spin-order-transfer sequence is applied. First data indicate, that interposition of an ion-exchange filter at the outlet of the polarizer can remove most of the rhodium. A solid-supported catalyst would overcome this problem entirely. Promising results in this respect were reported recently [69].

Sterility
of agent and entire apparatus is an important next step. One approach may be to replace the present construction by one consisting of disposable lines, reactor and isolated valves. A second approach, less expensive and equally readily achieved with the present PASADENA polarizer design is to substitute heat-resistant, autoclaveable components, or items which can be sterilized. A second, dismountable reaction chamber would allow for uninterrupted experimentation during sterilization of one reactor while the polarizer remains operational.

To conclude this section, the application of a biologically relevant PASADENA compound was demonstrated for the first time *in vivo*: In all MRI and MRS experiments, strong ^{13}C signal enhancement observed. This is an advancement of the PASADENA technique, and demonstrates the feasibility for biomedical research *in vivo.*
Future improvements are envisaged in the areas of faster sample delivery to avoid signal loss, removal of the catalyst prior to *in vivo* administration and sterility of apparatus and solution.

Chapter 5: Conclusions and Outlook

Conclusion

The developed PASADENA polarizer allows for hyperpolarization for biomolecules in aqueous solution in intervals of minutes, suitable for small animal research.
The strong hyperpolarization ($P \sim 0.1$) of 1-^{13}C, 2,3-D_2 succinate, a biomolecule with the potential application to the detection of brain tumors [2, 4, 26], qualifies for *in vivo* application. Moreover, the lifetime of succinate hyperpolarization was extended 10-fold: A much longer time span is now available for the ^{13}C label to penetrate metabolic processes *in vivo* [58]. Tetrafluorroproyl propionate (TFPP) was also hyperpolarized: It is the first *functional receptor-specific* agent, which harnesses the signal gain owing to PASADENA to specifically image a target (plaque, in this case) [52, 65].
A detailed description of the essential steps to extend the pool of PASADENA agents is provided, including a numerical method to calculate spin-order-transfer sequence.
The feasibility of biomedical research with the presented polarizer and *metabolic tracers* and *functional agents* was proven by ^{13}C MR imaging and spectroscopy *in vivo*. Altogether, the experimental fundament for routine biomedical *in vivo* studies by means of PASADENA was established.

Outlook

The extension of the pool of PASADENA agents remains a priority. The following potential PASADENA agents with biomedical significance were identified and are currently under investigation in our laboratory:

^{15}N-choline, a tumor marker in clinical ^{1}H MRS.
^{13}C-glucose, a basic energy source for cellular metabolism,
^{13}C-glutamine, an essential amino acid capable of passing over the blood-brain barrier
^{13}C-glutamate, another essential amino acid and neurotransmitter.

The handling and use of the PASADENA polarizer for routine biomedical application will be further improved by the suggested measures. Potential future innovations include hyperpolarization within a whole-body MR system, and continuous production of hyperpolarized samples.

Most interestingly, though, is the application *in vivo.* The metabolism of succinate (soon including the above mentioned agents) in a tumor (rat) using PASADENA hyperpolarized ^{13}C *in vivo* is currently under investigation: New parameters for diagnosis and treatment response of cancer may be derived [4, 70].

.

References

[1] Goldman M., and Johannesson H. (2005) Conversion of a Proton Pair Para Order into C-13 Polarization by Rf Irradiation, for Use in MRI. C.R. Phys. 6: 575-581.

[2] Hövener J.-B., Chekmenev E.Y., Norton V.A., Harris K.C., Perman W.H., Weitekamp D.P., Ross B.D., and Bhattacharya P. (2008) Quality Assurance of Pasadena Hyperpolarization for 13C Biomolecules. Magn. Reson. Mater. Phys. submitted.

[3] Hövener J.-B., Chekmenev E.Y., Norton V.A., Weitekamp R., Harris K.C., Perman W.H., Robertson L., Weitekamp D.P., Ross B.D., and Bhattacharya P. (2008) Pasadena Hyperpolarization of 13C Biomolecules: Equipment Design and Installation. Magn. Reson. Mater. Phys. submitted.

[4] Bhattacharya P., Chekmenev E.Y., Perman W.H., Harris K.C., Lin A.P., Norton V.A., Tan C.T., Ross B.D., and Weitekamp D.P. (2007) Towards Hyperpolarized 13C-Succinate Imaging of Brain Cancer. J. Magn. Reson. 186: 108-113.

[5] Ladriere L., Grue-Sorensen G., Bjorkling F., and Malaisse W.J. (1999) Metabolism of Glycerol-1,2,3-Trimethylsuccinate in Rat Hepatocytes. Mol. Cell. Biochem. 198: 135-139.

[6] Zhang Q.W., Zhang H., Lakshmi K.V., Lee D.K., Bradley C.H., and Wittebort R.J. (1998) Double and Triple Resonance Circuits for High-Frequency Probes. J. Magn. Reson. 132: 167-171.

[7] Tam S., and Fajardo M.E. (1999) Ortho/Para Hydrogen Converter for Rapid Deposition Matrix Isolation Spectroscopy. Rev. Sci. Instrum. 70: 1926-1932.

[8] Naressi A., Couturier C., Devos J.M., Janssen, M.,, Mangeat C., de Beer R., and Graveron-Demilly D. (2001) Java-Based Graphical User Interface for the Mrui Quantitation Package. Magn. Reson. Mater. Phys. 2-3: 141-52.

[9] Vanhamme L., van den Boogaart A., and Van Huffel S. (1997) Improved Method for Accurate and Efficient Quantification of MRS Data with Use of Prior Knowledge. J. Magn. Reson. 129: 35-43.

[10] Gerlach W., and Stern O. (1922) Das Magnetische Moment Des Silberatoms. Zeitschrift für Physik 9: 353-355.

[11] Rabi I.I., Zacharias J.R., Millman S., and Kusch P. (1938) A New Method Fro Measuring Nuclear Magnetic Moment. Phys. Rev. Lett. 53: 318.

[12] Bloch F. (1946) Nuclear Induction. Phys. Rev. Lett. 70: 460-474.

[13] Purcell E.M., Torrey H.C., and Pound R.V. (1946) Resonance Absorption by Nuclear Magnetic Moments in a Solid. Phys. Rev. Lett. 69: 37.

[14] Lauterbur P. (1973) Image Formation by Induced Local Interactions: Examples Employing Nuclear Magnetic Resonance. Nature 242: 190-191.

[15] Bachert P., Bellemann M.E., Layer G., Koch T., Semmler W., and Lorenz W. (1992) In Vivo 1H, 31P-{1H} and 13C-{1H} Magnetic Resonance Sectroscopy of Malignant Histocytoma and Skeletal Muscle Tussue in Man. NMR Biomed. 5: 161-170.

[16] Ardenkjaer-Larsen J.H., Fridlund B., Gram A., Hansson G., Hansson L., Lerche M.H., Servin R., Thaning M., and Golman K. (2003) Increase in Signal-to-Noise Ratio of > 10,000 Times in Liquid-State NMR. Proc. Natl. Acad. Sci. U. S. A. 100: 10158-10163.

[17] Golman K., Axelsson O., Johannesson H., Mansson S., Olofsson C., and Petersson J.S. (2001) Parahydrogen-Induced Polarization in Imaging: Subsecond C-13 Angiography. Magn. Reson. Med. 46: 1-5.

[18] Abragam A., and Goldman M. (1978) Principles of Dynamic Nuclear-Polarization. Rep. Prog. Phys. 41: 395-467.

[19] Comment A., Rentsch J., Kurdzesau F., Jannin S., Uffmann K., van Heeswijk R.B., Hautle P., Konter J.A., van den Brandt B., and van der Klink J.J. (2008) Producing over 100 Ml of Highly Concentrated Hyperpolarized Solution by Means of Dissolution Dnp J. Magn. Reson. 194: 152-155.

[20] Schroeder M., Cochlin L., Heather L., Clarke K., Radda G., Tyler D., and Shulman R. (2008) In Vivo Assessment of Pyruvate Dehydrogenase Flux in the Heart Using Hyperpolarized Carbon-13 Magnetic Resonance. Proc. Natl. Acad. Sci. U. S. A. 105: 12051-12056.

[21] Golman K., Petersson J.S., Magnusson P., Johansson E., Akselson P., Chai C., Hansson G., and Mansson S. (2008) Cardiac Metabolism Measured Noninvasively by Hyperpolarized 13C MRI. Magn. Reson. Med. 59: 1005-13.

[22] Bowers C.R., and Weitekamp D.P. (1986) Transformation of Symmetrization Order to Nuclear-Spin Magnetization by Chemical-Reaction and Nuclear-Magnetic-Resonance. Phys. Rev. Lett. 57: 2645-2648.

[23] Bowers C.R., and Weitekamp D.P. (1987) Para-Hydrogen and Synthesis Allow Dramatically Enhanced Nuclear Alignment. J. Am. Chem. Soc. 109: 5541-5542.

[24] Pravica M.G., and Weitekamp D.P. (1988) Net Nmr Alignment by Adiabatic Transport of Para-Hydrogen Addition-Products to High Magnetic-Field. Chem. Phys. Lett. 145: 255-258.

[25] Mansson S., Johansson E., Magnusson P., Chai C., Hansson G., Petersson J.S., Stahlberg F., and Golman K. (2006) 13C Imaging - a New Diagnostic Platform. Eur. Radiol. 16: 57-67.

[26] Chekmenev E.Y., Hövener J.-B., Norton V.A., Harris K.C., Batchelder L.S., Bhattacharya P., Ross B.D., and Weitekamp D.P. (2008) Pasadena Hyperpolarization of Succinic Acid for MRI and NMR Spectroscopy. J. Am. Chem. Soc. 130: 4212-4213.

[27] Perman W.H., Bhattacharya P., Leupold J., Lin A.P., Harris K.C., Norton V.A., Hövener J.-B., Weitekamp D.P., and Ross B.D. (2008) Fast Volumetric Spatial-Spectral Mr Imaging of Hyperpolarized 13C-Labeled Compounds Using Multiple Echo 3d Fiesta. J. Magn. Reson. Imaging submitted.

[28] Sakurai J.J., Modern Quantum Mechanics, Addison-Wesley Publishing Company, 1994.

[29] Abragam A., Principles of Nuclear Magnetism, Oxford University Press, London New York Toronto, 1985.

[30] Levitt M.H., Spin Dynamics, John Wiley and Sons Ltd., Chichester, GB, 2007.

[31] Schlichter C.P., Principles of Magnetic Resonance, Springer, Berlin Heidelberg New York, 1990.

[32] de Graaf R.A., In Vivo NMR Spectroscopy: Principles and Techniques, John Wiley & Sons Ltd, West Sussex, 2007.

[33] Eisenschmid T.C., Kirss R.U., Deutsch P.P., Hommeltoft S.I., Eisenberg R., Bargon J., Lawler R.G., and Balch A.L. (1987) Para Hydrogen Induced Polarization in Hydrogenation Reactions. J. Am. Chem. Soc. 109: 8089-8091.

[34] Hommeltoft S.I., Berry D.H., and Eisenberg R. (1986) A Metal-Centered Radical-Pair Mechanism for Alkyne Hydrogenation with a Binuclear Rhodium Hydride Complex - Cidnp without Organic Radicals. J. Am. Chem. Soc. 108: 5345-5347.

[35] Goldman M., Johannesson H., Axelsson O., and Karlsson M. (2006) Design and Implementation of C-13 Hyperpolarization from Para-Hydrogen, for New MRI Contrast Agents. C. R. Chim. 9: 357-363.

[36] Bhattacharya P., Harris K., Lin A.P., Mansson M., Norton V.A., Perman W.H., Weitekamp D.P., and Ross B.D. (2005) Ultra-Fast Three Dimensional Imaging of Hyperpolarized C-13 in Vivo. Magn. Reson. Mater. Phys. 18: 245-256.

[37] Mansson S., Johansson E., Magnusson P., Chai C.M., Hansson G., Petersson J.S., Stahlberg F., and Golman K. (2006) C-13 Imaging - a New Diagnostic Platform. Eur. Radiol. 16: 57-67.

[38] Norton V.A., and Weitekamp D.P., New Techniques for Interconversion of Non-Equilibrium Spin Order, Proceedings of the 48th Experimental NMR Conference, Asilomar, CA, USA, 2007.

[39] Bowers C.R., Pravica M.G., and Weitekamp D.P. (1989) Parahyrdrogen as a High Sensitivity Spin Lable for Catalysis. Abstracts of Papers of the American Chemical Society 197: 34-COLL.

[40] Brown J.M., Evans P.L., and Lucy A.R. (1987) Stereochemistry of Intermediates in Homogeneous Hydrogenation Catalyzed by Tristriphenylphosphinerhodium Chloride, Employing Nuclear-Magnetic-Resonance Magnetization Transfer. Journal of the Chemical Society-Perkin Transactions 2: 1589-1596.

[41] Hubler P., Natterer J., and Bargon J. (1998) Indirect Characterisation of Hydrogenation Intermediates Using Pasadena NMR Spectroscopy - Evolution of Zero-Quantum Coherence in Ab Spin Systems. PCCP 102: 364-369.

[42] Lopez-Serrano J., Duckett S.B., Aiken S., Lenero K.Q.A., Drent E., Dunne J.P., Konya D., and Whitwood A.C. (2007) A Para-Hydrogen Investigation of Palladium-Catalyzed Alkyne Hydrogenation. J. Am. Chem. Soc. 129: 6513-6527.

[43] G. van Rossum et al., Python Language Website, http://www.python.org.

[44] Oliphant T.E. (2007) Python for Scientific Computing. Computing in Science and Engineering 9: 10-20.

[45] Jones E., Oliphant T., Peterson P., and *al. e.* (2001) *Scipy:* Open Source Scientific Tools for *Python*.

[46] Bonhoeffer K.F., and Harteck P. (1929) Para- and Ortho Hydrogen. Zeitschrift Fur Physikalische Chemie-Abteilung B-Chemie Der Elementarprozesse Aufbau Der Materie 4: 113-141.

[47] Born M., and Heisenberg W. (1924) The Quantum Theory of Molecules. Annalen Der Physik 74: 1-31.

[48] Eucken A., and Hiller K. (1929) The Detection of the Conversion of Othohydrogen in Parahydrogen by Means of Measurement of the Specific Heat. Zeitschrift Fur Physikalische Chemie-Abteilung B-Chemie Der Elementarprozesse Aufbau Der Materie 4: 142-157.

[49] Gridnev I.D., Higashi N., Asakura K., and Imamoto T. (2000) Mechanism of Asymmetric Hydrogenation Catalyzed by a Rhodium Complex of (S,S)-1,2-Bis(Tert-Butylmethylphosphino)Ethane. Dihydride Mechanism of Asymmetric Hydrogenation. J. Am. Chem. Soc. 122: 7183-7194.

[50] Gridnev I.D., and Imamoto T. (2004) On the Mechanism of Stereoselection in Rh-Catalyzed Asymmetric Hydrogenation: A General Approach for Predicting the Sense of Enantioselectivity. Acc. Chem. Res. 37: 633-644.

[51] Chekmenev E.Y., Tofan D., Chow S.K., Hövener J.-B., Ross B.D., Weitekamp D.P., and Bhattacharya P. (2008) Towards Receptor Targeted 13C Hyperpolarized Mr Contrast Agents. J. Am. Chem. Soc. submitted.

[52] Chekmenev E.Y., Chow S.K., Tofan D., Weitekamp D.P., Ross B.D., and Bhattacharya P. (2008) Fluorine-19 NMR Chemical Shift Probes Molecular Binding to Lipid Membranes. J. Phys. Chem. 112: 6285-6287.

[53] Wikipedia, Citric Acid Cycle.

[54] Esteban M.A., and Maxwell P.H. (2005) Hif, a Missing Link between Metabolism and Cancer. Nat. Med. 11: 1047-1048.

[55] Rustin P. (2002) Mitochondria, from Cell Death to Proliferation. Nat. Genet. 30: 352-353.

[56] Rustin P., Munnich A., and Rotig A. (2002) Succinate Dehydrogenase and Human Diseases: New Insights into a Well-Known Enzyme. Europ. J. Hum. Genet. 10: 289-291.

[57] Hövener J.-B., Bhattacharya P., Chekmenev E.Y., Norton V.A., Perman W.H., Lin A.P., Harris K.C., Weitekamp D.P., and Ross B.D., Reproducibility and Quality Assurance in Hyperpolarized ^{13}C MRI and MRS Proceedings of the joint annual meeting of the ISMRM and ESMRMB, Berlin, Germany, 2007, pp. 278.

[58] Hövener J.-B., Strategies to Prolong the T_1 Time of Hyperpolarized Molecules, Proceedings of the 16th annual meeting of the International Society for Magentic Resonance in Medicine, Toronto, Canada, 2008, pp. 336.

[59] Smith S.A., Levante T.O., Meier B.H., and Ernst R.R. (1994) Computer-Simulations in Magnetic-Resonance - an Object-Oriented Programming Approach. J. Magn. Reson., Ser A 106: 75-105.

[60] Sauerwald T, Demmelmair H, and B K. (1997) Safety of Stable Isotope Use. Eur. J. Pediatr. 144, Suppl. 1: S12-S17.

[61] Bottomley P.A., Foster T.H., Argersinger R.E., and Pfeifer L.M. (1984) A Review of Normal Tissue Hydrogen NMR Relaxation Times and Relaxation Mechanism from 1-100 MHz: Dependence on Tissue Type, NMR Frequency, Temperature, Species, Excision, and Age. Med. Phys. 11: 425-448.

[62] Escanye J.M., Canet D., and Robert J. (1982) Frequency Dependence of Water Proton Longitudinal Nuclear Magnetic Relaxation Times in Mouse Tissues at 20 Degrees C. Biochim Biophys Acta 721: 305-11.

[63] Biological Magnetic Resonance Data Bank BMRB, Department of Chemsitry, University of Wisconsin-Madison, USA.

[64] Bachert P., Schad L.R., Bock M., Knopp M.V., Ebert M., Grossmann T., Heil W., Hofmann D., Surkau R., and Otten E.W. (1996) Nuclear Magentic Resonance Imaging of Airways in Humans with Use of Hyperpolarized 3he. Magn. Reson. Med. 36: 192-6.

[65] Chekmenev E.Y., Norton V.A., Hövener J.-B., Perman W.H., Reynolds W.F., Weitekamp D.P., Ross B.D., and Bhattacharya P., Hyperpolarized Pasadena 13C Tracers for True Mr Metabolic Imaging, Proceedings of the International Conference on Magnetic Resonance in Biological Systems, San Diego, CA, USA, 2008.

[66] Hövener J.-B., Chekmenev E.Y., Norton V.A., Weitekamp R.A., Harris K.C., Perman W.H., Robertson L.W., Ross B.D., Weitekamp D.P., and Bhattacharya P., Quality Assurance of Pasadena Hyperpolarization for ^{13}C Biomolecules, Proceedings of the 49th Experimental NMR Conference, Asilomar, CA, USA, 2008.

[67] Canet D., Aroulanda C., Mutzenhardt P., Aime S., Gobetto R., and Reineri F. (2006) Para-Hydrogen Enrichment and Hyperpolarization. Conc. Magn. Reson. A 28A: 321-330.

[68] Norton V.A., and Weitekamp D.P., Pulses for Low-Field NMR, Proceedings of the 49th Experimental NMR conference, Asilomar, CA, USA, 2008.

[69] Kovtunov K.V., I.E. B., V.I. B., and Koptyug I.V. (2008) Observation of Parahydrogen-Induced Polarization in Heterogeneous Hydrogenation on Supported Metal Catalysts. Angew. Chem. Int. Ed. 47: 1492-1495.

[70] Day S.E., Kettunen M.I., Gallagher F.A., Hun D.E., Lerche M., Wolber J., Golman K., Ardenkjaer-Larsen J.H., and Brindle K.M. (2007) Detecting Tumor Response to Treatment Using Hyperpolarized 13C Magnetic Resonance Imaging and Spectroscopy. Nat. Med. 13: 1382-1387.

Appendix I

Source code of “PASADENAintervals.py”

```
#!/usr/bin/env python
# -*- coding: utf-8 -*-

import numpy
import scipy
import pylab

from numpy import *
from scipy import *
from pylab import *

from scipy.linalg.matfuncs import *
print ‘\nFree-evolution intervals, and polarization yield of PASADENA
experiment,\nfollowing Goldman et. al., CR Physique (6) 2005, pp. 575.’
print ‘\n\t* input: J-couplings J12, J1S, J2S. \n\t* output: T1, t2, t3, P.\n’
print ‘\nThe following spin system and Hamiltonian are considered:\n\n\t*
3-spin-system: two spins (I1 I2)in the para-state, s is unordered (all l=1/2).’
print ‘\t* isotr. liqu. state Hamiltonian in low-field (no chemical shift), rotating
frame: \n\t\tH = J12*I1*I2 + J1S*I1zSy + J2S*I2z*Sz’

# guess of t2 interval
t2g=0.02

# input: J-couplings
J12HEP=7.57
J1SHEP=7.24
J2SHEP=-5.62

J12Suc=7.15
J1SSuc=-5.82
J2SSuc=7.41
J12=J12Suc
J1S=J1SSuc
J2S=J2SSuc
“”””
J12=J12HEP
J1S=J1SHEP
J2S=J2SHEP
“”””

# start calculations for T1, t3
print ‘_____’

a=0.5*(J1S-J2S)
b=J12
θ=arctan(b/a)
s=sin(θ)
c=cos(θ)
Ω=sqrt(a**2+b**2)

print ‘\nInput: J12=’, J12, ‘Hz, J1S=’, J1S, ‘Hz, J2S=’, J2S, ‘Hz’
print ‘\na=’,a,’Hz, \nb=’,b,’Hz, \nθ=’,θ*360/2/pi,’deg, \nΩ=’, Ω,’2pi Hz’

# calculate intervals T1, t3
T1=(1/(Ω*2*pi))* arccos((s*c*a/b-(s**2)) / (s*c*a/b+c**2) )
t3=pi/(Ω*2*pi)
print ‘\nT1 calculated..’
print ‘t3 calculated..’
print ‘optimize t2..\n’

# simulate PASADENA NMR experiment to determine t2
# setup basic matrices
ID2=mat(eye(2))
ID4=mat(eye(4))
ID8=mat(eye(8))
Ix=matrix([(0, 0.5),(0.5, 0)])
Iy=matrix([(0, -0.5j), (0.5j, 0)])
Iz=matrix([(0.5, 0), (0, -0.5)])
Iup=Ix+1j*Iy

# product operators for hydrogens
Ix1=2*kron(Ix, 0.5*ID2)
```

```
Iy1=2*kron(Iy, 0.5*ID2)
Iz1=2*kron(Iz, 0.5*ID2)
Ix2=2*kron(0.5*ID2, Ix)
Iy2=2*kron(0.5*ID2, Iy)
Iz2=2*kron(0.5*ID2, Iz)

# product operators for the whole system
I3x1=2*kron(2*kron(Ix, 0.5*ID2),0.5*ID2)
I3y1=2*kron(2*kron(Iy, 0.5*ID2), 0.5*ID2)
I3z1=2*kron(2*kron(Iz, 0.5*ID2), 0.5*ID2)
I3x2=2*kron(2*kron(0.5*ID2, Ix), 0.5*ID2)
I3y2=2*kron(2*kron(0.5*ID2, Iy), 0.5*ID2)
I3z2=2*kron(2*kron(0.5*ID2, Iz), 0.5*ID2)
S3x=2*kron(2*kron(0.5*ID2, 0.5*ID2), Ix)
S3y=2*kron(2*kron(0.5*ID2, 0.5*ID2), Iy)
S3z=2*kron(2*kron(0.5*ID2, 0.5*ID2), Iz)

I3x=I3x1+I3x2
I3y=I3y1+I3y2
I3z=I3z1+I3z2
S3up=S3x-1j*S3y

# Goldmans operators
Kx=I3x1*I3x2+I3y1*I3y2
Kz=0.5*(I3z1-I3z2)
Ky=I3y1*I3x2-I3x1*I3y2
omega=a*Kz +b*Kx
eta=b*Kz+a*Kx
etam=-b*Kz+a*Kx

# Eigen kets etc, as well done by kron product
up=transpose(matrix([(1, 0)]))
down=transpose(matrix([(0),(1)]))

evHH1=kron(up, up)
evHH2=kron(up, down)
evHH3=kron(down, up)
evHH4=kron(down, down)

evHHC1=kron(evHH2,up)
evHHC2=kron(evHH2, down)
evHHC3=kron(evHH3, up)
evHHC4=kron(evHH3, down)

# singlet kets
singlet2=1/sqrt(2)*(evHH2-evHH3)
singlet3up=1/sqrt(2)*(evHHC1-evHHC3)
singlet3down=1/sqrt(2)*(evHHC2-evHHC4)

#other variables
data=[]
POLdata=[]
i=0

# density matrix for whole system
density13C=0.5*ID2
r0=kron(singlet2*singlet2.H, density13C)

#r0=Kx/2 # Goldmans density operator
# Hamiltonian operator: Zeeman drops out -> field low enough that wa ~ wb
H=J12*(I3z1*I3z2+I3y1*I3y2+I3x1*I3x2) + J1S*I3z1*S3z + J2S*I3z2*S3z

# time evolution operators U for T1, t2, t3
U1=mat(expm2(-1j*2*pi*H*T1))
U2=mat(expm2(-1j*2*pi*H*t2g))
U3=mat(expm2(-1j*2*pi*H*t3))

# ideal pulses: rotation operators
pulse1=mat(expm2(-1j*pi*I3x))    # 180° Ix
pulse2=mat(expm2(-1j*(pi/2)*S3y))  # 90° Sy
pulse3=mat(expm2(-1j*(pi/2)*S3x))  # 90° Sx


# PASADENA sequence: three free-evolutions, three pulses
#*****************************************************

# 1. step of sequence. Evolve r0 for T1. .H gives transpose conjugate.
r1=U1*r0*U1.H

# 2. next in the sequence, pulse for 180 around Iy
r2=pulse1*r1*pulse1.H
```

```
# 3. now, evolve for t2 = 30ms
r3=U2*r2*U2.H

# 4. pulse 90y on S
r4=pulse2*r3*pulse2.H

# 5. evolve for t3
r5=U3*r4*U3.H

# 6. pulse 90x on S
r6=pulse3*r5*pulse3.H

# Now it should be polarized. Pulse 90°y S.
r7=pulse2*r6*pulse2.H

# Variation of the t2 interval to find optimum
t2a=arange(0, t2g+0.05, 0.001)

for t2i in t2a:
U2a=mat(expm2(-1j*2*pi*H*t2i))
# 3. now, evolve for t2 = 30ms
r3=U2a*r2*U2a.H

# pulse..
r4=pulse2*r3*pulse2.H

# 5. evolve for t3
r5=U3*r4*U3.H

# 6. pulse 90x on S
r6=pulse3*r5*pulse3.H

# Now it should be polarized. Do 90x° on S
r7=pulse2*r6*pulse2.H
P=2*abs(trace(r7*S3up))
#print 'P=',P, '\tt2=',t2i
POLdata.append(P+1j*t2i)
i=i+1

# take optimal t2 value
t2=imag(max(POLdata))
print 'done.'
print '_____'

# output
print '\n\nResults:\n\nT1 calculated', T1,'s'
print 't2 optimized', t2,'s'
print 't3 calculated', t3,'s'
print '\npolarization with guessed t2=',t2g,'s -> P=',2*abs(trace(r7*S3up))
print 'polarization with optimized t2=',imag(max(POLdata)),'s -> P=',
real(max(POLdata))
```

Output of program „PASADENAintervals.py“, for molecule HEP:

Free-evolution intervals, and polarization yield of PASADENA experiment, following Goldman et. al., CR Physique (6) 2005, pp. 575.

- input: J-couplings J12, J1S, J2S.
- output: T_1, t_2, t_3, P.

The following spin system and Hamiltonian are considered:

- 3-spin-system: two spins (I1 I2)in the para-state, s is unordered (all l=1/2).
- isotr. liqu. state Hamiltonian in low-field (no chemical shift), rotating frame:

H = J12*I1*I2 + J1S*I1zSy + J2S*I2z*Sz

Input: J12= 7.57 Hz, J1S= 7.24 Hz, J2S= -5.62 Hz
a= 6.43 Hz,
b= 7.57 Hz,
θ= 49.6552425683 deg,
Ω= 9.93226056847 2pi Hz

T_1 calculated..
t_3 calculated..
optimize t_2..

done.

Results:
T_1 calculated 0.0282828436447 s
t_2 optimized 0.036 s
t_3 calculated 0.0503410071205 s

polarization with guessed t_2= 0.02 s -> P= 0.452325967151
polarization with optimized t_2= 0.036 s -> P= 0.986749581139

Output of program „PASADENAintervals.py“, for molecule Suc:

Free-evolution intervals, and polarization yield of PASADENA experiment, following Goldman et. al., CR Physique (6) 2005, pp. 575.

- input: J-couplings J12, J1S, J2S.
- output: T_1, t_2, t_3, P.

The following spin system and Hamiltonian are considered:

- 3-spin-system: two spins (I1 I2)in the para-state, s is unordered (all l=1/2).
- isotr. liqu. state Hamiltonian in low-field (no chemical shift), rotating frame:

H = J12*I1*I2 + J1S*I1zSy + J2S*I2z*Sz

Input: J12= 7.41 Hz, J1S= –5.82 Hz, J2S= –7.15 Hz
a= -6.615 Hz,
b= 7.15 Hz,
θ= -47.2257770348 deg,
Ω= 9.74067374466 2pi Hz

T_1 calculated..
t_3 calculated..
optimize t_2..

done.

Results:
T_1 calculated 0.0270421045541 s
t_2 optimized 0.038 s
t_3 calculated 0.0513311515309 s

polarization with guessed t_2= 0.02 s -> P= 0.330696771796
polarization with optimized t_2= 0.038 s -> P= 0.99691598224

Source code of program „HypMetabolism.cc“uc:

```
#include <gamma.h>
#include
"/Users/janhoevener/Documents/Physik/programming/Gamma/Programs/includes
/PASADENAjb.cc"
#include
"/Users/janhoevener/Documents/Physik/programming/Gamma/Programs/includes
/polarized.cc"

using namespace std;
//This code simulates a polarized spin undergoing a molecular change in a bSSFP
sequence.
//This is realized in a chemical exchange process (defined by two rates, to and fro)
between two spins with different chemical shift (sys file), J-couplings (sys file),
relaxation rates (this code).
//To simulate a one-way process, as it may be the case when hyperpolarized media
are administered, the return rate is set to zero. As it turns out, the second signal
comes in antiphase.
//The signal of a bSSFP sequence is calculated, and exported in a matlab file.


int main(int argc, char*argv[])
{

//  ***************************************************Dialog
section*****************************************
int qn=1;
cout << "********* Simulation of bFFE sequencs with chemical exchange
*************\n\n";
cout << "********* Set up spin system *************\n\n";
//the sys file is read to obtain parameters.
// other parameters are acquired interactively:


sys_dynamic sys;

string filein("forKandR");
ask_set(argc, argv, qn++,
"\n\nSpin system filename ["+filein+"] ", filein);          // Ask for file or read file
sys.read(filein+".sys");
  string IsoD = "13C";//sys.symbol(2);                    // Get 1st spins isotope type

  double Kf = 100;                                  // Default spectral width
  ask_set(argc, argv, qn++,                         // Get the spectral width
"\n\tKf exchange - forward [100]? ", Kf);
   cout << "\t\t\t\t\t\t\tKf: " << Kf;          // Write the system t

 double Kr = 0;                                 // Default spectral width
  ask_set(argc, argv, qn++,                         // Get the spectral width
"\n\tk exchange - backwards [0]? ", Kr);
  cout << "\t\t\t\t\t\t\tKr: " << Kr;          // Write the system t

            double T1ofS0 = 1;                              // Default spectral width
  ask_set(argc, argv, qn++,                         // Get the spectral width
"\n\tT1 relaxation time of spin 0 [1s]? ", T1ofS0);
            cout << "\t\t\t\t\t\t\tT1 of spin0: " << T1ofS0;          // Write the system t

            double T1ofS1 = 1;                              // Default spectral width
  ask_set(argc, argv, qn++,                         // Get the spectral width
"\n\tT1 relaxation time of spin 1 [1s]? ", T1ofS1);
  cout << "\t\t\t\t\t\t\tT1 of spin1: " << T1ofS1;          // Write the syste m t

 double T2ofS0 = 0.1;                               // Default spectral width
  ask_set(argc, argv, qn++,                         // Get the spectral width
"\n\tT2 relaxation time of spin 0 [0.1s]? ", T2ofS0);
  cout << "\t\t\t\t\t\t\tT2 of Spin0: " << T2ofS0;          // Write the system t

           double T2ofS1 = 0.1;                             // Default spectral width
  ask_set(argc, argv, qn++,                         // Get the spectral width
"\n\tT2 relaxation time of spin 1 [0.1s]? « , T2ofS1);
cout << « \t\t\t\t\t\t\tT2 of S1: «  << T2ofS1;          // Write the system t
cout << « \n\n\n\t *****setup sequence********** »;
 double dwelltime = 0.001;                              // Default spectral width
  ask_set(argc, argv, qn++,                         // Get the spectral width
"\n\tdwelltime [0.001s]? ", dwelltime);
  cout << "\t\t\t\t\t\t\tdwell time: " << dwelltime;          // Write the system t

double Tr= 0.01;                                    // Default spectral width
  ask_set(argc, argv, qn++,                         // Get the spectral width
"\n\tTr [0.01s]? ", Tr);
```

```
   cout << "\t\t\t\t\t\t\tTr: " << Tr;          // Write the system t

double beta = 10;                                // Default spectral width
  ask_set(argc, argv, qn++,                      // Get the spectral width
"\n\tPreparation pulse beta [10deg]? ", beta);
  cout << "\t\t\t\t\t\tbeta: " << beta;          // Write the system t

double alpha = 20;                               // Default spectral width
  ask_set(argc, argv, qn++,                      // Get the spectral width
"\n\tFlip angle alpha [20deg]? « , alpha);
cout << »\t\t\t\t\t\talpha: «  << alpha;          // Write the system t
int datapoints(1);//(32768);
ask_set(argc, argv, qn++,                        // Get the spectral width
« \n\tdata points [1]? « , datapoints);
cout << « \t\t\t\t\t\tdatapoints: «  << datapoints;          // Write the system t
int acquisitions(128);//(32768);
ask_set(argc, argv, qn++,                        // Get the spectral width
« \n\tacquisitions [128]? « , acquisitions);
  cout << « \n\t\t\t\t\t\tacquisiton cycles «  << acquisitions;          // Write the
system t

  cout << « \n\t\t\t\t\t\tAcquisition time: «  << datapoints*dwelltime;          //
Write the system t


string domain="ftt";
ask_set(argc, argv, qn++,                        // Get the spectral width
"\n\n\tdisplay data in domain  [time] ", domain);
 cout << « \t\t\t\t\t\tdomain= «  << domain;          // Write the system t

 cout << "\n\n        ****** Simulation of bFFE sequence ******\n\n";

// ******** SET UP VARIABLES ********
int KfMax(16), i(0), iterations(0);
complex z(0);
row_vector fft(acquisitions);
matrix R(16,16), K(16,16), U(16,16), Uinv(16,16), RandK(16,16);
matrix data0(acquisitions, 1, complex0), data1(acquisitions, 1, complex0);
double R2ofS0(1/T2ofS0), R2ofS1(1/T2ofS1), R1ofS0(1/T1ofS0),
R1ofS1(1/T1ofS1);
double h(0.5);
complex ih(0,0.5);
int Kfint;

complex temp;
row_vector fidvector(acquisitions);
row_vector fid0(datapoints), fid1(datapoints);

//The time evolution is determined by the hamiltonian, the relaxation, and the
exchange. The according matrix representations are calculated here.
// The matrix are in jason space (easy-to-understand), which requires a
transformation into gamma space. This is accomplished with U.
// R = relaxation
// K = exchange
// U = basis transformation matrix: from easy-to-understand to gamma basis.


// relaxation superoperator
R.put(-R2ofS0,0,0);     R.put(0,0,1);           R.put(0,0,2);
        R.put(0,0,3);           R.put(0,0,4);           R.put(0,0,5);
R.put(0,1,0);           R.put(-R2ofS0,1,1);     R.put(0,1,2);
        R.put(0,1,3);           R.put(0,1,4);           R.put(0,1,5);
R.put(0,2,0);           R.put(0,2,1);           R.put(-R1ofS0,2,2);
        R.put(0,2,3);           R.put(0,2,4);           R.put(0,2,5);
R.put(0,3,0);           R.put(0,3,1);           R.put(0,3,2);           R.put(-
R2ofS1,3,3);    R.put(0,3,4);           R.put(0,3,5);
R.put(0,4,0);           R.put(0,4,1);           R.put(0,4,2);
        R.put(0,4,3);           R.put(-R2ofS1,4,4);     R.put(0,4,5);
R.put(0,5,0);           R.put(0,5,1);           R.put(0,5,2);
        R.put(0,5,3);           R.put(0,5,4);           R.put(-R1ofS1,5,5);

// chemical exchange superop
K.put(-Kf,0,0);         K.put(0,0,1);           K.put(0,0,2);
        K.put(Kr,0,3);          K.put(0,0,4);           K.put(0,0,5);
K.put(0,1,0);           K.put(-Kf,1,1);         K.put(0,1,2);
        K.put(0,1,3);           K.put(Kr,1,4);          K.put(0,1,5);
K.put(0,2,0);           K.put(0,2,1);           K.put(-Kf,2,2);
        K.put(0,2,3);           K.put(0,2,4);           K.put(Kr,2,5);
K.put(Kf,3,0);          K.put(0,3,1);           K.put(0,3,2);           K.put(-
Kr,3,3);        K.put(0,3,4);           K.put(0,3,5);
K.put(0,4,0);           K.put(Kf,4,1);          K.put(0,4,2);
        K.put(0,4,3);           K.put(-Kr,4,4);         K.put(0,4,5);
```

```
K.put(0,5,0);	K.put(0,5,1);	K.put(Kf,5,2);
	K.put(0,5,3);	K.put(0,5,4);	K.put(-Kr,5,5);

// transformation matrix
U.put(0,0,0);	U.put(0,0,1);	U.put(h,0,2);
	U.put(0,0,3);	U.put(0,0,4);	U.put(h,0,5);
	U.put(0,0,6);	U.put(0,0,7);	U.put(0,0,8);
	U.put(0,0,9);	U.put(0,0,10);	U.put(0,0,11);
	U.put(0,0,12);	U.put(0,0,13);	U.put(h,0,14);
	U.put(h,0,15);
U.put(0,1,0);	U.put(0,1,1);	U.put(0,1,2);
	U.put(h,1,3);	U.put(-ih,1,4);	U.put(0,1,5);
	U.put(0,1,6);	U.put(0,1,7);	U.put(0,1,8);
	U.put(0,1,9);	U.put(0,1,10);	U.put(0,1,11);
	U.put(h,1,12);	U.put(-ih,1,13);	U.put(0,1,14);
	U.put(0,1,15);
U.put(h,2,0);	U.put(-ih,2,1);	U.put(0,2,2);
	U.put(0,2,3);	U.put(0,2,4);	U.put(0,2,5);
	U.put(0,2,6);	U.put(0,2,7);	U.put(h,2,8);
	U.put(0,2,9);	U.put(0,2,10);	U.put(h,2,11);
	U.put(0,2,12);	U.put(0,2,13);	U.put(0,2,14);
	U.put(0,2,15);
U.put(0,3,0);	U.put(0,3,1);	U.put(0,3,2);
	U.put(0,3,3);	U.put(0,3,4);	U.put(0,3,5);
	U.put(h,3,6);	U.put(-ih,3,7);	U.put(0,3,8);	U.put(-
ih,3,9);	U.put(ih,3,10);	U.put(0,3,11);	U.put(0,3,12);
	U.put(0,3,13);	U.put(0,3,14);	U.put(0,3,15);
U.put(0,4,0);	U.put(0,4,1);	U.put(0,4,2);
	U.put(h,4,3);	U.put(ih,4,4);	U.put(0,4,5);
	U.put(0,4,6);	U.put(0,4,7);	U.put(0,4,8);
	U.put(0,4,9);	U.put(0,4,10);	U.put(0,4,11);
	U.put(h,4,12);	U.put(ih,4,13);	U.put(0,4,14);
	U.put(0,4,15);
U.put(0,5,0);	U.put(0,5,1);	U.put(h,5,2);
	U.put(0,5,3);	U.put(0,5,4);	U.put(-h,5,5);
	U.put(0,5,6);	U.put(0,5,7);	U.put(0,5,8);
	U.put(0,5,9);	U.put(0,5,10);	U.put(0,5,11);
	U.put(0,5,12);	U.put(0,5,13);	U.put(-h,5,14);
	U.put(h,5,15);
U.put(0,6,0);	U.put(0,6,1);	U.put(0,6,2);
	U.put(0,6,3);	U.put(0,6,4);	U.put(0,6,5);
	U.put(h,6,6);	U.put(-ih,6,7);	U.put(0,6,8);	U.put(-
ih,6,9);	U.put(-ih,6,10);	U.put(0,6,11);	U.put(0,6,12);
	U.put(0,6,13);	U.put(0,6,14);	U.put(0,6,15);
U.put(h,7,0);	U.put(-ih,7,1);	U.put(0,7,2);
	U.put(0,7,3);	U.put(0,7,4);	U.put(0,7,5);
	U.put(0,7,6);	U.put(0,7,7);	U.put(-h,7,8);
	U.put(0,7,9);	U.put(0,7,10);	U.put(ih,7,11);
	U.put(0,7,12);	U.put(0,7,13);	U.put(0,7,14);
	U.put(0,7,15);
U.put(h,8,0);	U.put(ih,8,1);	U.put(0,8,2);
	U.put(0,8,3);	U.put(0,8,4);	U.put(0,8,5);
	U.put(0,8,6);	U.put(0,8,7);	U.put(h,8,8);
	U.put(0,8,9);	U.put(0,8,10);	U.put(ih,8,11);
	U.put(0,8,12);	U.put(0,8,13);	U.put(0,8,14);
	U.put(0,8,15);
U.put(0,9,0);	U.put(0,9,1);	U.put(0,9,2);
	U.put(0,9,3);	U.put(0,9,4);	U.put(0,9,5);
	U.put(h,9,6);	U.put(-ih,9,7);	U.put(0,9,8);
	U.put(ih,9,9);	U.put(-ih,9,10);	U.put(0,9,11);
	U.put(0,9,12);	U.put(0,9,13);	U.put(0,9,14);
	U.put(0,9,15);
U.put(0,10,0);	U.put(0,10,1);	U.put(-h,10,2);
	U.put(0,10,3);	U.put(0,10,4);	U.put(h,10,5);
	U.put(0,10,6);	U.put(0,10,7);	U.put(0,10,8);
	U.put(0,10,9);	U.put(0,10,10);	U.put(0,10,11);
	U.put(0,10,12);	U.put(0,10,13);	U.put(-h,10,14);
	U.put(h,10,15);
U.put(0,11,0);	U.put(0,11,1);	U.put(0,11,2);
	U.put(h,11,3);	U.put(-ih,11,4);U.put(-0,11,5);
	U.put(0,11,6);	U.put(0,11,7);	U.put(0,11,8);
	U.put(0,11,9);	U.put(0,11,10);	U.put(0,11,11);
	U.put(-h,11,12);	U.put(ih,11,13);	U.put(0,11,14);
	U.put(0,11,15);
U.put(0,12,0);	U.put(0,12,1);	U.put(0,12,2);
	U.put(0,12,3);	U.put(0,12,4);	U.put(0,12,5);
	U.put(h,12,6);	U.put(ih,12,7);	U.put(0,12,8);
	U.put(ih,12,9);	U.put(ih,12,10);	U.put(0,12,11);
	U.put(0,12,12);	U.put(0,12,13);	U.put(0,12,14);
	U.put(0,12,15);
U.put(h,13,0);	U.put(ih,13,1);	U.put(-0,13,2);
	U.put(0,13,3);	U.put(0,13,4);	U.put(0,13,5);
```

```
        U.put(0,13,6);          U.put(0,13,7);          U.put(-h,13,8);
        U.put(0,13,9);          U.put(0,13,10);         U.put(0,13,11);
        U.put(-ih,13,12);       U.put(0,13,13);         U.put(0,13,14);
        U.put(0,13,15);
U.put(0,14,0);          U.put(0,14,1);          U.put(0,14,2);
        U.put(h,14,3);          U.put(ih,14,4);         U.put(0,14,5);
        U.put(0,14,6);          U.put(0,14,7);          U.put(0,14,8);
        U.put(0,14,9);          U.put(0,14,10);         U.put(0,14,11);
        U.put(-h,14,12);        U.put(-ih,14,13);       U.put(0,14,14);
        U.put(0,14,15);
U.put(0,15,0);          U.put(0,15,1);          U.put(-h,15,2);
        U.put(0,15,3);          U.put(0,15,4);          U.put(-h,15,5);
        U.put(0,15,6);          U.put(0,15,7);          U.put(0,15,8);
        U.put(0,15,9);          U.put(0,15,10);         U.put(0,15,11);
        U.put(0,15,12);         U.put(0,15,13);         U.put(h,15,14);
        U.put(h,15,15);

Uinv=inv(U);

// add both relaxation and exchange superpoerators for lioville space.

 RandK=R+K;
 int gradsteps=10;
 gen_op H[gradsteps];
 super_op L[gradsteps];
 sys_dynamic sys_multi[gradsteps];

 for (ii=0; ii<gradsteps; ii++)
   {

    sys.Omega(OmegaCenter+((-gradsteps/2)+ii)*GzMHz);
    sys_multi[ii]=sys;
    H[ii]=Ho(sys_multi[ii]);

    L[ii]=complexi*Hsuper(H[ii])-(U*RandK*Uinv);
    if (verbose==”y”)
 {
    cout <<”\n\n\nthis is H[”<<ii<<”] of omega=”<<sys.Omega()<<”\n”<< H[ii];
    cout <<”\n\n\nthis is L[”<<ii<<”] of omega=”<<sys.Omega()<<”\n”<< L[ii];
 }
 }
```

```
//generate the starting density operator from sys, called sigma_ex, with specified
temperature. This is a custom made sigma_ex, polarizing only the specified spin

  gen_op sigma_start=Ipol(sys,1/2,0); // Ipol is the polarization operator, giving
P=100% on spin i
  gen_op sigma_seq=sigma_start, sigma_fid;

// setup the detection operator. The expectation value of this operator (and the
desity operator) will be saved in the FID (at each timepoint)

//acquire total signal
//gen_op D=Fm(sys, IsoD);

//acquire spins separatly

 gen_op D0=Im(sys,0);
 gen_op D1=Im(sys,1);

// generate the  Ho, high resolution isotropic hamiltonian,
//gen_op Ht=Ho(sys);
 // cout <<”\n\nHt=”<<Ht;


 // now take the hamiltoian and make it a superoperator
 //super_op L=complexi*Hsuper(Ht);

//********* Transform, than add the exchange and relaxation super operator to
the liouvillian.
//Note, gamma takes positive relaxation values. Since I set the rates negative,
substract here.

  //******** start pulse sequence ********
  //******** preparation sequence ********

sigma_seq=Iypuls(sys, sigma_seq, IsoD, beta);
sigma_seq=evolve(sigma_seq, L, Tr/2);

 for (space=0; space<gradsteps; space++)
   {
```

```
//******** FFE sequence ********
  for(iterations=0;iterations<acquisitions; iterations++)
 {

 sigma_seq=Iypuls(sys, sigma_seq, IsoD, pow(-1.,iterations)*alpha);
 sigma_fid=sigma_seq;
 FID(sigma_fid, D0, L, dwelltime, datapoints, fid0); //acquire fid signal
 FID(sigma_fid, D1, L, dwelltime, datapoints, fid1); //acquire fid signal
 sigma_seq=evolve(sigma_seq, L, Tr);
 data0.put_block(iterations,0, fid0); // store signal in matrix
 data1.put_block(iterations,0, fid1); // store signal in matrix

 }
  }

fidvector=transpose(data0.get_block(1,1,acquisitions, 1));

// generate a matlab file.
// Header in Matlab file to hand over parameters for processing
// Structure: 'parameters' = datapoints, dwelltime, frequency, datasets
// fid: complex datasets in rows

//calculate parameters
Isotope observe(IsoD); // set observed isotope for postprocessing of spectra.
double frequency(sys.Omega()*observe.gamma()/GAMMA1H);
int datasets(KfMax);

//write parameters in row vector
row_vector parameters(20);
parameters.put(datapoints, 0);
parameters.put(dwelltime*1e3, 1);
parameters.put(frequency, 2);
parameters.put(datasets, 3);
parameters.put(acquisitions, 4);
parameters.put(Tr, 5);
parameters.put(T1ofS0, 6);
parameters.put(T1ofS1, 7);
parameters.put(T2ofS0, 8);
parameters.put(T2ofS1, 9);
parameters.put(Kf, 10);
parameters.put(Kr, 11);
parameters.put(alpha, 12);
parameters.put(beta, 13);
parameters.put(sys.shift(0), 14);
parameters.put(sys.shift(1), 15);

cout << "\nparameters: " << parameters;
MatLabFile fp("mbFFE.mat", std::ios::binary|std::ios::out); // make matlab file to
export fid matricies

//write parameters in matlab file
fp.write("parameters", parameters, 0);

//write data in matlab file
fp.write("fid0", data0, 1);
fp.write("fid1", data1, 1);

//********GNU plot ********
// fidvector=abs(fidvector);

  GP_1D("gnufid.asc", fidvector, 0, 0);          // Output in gnuplot (ASCII)
  GP_1Dplot("gnufid.gnu", "gnufid.asc");         // Interactive 1D gnuplot
     }
```

Appendix II

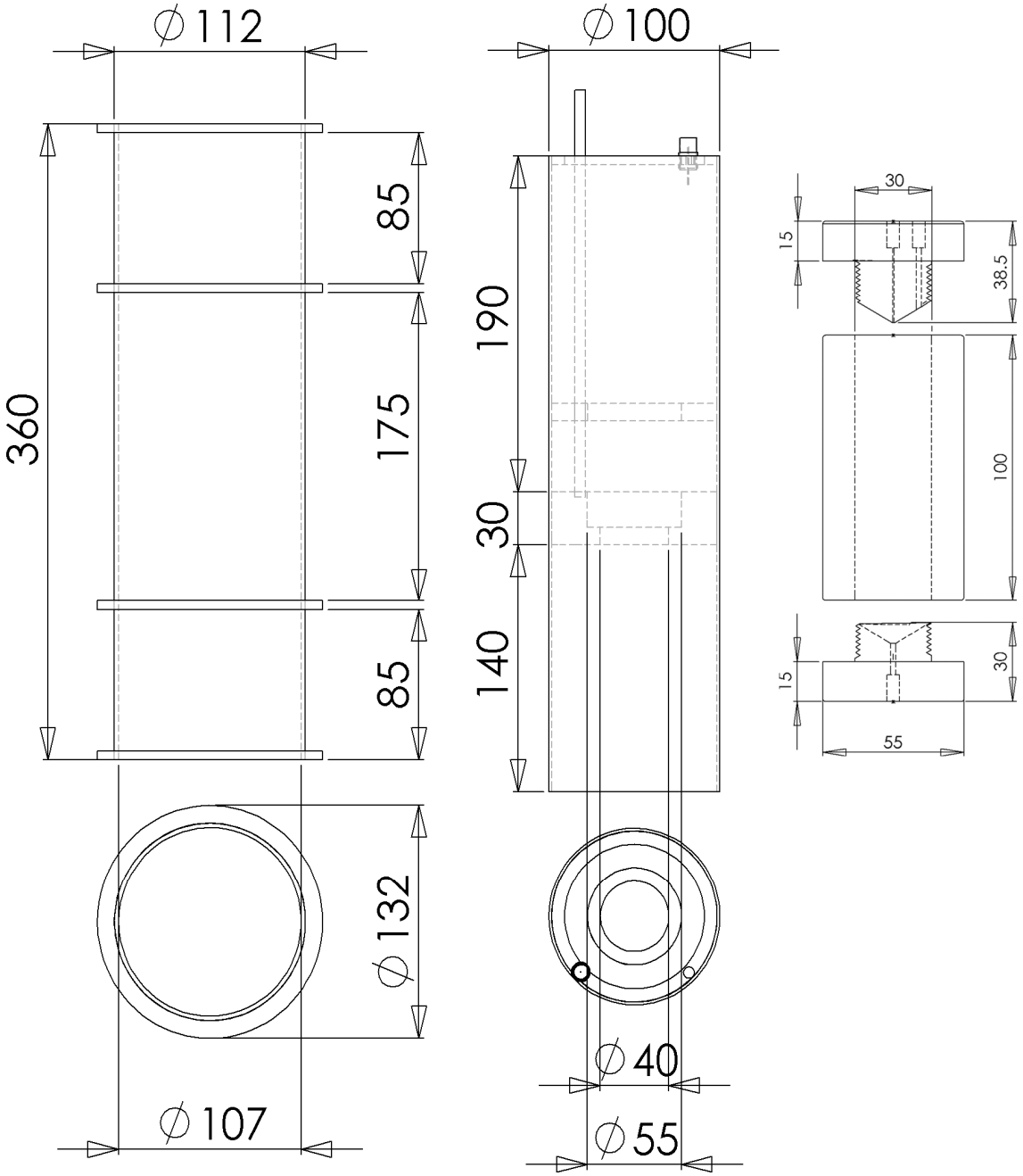

Fig. 52: Engineering drawings of B_0 coil, B_1 coil, and reactor No. 3. Units are in mm.

Tab. 12: List of all parts of the fluid-control unit of the polarizer as described in this work.

Subunit	Part	Description	C.A.
Transport and reaction	Tubing	PTFE tubing	Y[1]
	Valves	Electromagnetic solenoid and manual valves	Y[2, 3, 4]
	Ante chamber	PTFE tubing	Y[1]
	Reaction chamber	Injection cap, reactor body, end cap	-
Auxiliary	T control	Heater, fan, controller, relay	Y[5]
	Injection timer	On-delay relay	Y[6]
	Intake precursor	rubber piston syringe	Y[7]

— *Abbreviations:* C.A.: commercially available, Y: yes, PTFE: polytetrafluoroethylene. The superscript refers to the list of suppliers in Tab. 17.

Tab. 13: List of all parts of the low-field NMR unit of the polarizer as described in this work.

Subunit	Part	Description	C.A.
B_1 field	B_1 coil	Saddle-shaped coil	-
	Synthesizer	DAC analog-out	Y[8]
	Amplifier	Audio amplifier	Y[9]
	Filter	150 kHz low-pass filter	Y[10]
	Monitoring	Oscilloscope	Y[11]
	Cables	Coaxial cable RG58	Y[12]
B_0 field	B_0 coil	Solenoid coil	-
	Power supply	DC power supply	Y[13]
	Monitoring	Gauss meter	Y[14]

— *Abbreviations:* C.A.: commercially available, Y: yes, DAC: digital-to-analog converter, DC: direct current. The superscript refers to the list of suppliers in Tab. 17.

Tab. 14: List of all parts of the process-control unit of the polarizer as described in this work.

Subunit	Part	Description	C.A.
Software	Platform	LabView	Y[15]
	Program	PASADENA control V1.1	-
Hardware	Synthesizer	DAC analog-out	Y[8]
	Valve, trigger control	DAC digital-out	Y[16]
		Relays	Y[17]

— *Abbreviations:* C.A.: commercially available, Y: yes, DAC: digital-to-analog converter. The superscript refers to the list of suppliers in Tab. 17.

Tab. 15: List of chemistry and auxiliary equipment, used in this work.

Category	Part	Description	C.A.
Chemicals	Precursor	1-^{13}C, 2,3-D_2 Fum, 1-^{13}C, 2,3,3-D_3 HEA	Y[35, 36]
	Catalyst	Rh-complex and ligand	Y[37, 38]
	Solvent	D_2O, H_2O, buffer	Y[39]
Aux Lab Equipment		Schlenk line with vacuum, N_2, in fume hood	Y[39]
		Glassware	Y[39]
		Precession scale	Y[39]

— *Abbreviations:* C.A.: commercially available, Y: yes. Rh: Rhodium. Fum: fumarate, HEA: hydroxyethyl acrylate. The superscript refers to the list of suppliers in Tab. 17.

Tab. 16: List of all parts of the parahydrogen generator, as used in this work.

Function	Description	C.A.
Low T Unit	Helium two stage cold head	Y[18]
	Pressure gauge	Y[19]
	Vacuum shroud	Y[20]
	Helium compressor / cryodrive	Y[21]
	Vacuum pump	Y[22]
	Valve	Y[23]
	Flow limiter	Y[24]
	Relay	Y[25]
	Pressure display	Y[26]
	Water cooler	Y[27]
	Tubing connectors	Y[28]
	Regulator for H_2 supply	Y[29]
	Tubing at ambient temeratures	Y[30]
	Flow meter	Y[31]
Catalytic converter	Low-temperature catalyst container	Y[32]
	Catalyst	Y[33]
Storage	Cylinder	Y[34]

— *Abbreviations:* C.A.: commercially available, Y: yes. The superscript refers to the list of suppliers in Tab. 17

Tab. 17: List of suppliers and manufacturers for parts of the polarizer.

1 PTFE tubing, OD / ID/ WT: 1/8, 1/16, 1/32 “, Nalgene, NY, USA.
2 Two-ways rocker valve, mod. 6126 (id. 431568, for liquids), Buerkert Fluid Control Systems, Indelfingen, Germany.
3 Addition to 6126 by Promech lab AB, Malmø , Sweden.
4 Solenoid valve, mod. H22G9DGV (for gases), Peter Paul Co., CN, USA.
5 Mod. CN132, Omega Engineering, CN, USA.
6 Mod. 814 Syrelec, Crouzet, TX, USA.
7 BD, Franklin Lanes, NJ, 07417, USA.
8 Mod. PXI 1042, PXI 8331, PXI 6251, National Instruments, TX, USA.
9 Mod. 8522 TX, Onkyo, USA.
10 Mod. 3200, Krohn Hite, USA.
11 Mod. TDS 3012 B 100 MHz 1.25 Gs/s, Tectronix, USA.
12 Generic.
13 Mod. 3615°, Agilent, USA.
14 Gaussmeter 450 with axial probe MMA 2508 VH, Lake shore, USA.
15 LabView (V. 8.0), National Instruments, TX, USA.
16 Mod. USB 6501, NI, TX, USA.
17 Mod. ER-16, NI, TX, USA.
18 Mod. B51907000 6130 cold head assembly, Edwards, MA, USA.
19 Active pirani gauge, APG M NW 25 ST/ST, PN: D0217200 SN: 02723484.
20 Generic, S.C.B., Herrmann-Cossmann-Str. 19, D-41472 Neuss, Germany.
21 3.0kW He cryodrive, Edwards, MA, USA.
22 Mod. RV3, with oil mist filter EMF 10, Edwards, MA, USA.
23 Mod. LCPV2 5 EKA, Edwards, MA, USA.
24 Needle valve HAKE 1315G4s 5000PSI 1345b 1 0553, set 4.5.
25 Generic, 240V.
26 Mod. AGD, set to ~ 2x10-4 b, Edwards, MA, USA.
27 Mod. Neslab Merlin M150, Thermo Fischer Scientific, MA, USA.
28 “Instrumentation-quick-connect” (SS), Swagelok, OH, USA.
29 Regulator 250 b to 68 b, Advanced specialty gas equipment, NJ, USA.
30 ¼ “ copper / ¼” SS generic, 7RSW SAE 100 R7-4 ¼ 2750 PSI swagelok, OH, USA.
31 Mod. 7101 043001A, King Instruments, CA, USA.
32 ¼ “copper tubing, generic.
33 Ionex-Type O-P catalyst (hydrous ferric oxide), Molecular products, CO, USA.
34 7 L volume, M25x2 150, CBM produkter AB, Box 47, 131 06 Nacka, Sweden, or P2795z, Luxfer, CA, USA.
35 Fumaric acid, 1-^{13}C (99%), 2,3-D_2 (96%), Cambridge Isotope Laboratories, MA, USA.
36 2-Hydroxyethyl 1-^{13}C (99%), 2,3,3-D_3 (98%) acrylate, Isotech, Sigma-Aldrich, MO, USA.
37 Bis(norbornadiene)rhodium(I) tetrafluroborate, catalog number 45-0230, CAS 36620-11-8, >96%, Strem Chemicals, MA, USA.
38 1, 4-bis[(phenyl-3-propanesulfonate) phosphine] butane disodium salt, Q36333, Isotech, Sigma Aldrich, MO, USA.
39 Generic.

Appendix III

Statistic errors

The term *standard deviation* (SD, σ_x, Eq. 69), the square root of the sample variance, characterizes the accuracy of a measurement: The probability of a of a *single sample* x_i be within an interval of one (two, three) standard deviation(s) of the 'true', but unknown value x_0 is 68% (95%, 98%), respectively. The statistic measure for the accuracy of a *mean value*, which was obtained from n-single samples, is the *standard error* (SE, $\sigma_{\bar{x}}$, Eq.70). To obtain an estimate for the SD or SE, multiple samples (e.g. n-measurements) need to be taken. While the SD of the individual values converges with n towards a constant, the SE of the mean value decreases with $n^{-\frac{1}{2}}$: The more measurements are taken, the closer is the mean to the "true" value.

A dimensionless measure for the accuracy of an individual sample is the SD normalized by the sample mean, denoted as coefficient of variance (c_v, Eq. 71).

$$SD = \sigma_x = \sqrt{\frac{1}{(n-1)}\sum_{i=1}^{n}(x_i - \bar{x})^2} \tag{69}$$

$$\begin{aligned} SE = \sigma_{\bar{x}} &= \sqrt{\frac{1}{n(n-1)}\sum_{i=1}^{n}(x_i - \bar{x})^2} \\ &= \frac{1}{\sqrt{n}}\sigma_x \end{aligned} \tag{70}$$

$$c_v = \frac{\sigma_x}{\bar{x}} \tag{71}$$

Systematic errors

Systematic errors are derived e.g. by the errors of the involved instruments (e.g. meter-reading uncertainty). If a value is a function of several measurands, the Gaussian error propagation is applied:

The Gaussian error propagation allows for the estimation of an error Δ_q^{Gauss} for a quantity $q(x_i)$ of observables x_i, which can not be measured directly. The error of $q(x_i)$, Δ_q^{Gauss} is determined using the individual x_i, and the corresponding individual errors Δx_i. Gaussian normal distribution is assumed.

$$\Delta_q^{Gauss} = \sqrt{\sum_{i=1}^{n}\left(\frac{\partial q}{\partial x_i}\right)^2 \Delta_{xi}^2} \tag{72}$$

In this work, the standard deviation is given for an individual sample (single measurement): $T_1^i = (x_i \pm SD)$. The standard error is noted for means: $\overline{T}_1^i = (\overline{x} \pm SE)$.
For individual measureands where the SD is unknown, the systematic error is noted.

In the following, the error-calculation of selected experiments is discussed.

B_0 and B_1 calibration

^{13}C and ^{1}H NMR signals (S) were acquired at $B_0 = 7$ T as a function of the strength of the B_0 field in the polarizer and pulse widths of the SOT sequence, $S(B_0)$ and $S(B_1)$. Due to relaxation processes, variable magnetic fields and pulses, it is difficult to give an analytical expression for the uncertainties of the measurement of $S(B_0)$ and $S(B_1)$. However, certain errors can be estimated: The major contribution to the uncertainty of for both terms originates from the 'delivery time', the period for transportation between high-field NMR and polarizer: (14 ± 0.5) s. Based on the T_1 of the NMR agents of the order of 5 s for ^{1}H, 30 s for ^{13}C, the total error is estimated to 10 % (^{1}H), and 2 % (^{13}C), respectively (Gaussian error propagation, see above). Furthermore, the numerical integration of the peaks is estimated to have a maximal error of 2 %. The errors of the pulse widths of the SOT sequence and the settings of B_0 (promille precision) are negligible. In total, a relative error for $S(B_0)$ and $S(B_1)$ of 11 % (^{1}H), and 3 % (^{13}C) is estimated.

Quantification of hyperpolarization

The degree of polarization is calculated according to the following formula:

$$P_{hyp}^{t_a} = \frac{S_{hyp}^{t_a}}{S_{ref}} \cdot \frac{c_{ref}}{c_{hyp}} P_B , \tag{73}$$

where $S_{hyp}^{t_a}$, S_{ref}, c_{hyp} and c_{ref} are the signal intensities (peak areas) and molar concentrations of hyperpolarized- and reference sample. $P_{hyp}^{t_a}$ denotes the hyperpolarization degree at a time t_a after the production of the sample, P_B is the Boltzmann polarization.

Statistical error.
The statistical errors of the hyperpolarization degree of 1-^{13}C, 2,3-D_2 Suc in H_2O and D_2O were determined in section (section 3.3, pp. 73). The mean values, standard errors ($\overline{P}_{hyp}^{t_a}$ ± SE), as well as the standard deviations ($P_{hyp}^{t_a}$ ± SD) are given in Tabs. 8 and 9.

Systematic error.
The systematic error for the hyperpolarization yield is calculated using the Gaussian error propagation. Only the error of the signal intensities ($S_{hyp}^{t_a}$, S_{ref}) and the concentration of the hyperpolarized agent (c_{hyp}) contribute:

$$\Delta P_{hyp}^{t_a=33s} = \sqrt{\left(\frac{\partial P_{hyp}^{t_a=33s}}{\partial S_{hyp}} \Delta S_{hyp}\right)^2 + \left(\frac{\partial P_{hyp}^{t_a=33s}}{\partial S_{ref}} \Delta S_{ref}\right)^2 + \left(\frac{\partial P_{hyp}^{t_a=33s}}{\partial c_{hyp}} \Delta c_{hyp}\right)^2} \tag{74}$$

The error of the concentration of the hyperpolarized agent is calculated similarly:

$$\Delta c_{hyp} = \sqrt{\left(\frac{\partial c_{hyp}}{\partial M}\Delta M\right)^2 + \left(\frac{\partial c_{hyp}}{\partial V}\Delta V\right)^2} \tag{75}$$

Where M denotes the moles of the hyperpolarized agent and V is the volume of solvent.
The calculation is demonstrated for measurement No. 2 in Tab.8:

Concentration
A weight of (5.2 ±0.1) mg of 1-^{13}C, 2,3-D_2 Fum solved in V = (25 ± 1) ml yield a concentration of c_{hyp} = (1.71 ± 0.08) mM (molecular weight mw(Fum) = 121 g/mol).

Polarization yield
With $S_{hyp}^{t_a=33s}$ = 186.3, S_{ref} = 1, c_{hyp} = (1.71 ± 0.08) mM, c_{ref} = 188.0 mM and B_0 = 4.7 T, the ^{13}C polarization calculates to:

$$P_{hyp}^{t_a=33s} = 0.084 \pm 0.004\,, \tag{76}$$

The contributions to the total error of S_{ref} and c_{hyp} are four orders of magnitude higher than the contribution of $S_{hyp}^{t_a=33s}$. To estimate the polarization at t_a = 0,

$$P_{hyp}^{t\ =0} = \frac{I_{hyp}^{t_a}}{I_{ref}} \cdot \frac{c_{ref}}{c_{hyp}} P_B \cdot \exp\left(\frac{t_a}{T_1}\right), \tag{77}$$

the error originating from the exponential function had to be added:

$$\Delta P_{hyp}^{t_a=0} = \sqrt{\left(\frac{\partial P_{hyp}^{t_a=0}}{\partial S_{hyp}}\Delta S_{hyp}\right)^2 + \left(\frac{\partial P_{hyp}^{t_a=0}}{\partial S_{ref}}\Delta S_{ref}\right)^2 + \left(\frac{\partial P_{hyp}^{t_a=0}}{\partial c_{hyp}}\Delta c_{hyp}\right)^2 + \left(\frac{\partial P_{hyp}^{t_a=0}}{\partial t_a}\Delta t_a\right)^2 + \left(\frac{\partial P_{hyp}^{t_a=0}}{\partial T_1}\Delta T_1\right)^2} \tag{78}$$

Assuming t_a = (33.0 ± 0.1) s, and the T_1 = (39.6 ± 0.6) s measured at B_0 = 4.7 T, the polarization at t_a = 0 is calculated to:

$$P_{hyp}^{t=0} = 0.194 \pm 0.01\,. \tag{79}$$

However, since the exact dependence of T_1 on B_0 is not known, and the hyperpolarized sample experiences field strengths of B_0 = mT – T for >20 s (during the transportation), the actual polarization degree at t_a = 0 ($P_{HP}^{t_a=0}$) is only an estimate.

T_1 is expected to decrease in lower fields, as described in [61, 62]:

$$T_1 \approx A\nu^B \tag{80}$$

where A and B are empirical parameters, is the ν resonance frequency.
Since the T_1 values used were obtained at $B_0 = 4.7$ T, the calculation above *underestimates* the degree of polarization at $t_a = 0$: $P_{HP}^{t_a=0}$ is assumed to be a lower limit.

T_1 constants

The decaying hyperpolarization of a sample was probed by successive low-angle pulse-and-collect experiments (small-excitation-angle approximation, SEA). The signal strength was determined by numerical integration (systematic error ~ 2%), and normalized by the first data point. An exponential function, corrected for the signal loss caused by the r.f. pulses, was fitted to the data (Eq. (63) to extract the lifetimes (T_1). (Origin, OriginLabs, USA)

A systematic error can be observed in these experiments: the first data point is regularly below the fitted function. This effect may be attributed to radiation damping for the first point, when the signal is strongest (the effect is not observed at a later point, when the signal has further decayed). For this reason, the first data point is omitted for the fitting, which improved the statistical errors strongly (demonstrated in the following paragraph).

A representative example for the determination of T_1 is discussed in detail in the following: n = 4 SEA experiments on 1-^{13}C,2,3-D_2 succinate in D_2O were carried out and processed individually as described above. Four individual T_1 values were obtained, which allowed for the calculation of a mean T_1 and SE: $\overline{T_1} = (39.6 \pm 1.1)$ s. The SD of an individual T_1 value is $\sigma_{T_1} = 2.2$ s. If the first (erroneous) data point is taken into account, the values are $\overline{T_1} = (43.5 \pm 3.2)$ s, and $\sigma_{T_1} = 6.4$ s.

To estimate the statistical error of each acquisition *within* one decay / experiment, the signals at each time point of all four experiments were averaged (TR = 20 s). The average SD of the individual signals, $\sigma_S = 0.02$ a.u., was used for all plots.

Acknowledgements

I would like to thank all who contributed to the success of this work very much. In particular,

PhD advisor Prof. Dr. P. Bachert, referee Prof. Dr. Dr. C. Cremer and Prof. Dr. Dr. W. Semmler, DKFZ and University of Heidelberg;

Ass. Prof. Dr. P. Bhattacharya and Dr. E. Chekmenev from the Enhanced Magnetic Resonance Laboratories;

Prof. Dr. D. Weitekamp, Dr. J. Ollerenshaw, V. Norton, Dr. N. Lisitza at the California Institute of Technology;

Dr. K. Kanamori, Dr. P. Sailasuta, L. Robertson, Dr. B. Ross, Dr. K. Harris and Dr. W. Opel, L. Barros, Dr. Ingram and the summer students Siu-Kei Chow and Joshua C. Ewell at the Huntington Medical Research Laboratories, and Dr. W. H. Perman from St. Louis University;

The staff of the physics and chemistry machine shop and T. Dunn of the electronics shop at the California Institute of Technology;

The International Society of Magnetic Resonance in Medicine and Experimental NMR conference for travel stipends;

Jessica Bastiaansen, since this thesis would not have been written without her;

All my friend and colleagues, who supported me in many ways: Frederik Laun, Moriz Berger, Benedict von Harling, Heiko Schröder, all my roommates from 135 south chester, and many, many more.

To all of you: thank you very much!